ABSTRACT

KIYAK, YASAR EMRE. Nonwovens as Separation Media in Bioreactors (Under the direction of Dr. Behnam Pourdeyhimi and Dr. Benoît Mazé).

Membranes are employed as separation media in the membrane bioreactor process (MBR), which involves a combination of biotreatment and membrane separation. Pore size is likely the most critical parameter of a medium to determine the treatment performance for size-exclusion filtration. The first aim of this study was to develop a basis for predicting mean pore diameter of nonwovens. A comprehensive methodology, considering various structure properties was employed to predict the mean pore diameter of nonwovens. The investigation revealed that mean pore diameter is a function of two structure properties: fiber diameter and solid volume fraction. The developed mean pore size model has a good agreement with the experimental data for highly porous nonwovens having small fibers (<4µm). The second aim of the study was to form nonwoven membranes through post-processing techniques. Membrane-like nonwovens are required to have narrow pore size distribution, smooth surface, and a surface filter (rather than depth filter) structure. For this purpose, three different post-processing setups have been employed to form nonwoven membranes. According to the results, the heated calender rollers where the gap between the rollers is predetermined is the most promising route to forming nonwoven membranes. The third aim was to investigate the effects of nonwoven mean pore diameter on treatment performance in terms of fouling behavior and effluent quality. The results showed that effluent quality and fouling behavior are mainly governed by pore size characteristics of the nonwoven media.

Nonwovens as Separation Media in Bioreactors

by
Yasar Emre Kiyak

A dissertation submitted to the Graduate Faculty of
North Carolina State University
in partial fulfillment of the
requirements for the degree of
Doctor of Philosophy

Fiber and Polymer Science

Raleigh, North Carolina

2016

APPROVED BY:

_____	_____
Dr. Behnam Pourdeyhimi Committee Co-Chair	Dr. Benoît Mazé Committee Co-Chair
_____	_____
Dr. William Oxenham	Dr. Saad Khan

DEDICATION

To my wife Umran, my son Hamza, and all my family members

BIOGRAPHY

Yasar Kiyak was born in Bursa, Turkey in June 18, 1986. He received his bachelor and master degree in Textile Engineering at Istanbul Technical University in 2009 and 2011, respectively. He joined the College of Textiles at North Carolina State University in August 2012 to pursuit a PhD degree in Fiber and Polymer Science.

ACKNOWLEDGMENTS

First and foremost, I would like to recognize my GOD, Allah for his blessings, and for establishing me to complete this dissertation. I want to express my deepest gratitude to my wife for her encouragement and support throughout my dissertation. I would like to express the cordial appreciation to my committee chairs Dr. Mazé and Dr. Pourdeyhimi. I want to give special thanks to Dr. Mazé for his aspiring guidance, constructive criticism and patience. I acknowledge the generous support from Dr. Pourdeyhimi. He is not only a great advisor but also a great life coach. His profound guidance helped me a lot during my years at NC State. I would like to acknowledge my committee members Dr. William Oxenham and Dr. Saad Khan. I am especially thankful to Dr. Oxenham for his valuable time for constructive feedback. I also wish to acknowledge my former advisor, Dr. Ali Demir for his guidance in my career. He encouraged me to pursuit PhD in the College of Textiles. I am indebted to my family, especially my mom and dad, for the continuous support they have given me throughout my life. Lastly, I would like to thank all of the people who helped me with my research, especially staff of The Nonwovens Institute, my friends at the College and colleagues at the Institute.

TABLE OF CONTENTS

LIST OF TABLES

LIST OF FIGURES

1. Introduction

In previous centuries, with a lower global population and many uncontaminated water sources, people could easily find access to clean water. With the increase in population, things have changed and several problems such as water scarcity have been born.[1] Agricultural, industrial and domestic demand are the main reasons for water scarcity, while conservation, desalination of seawater and brackish water, discovering new water sources and wastewater recycling are the solutions[2].

Water reuse and recycling have gained vital importance recently due to water scarcity. Lack of clean water, growing populations, and more severe environmental regulations have created a compelling demand for wastewater recycling and reuse[2]. In the 3rd millennium, health problems related to water pollution appear almost solved in industrialized countries. However, developing countries have many problems in terms of sanitation and safe drinking water[3]. With regard to these problems, wastewater treatment technologies have been in use for a long time around the world[4]. Among water treatment technologies, membrane bioreactors (MBR) are promising, because they result in excellent treated water quality at reasonable costs, small space requirements, and lower energy demand compared to typical water treatment plants[5–7].

MBR systems have three main problems which are listed below[8,9]:

High-energy demand: Operating MBR requires high energy due to low flux.

Membrane cost: Membranes are expensive materials due to complex production procedure. In a water treatment plant, the membrane may account for up to 50% of the total capital cost. Additionally, when any type of cleaning is not able to recover the flux or trans-membrane pressure, membrane replacement is required.

Fouling: Due to the sieving mechanism, fouling is inevitable and can be severe in MBR processes. Fouling is the major obstacle for widespread usage of MBR.

Engineered nonwoven fabrics with high porosity[10], enhanced flux[11], controllable fiber size[12], high surface area[13], diverse functionality[11], and low cost[14] are potential substitutes for membranes in water treatment applications. Nonwovens can be a full or partial replacement of microfiltration membranes in bioreactors.

This dissertation is organized in seven chapters. Chapter 2 is devoted to the literature review of the wastewater processing and critical review of the nonwoven separation media used in MBRs. Research objectives are introduced in Chapter 3. The basis for predicting mean pore size of nonwovens is given in Chapter 4. Chapter 5 introduces the nonwoven membrane formation while Chapter 6 relates to water treatment experiments. Chapter 7 gives the overall conclusion and provides a background for future research in the area of wastewater filtration where nonwovens are used as separation media.

2. Literature Review

2.1 Wastewater Processing

Conventional wastewater processing (Figure 2.1) starts with pretreatment. According to the Environmental Protection Agency (EPA), objectives of pretreatment are to prevent interference with the operation of wastewater treatment, to prevent the introduction of pollutants that could pass through the treatment plant untreated into the receiving stream, to improve opportunities for reuse or recycle of wastewater and biosolids, and to prevent the introduction of pollutants that could cause health or safety problems to the public or the environment[15].

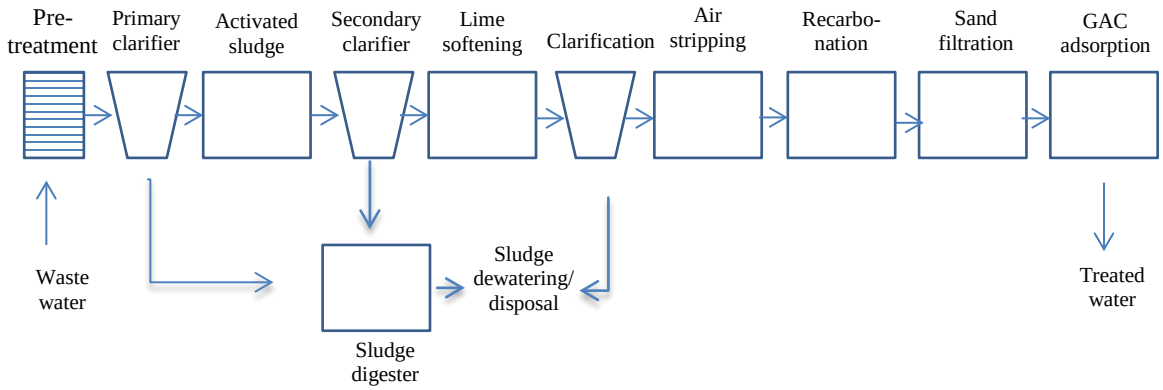

Figure 2.1 Conventional wastewater treatment process[16,17]

Primary clarifier removes the settleable and floatable solid from the wastewater[18]. Microorganisms digest the waste in activated sludge step, which creates biomass during treatment. Secondary clarifier removes this biomass. Digested sludge is disposed directly on land or dewatered on drying beds with the time[19].

Hardness is the result of the presence of some ions such as calcium and magnesium. Lime softening, which is used for removing heavy metals, radionuclides, dissolved organics, and viruses[20], reduces hardness in the wastewater when necessary. After lime softening, another clarification is applied to remove solids in the wastewater. Air stripping process removes volatile gases such as hydrogen sulfide, hydrogen cyanide and ammonia by blowing air through the wastewater. Basically, this process can be considered as a transformation from liquid phase to gas phase[21]. Generally, ammonia is removed by increasing pH. Sufficient air-water contact strips the ammonia gas from the solution[22]. It is important to raise the pH to the value of 11 or higher so that at least 95% of ammonia nitrogen is converted to the gas form. In other words, pH could be high after air stripping process because typically there is a contact between contaminated water and the air stream. So, pH reduction is done by recarbonation process[23]. Recarbonation process prepares the water for filtration; lowers the pH to a value that increases the efficiency of carbon adsorption of organics, and stabilizes the water with respect to scale formation on pipelines[24]. If water is allowed to enter the distribution system in this state, high pH may result in corrosion of pipes and the excess calcium carbonate can precipitate out, resulting in scale. In sand filtration, water is applied to a sand bed for filtration. Removal of microorganisms is achieved in sand filtration by physical and biological mechanisms[25]. Granular activated carbon (GAC) adsorption removes organics, tastes, and odors[26]. Frequently, activated carbon is used to adsorb organics, taste and odor compounds in drinking water treatment[27].

2.1.1 Membrane Bioreactor

A membrane bioreactor is defined as a flow reactor within which membranes are used as a separation medium to separate particles from the feed[28,29]. Briefly it is the combination of membrane separation and activated sludge process (Figure 2.2). The first U.S. patent was issued to W. Budd and R. Okey of Dorr-Oliver, Inc. for complete-mix activated sludge process with membrane technology in 1969[30].

MBR technology can be applied on a wide range of scales. 37.8 m^3/d of wastewater can be treated on a small MBR which can be found in office buildings, and hotels where water can be reused near the source. The global number of MBRs is estimated over 5000 installations as of 2011. Design capacities of 166 of these are greater than 3800 m^3/d. There are many MBR plants in operation, under construction, or being designed worldwide[30].

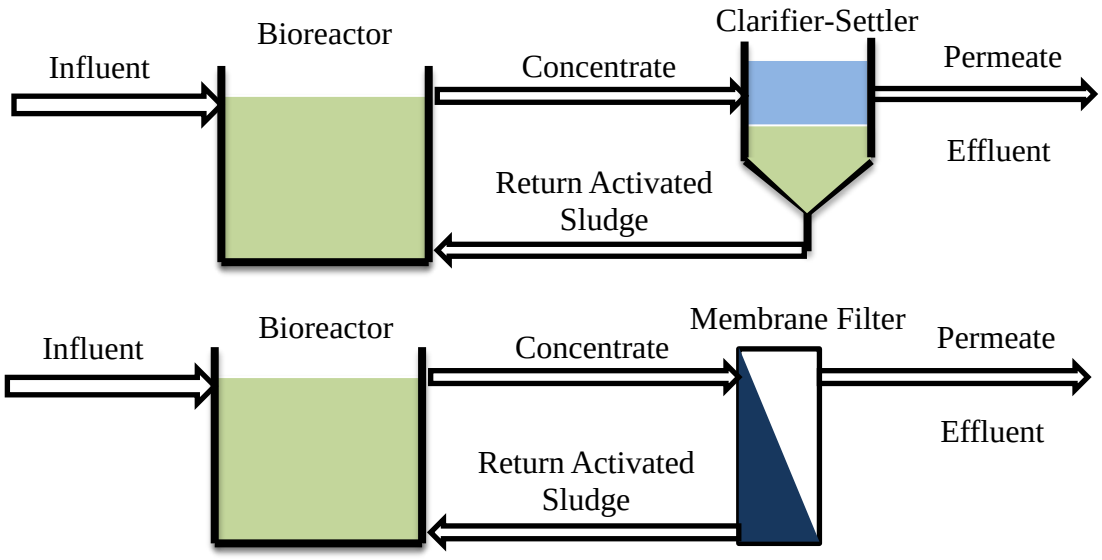

Figure 2.2 Conventional activated sludge process(a) and MBR process (b)[30].

Biological treatment depends on microorganisms to digest organic materials, to remove them from the wastewater and to convert them into new biomass. Microorganisms stick together as flocs, which are suspended in the wastewater. After treatment took place, the flocculated microorganisms must be separated from the water. In order to separate liquid and solid, conventionally a clarifier is used. However, in membrane bioreactor, the clarifier is replaced with a membrane for liquid-solid separation.

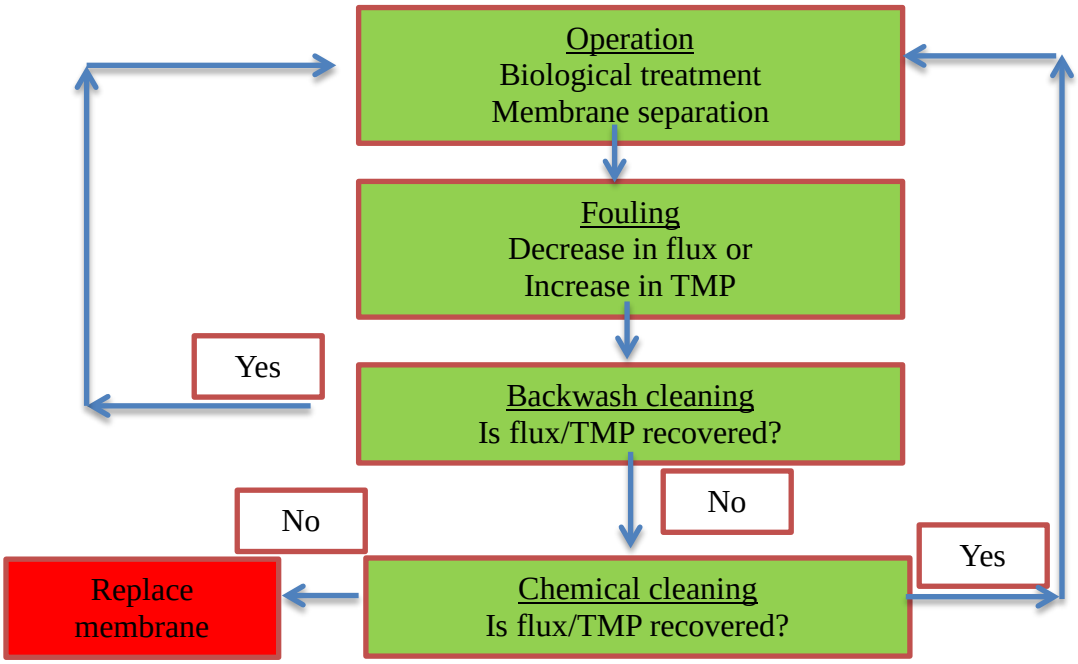

Figure 2.3 Operating cycle of MBR[31]

Some fundamental definitions are useful to understand the basics of the membrane bioreactor process. ***Flux,*** which is one of the most important parameters for MBR, is volumetric filtration rate for a given area of membrane. Cubic meter per square meter of membrane area per hour (m^3/m^2h) is the typical unit of the flux. When the flow rate is divided by the membrane area in service, instantaneous flux is calculated. ***Transmembrane pressure*** (TMP) is defined as pressure differential across the membrane. Generally, membrane flux is driven

by the vacuum pumping system on the permeate side. KPa (or PSI) is the unit of TMP. ***Permeability*** is the instantaneous flux divided by TMP. m^3/m^2.h.kPa is the unit of permeability[30].

2.1.1.1 Basic Operations

A membrane bioreactor has three main operations: biological degradation, membrane separation and maintenance. Relationships of these operations are shown in Figure 2.3.

Biological degradation is operated through microorganisms, which are in the form of flocs. Membrane separation is operated through membrane module. Fouling determines the maintenance frequency. Typical backwashing frequency for a flat-sheet membrane (Kubota) is 1/hr. Water treatment process will result in an increase of transmembrane pressure or a decrease of flux with the time. After a point this change in flux/transmembrane pressure has to be recovered by backwash since filtration is not applicable. After a point, backwashing will not be adequate for recovering the flux/transmembrane pressure. After this point chemical cleaning is required. When the chemical cleaning is not able to recover the flux/transmembrane pressure, then membrane replacement is required[31,32].

Constant Flux/Constant Pressure

The system can be operated either at constant transmembrane pressure or constant flux. Current trend for MBR is operating at constant flux. At constant flux, TMP is a variable while; flux is varying at constant pressure as a response to the changes in permeability. At constant flux, MBR should be run at moderate flux in order to limit fouling[33].

2.1.1.2 Biological Process

Membrane bioreactor is designed to remove organic materials and nutrients (nitrogen and phosphorus). Design of the conventional activated sludge (CAS) and MBR systems may be different but fundamentally biological processes are similar. Some of the related terms are defined below.

Hydraulic retention time (hydraulic residence time) (HRT) is defined as the measure of average length of time that the wastewater remains in a constructed bioreactor[34]. Minimum time required to allow influent organic matter to be adsorbed into the flocs before reaching the membranes is 3 hours[30].

Sludge retention time (SRT) also known as sludge age or mean cell residue time (MCRT) is the average time that microorganisms stay in the bioreactor[21]. Conventionally, SRT for MBR is no longer than 25 days. However, generally lower SRTs, which results in more manageable MLSS levels (10 to 15 kg/m^3) are desired[30].

Activated sludge is in the form of dispersed growth at the beginning (approximately two days). After that, flocculated organisms can be seen for a long time (until the 20^{th} day). After 20 days, dispersed floc formation is seen at the main tank (Figure 2.4). In other words, BOD removal efficiency increases continuously till the 2^{nd} day. After two days, BOD removal efficiency is almost the same[35].

Mixed liquor suspended solid (MLSS) is defined as the dry suspended solids in mixed liquor which is the measure of the concentration of matter in the biological treatment process.

Mixed liquor volatile suspended solids (MLVSS) is the volatile suspended solids, which are burnt up when a sample is heated to 550°C, in the mixed liquor which is the estimate of the active microorganisms in the mixed liquor[36].

Activated sludge includes organics, bacteria, and inorganics in the form of flocs whose size vary from 1 to 1000 μm. And microorganism concentration changes from 5 to 20% in the biological tank. It is accepted that there is enough oxygen inside the aeration tank. Normally, the outside (surface) of the floc is aerobic while the inside (center) of the floc is anaerobic, depending on oxygen accessibility[35].

Biosorption

Basically, organic matter is removed by biological metabolism. While oxygen is consumed by microorganisms, new cell mass is produced in addition to water, CO_2, dead leftover microorganism, etc. If the domestic wastewater is mixed up with sludge, sorption of the readily degradable organics may occur which is called biosorption[35].

Carbohydrates, proteins, fatty acids, and organic complex can be found in a real wastewater. These organics are named as readily degradable. Sorption of organics by flocs is done rapidly when the wastewater is contacted with sludge. This sorption can be regarded as biosorption, which depends on characteristics of the wastewater and activity of the biomass. In the absence of poorly degradable waste like amino acids and, acetate, this sorption may not take place.

Generally, one-third of the domestic waste is suspended solids, one-third is colloidal solids and the other one-third is soluble organics. When the wastewater gets in touch with the activated sludge, suspended solids are removed by flocs; colloidal organics are partially adsorbed and trapped in the flocs. And at the same time, a little portion of soluble organics are sorbed by flocs. Approximately, 85 percent of the removal of the total COD is done at an early stage of the bioprocess[35].

Food to Microorganism Ratio

Food to microorganism ratio (F/M) is the indication of operating criteria and design basis. F/M ratio is derived when the mass of organics (i.e. BOD or COD) is divided by MLVSS in the aeration tank.

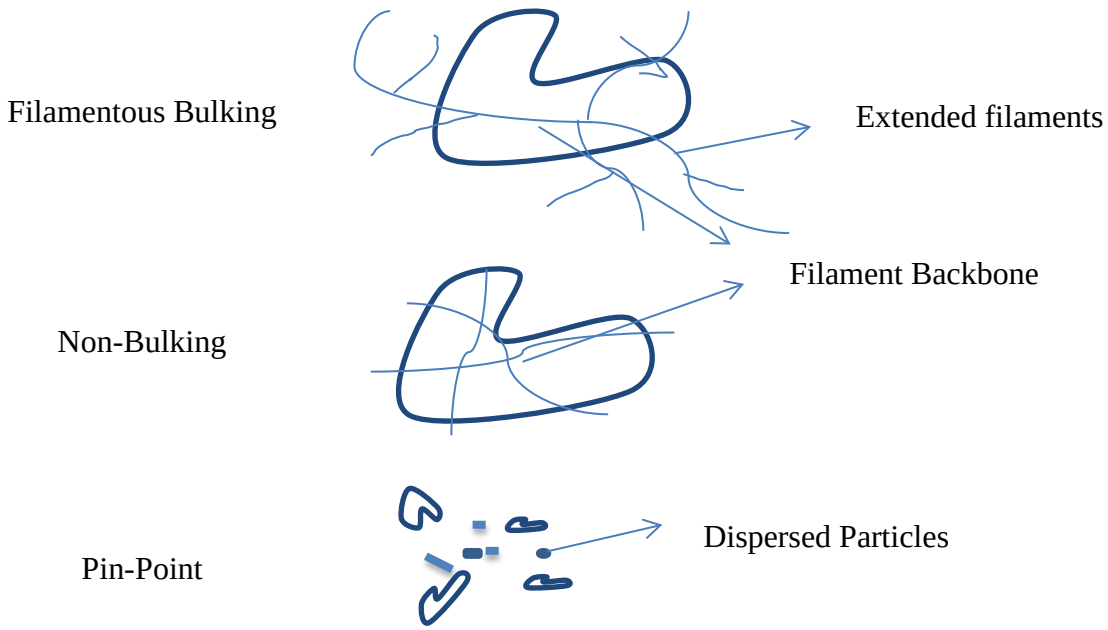

Figure 2.4 Activated Sludge Characteristics [35]

Temperature

Activated sludge process is mostly operated in the range of 4 to 39 ºC, which is called the mesophilic range. However, some trials have been made in the range of 45 to 55 ºC, which is called the thermophilic range. At these temperatures, mixed liquor was dispersed, and sludge was difficult to separate. As a result, effluent solid concentrations were high. Higher temperature will result in lower production rate of sludge production and reduction of aeration basin requirements. Bench or pilot scale membrane bioreactors can be operated at higher temperatures in order to figure out the sludge settling quality and oxygen transfer characteristics[35].

Nutrient Requirements

Good floc formation depends on required nutrients like Mn, Cu, Zn, and Ca. Generally these are present at required quantities in most wastewater. If the sufficient nutrient is not present in the solution, cellular material mass increases due to accumulation of polysaccharides. Nitrogen could be available in the form of ammonium (NH^{+}_{4}) or nitrate (NO^{-}_{3}). Nitrogen in the proteins or organics is supposed to be hydrolyzed in order to be consumed by biomass. Also, phosphorus is supposed to be in the form of soluble orthophosphate in order to be used by biomass. Maximum nutrient mass ratio should be 100:5:1 (BOD: N: P) to get the best removal. Otherwise, BOD removal will reduce and filamentous growth (Figure 2.4) -- which may result in the loss of sludge inventory to the effluent -- will occur which is a common and serious problem in activated sludge operation[35].

Acclimation

It is necessary to acclimate the biomass in the case of removal of organics. The time required for acclimation depends on the source of the seed biomass, operating temperature and sludge age. Optimum acclimation may take five to six weeks. As biodegradation and acclimation proceed, concentration of the solution in the main tank increases in small doses as long as it does not go beyond the inhibition threshold. When the oxygen uptake rate or residual organic concentration reaches a steady state condition, it can be assumed that acclimation of the biomass is complete[30,35].

Bioinhibition

There is a threshold concentration at which organics inhibit the digestion of organism in the activated sludge. In most cases, it is hard to determine this concentration. Sludge and composition of waste affect the inhibition. So, each system has its own inhibition threshold concentration[35].

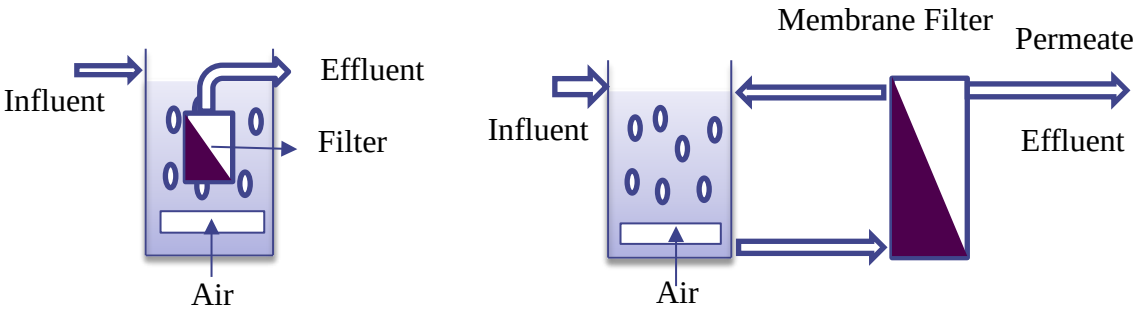

Figure 2.5 Submerged (left) and external (right) configurations[30]

Activated Sludge Quality

Mainly there are 3 different sludge characteristics, which are shown in Figure 2.4. Non-bulking has the optimum quality. Pin-point formation is seen at low F/M, which results in

high effluent TSS. Biomass bulking may be the result of insufficient mixed liquor dissolved oxygen, insufficient nutrient or low F/M ratio in the case of readily degradable wastewater[35].

2.1.1.3 Configurations

There have been many different membrane bioreactor configurations, which can be categorized according to process, type of membrane position, and type of removal and biocatalyst, etc. Internal (submerged or integrated) and external (recirculated or side-stream) MBRs are the two main configurations used today.

Internal (Submerged) / External (Sidestream)

Membrane module is placed in a biological tank at submerged (immersed) MBR (Figure 2.5). Activated sludge is located at the outside of the module. Shearing is created by aeration system at the outside of the membrane surface. Suction is the driving force in this process. For hollow fiber membrane modules, typically the permeate flows from outside to inside of the membrane module. Generally, hollow fiber and flat sheet membrane types are suitable for this process[30]. Internal bioreactor has some advantages compared to external bioreactor: low maintenance requirements, prevention of shear stress, sufficient oxygen supply, constant operating conditions, no additional investment costs, ease of sterilization, and low risk of contamination[37].

Biological tank is separated from membrane unit in external MBR. Driven force could be suction or pressure depending on permeate flow direction either from outside to inside or

from inside to outside[20]. External bioreactor has some advantages over internal bioreactors: fouling control, ease of replacement, and short mean residence time[37].

Aerobic/Anaerobic

If the microorganisms use air for degradation, it is regarded as aerobic/oxic. Anaerobic reactors are cost efficient. However, fouling can be severe for anaerobic systems compared to aerobic systems due to lack of aeration, which creates shear stress on membrane surface.

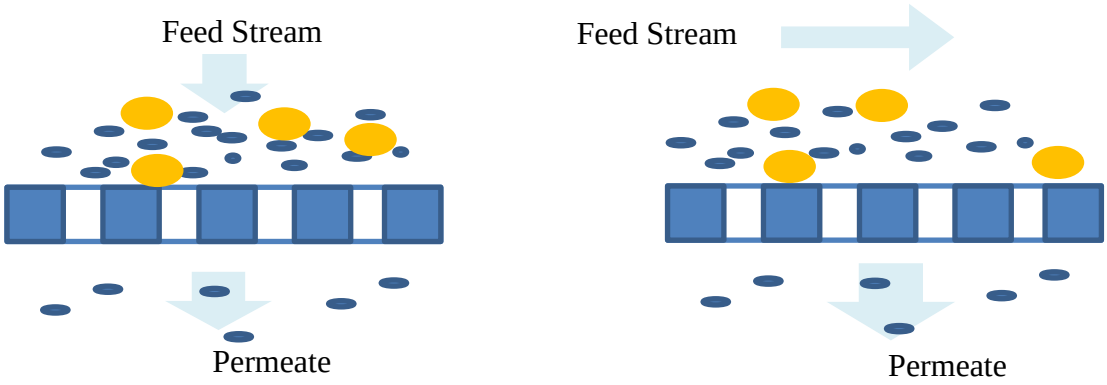

Figure 2.6 Dead-end filtration (left) vs. Tangential flow filtration (right)[38,39]

Moreover, different configurations are available especially for nitrogen removal. MBR configuration may include two-stage processes or four-stage processes like oxic/anoxic following subsequently. Also MBR could be designed in order to remove both nitrogen and phosphorus, which may have three or five stages[30].

Novel MBRs

Novel MBR configurations are more attractive nowadays but they are still at the stage of research. So, industrial applications of novel MBRs still need more development. Here are some of the novel membrane bioreactor configurations: hybrid biofilm MBR (HFMBR)[40], vertical submerged MBR[41], submerged rotating MBR[42], MBR with reverse osmosis[43], air-

sparging MBR[44], membrane distillation bioreactor[45], jet loop MBR[46], anaerobic ammonium oxidation (Anammox) MBR[47], fungi MBR, and membrane coagulation/adsorption bioreactor[48].

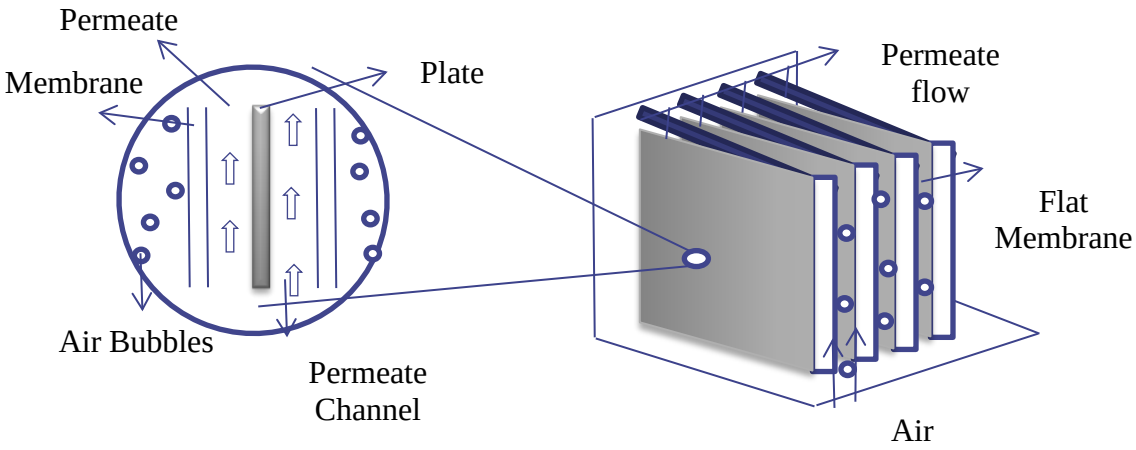

Figure 2.7 Flat-sheet plates[30]

2.1.1.4 Membrane Modules

Deposition modes known as filtration styles i.e. dead-end (direct) and tangential (cross flow or suspension) (Figure 2.6) are important two terms. In dead-end filtration contaminants are gathered on the surface, which may result in more fouling and damaging. The fouling clogs the membrane until filtration eventually stops. In tangential filtration, which involves the recirculation of retentate across the surface of the membrane, cross flow minimizes membrane fouling. Because the material stays safely in the solution, cross flow provides higher product recovery[38,39].

Membrane material has to be packed into a working unit. Module is defined as the smallest unit, which the membrane is packed into.

Plate and Frame

Plate and frame membrane module was the 1st large-scale membrane system where the membranes are settled one below another (Figure 2.7). There is a spacer between these membranes forming feed flow channel[39]. There is a large membrane area per unit volume in this type of the module. It is possible to clean and maintain the constant flux in plate and frame membrane. Operating costs are relatively high[30].

Tubular

Tubular membrane system is located in the porous stainless steel or plastic tube. Filtration takes place from inside to outside of the membrane tube. This type of module is very advantageous in terms of maintenance. However, it has relatively high investment and operating cost[39].

Hollow Fiber

Hollow fiber membranes are asymmetric in structure where hollow fibers are accumulated in a module with one side free at the end. Effluent can be fed either inside or outside of the fiber. The biggest benefit of this module is to have large membrane surface area to volume ratio. Therefore, hollow fiber modules are relatively smaller than others[39].

Spiral-wound

Spiral wound system is a rolled up plate and frame module. There are several different spiral wound module designs depending on the feed and permeate flow paths. Spiral wound is the most compressed, cheap design among the modules and commonly used with spacers in RO and UF applications. A permeate spacer is settled between two membranes. In order to form

a membrane envelope, three edges are attached together. The fluid is fed lengthwise along the unit, while filtration is forced through the membrane sheets into the permeate channel[39].

2.1.2 Fouling

Typically, fouling is defined as accumulation, attachment, or adsorption of foulant onto the membrane surface or into the membrane, decreasing the membrane performance over time[48]. Fouling is the main problem in MBR applications. Complex nature of foulants and sludge is the main reason that makes fouling hard to understand[8,49]. Despite the fact that fouling is inevitable, it can be controlled if the responsible substances and mechanisms are taken into account.

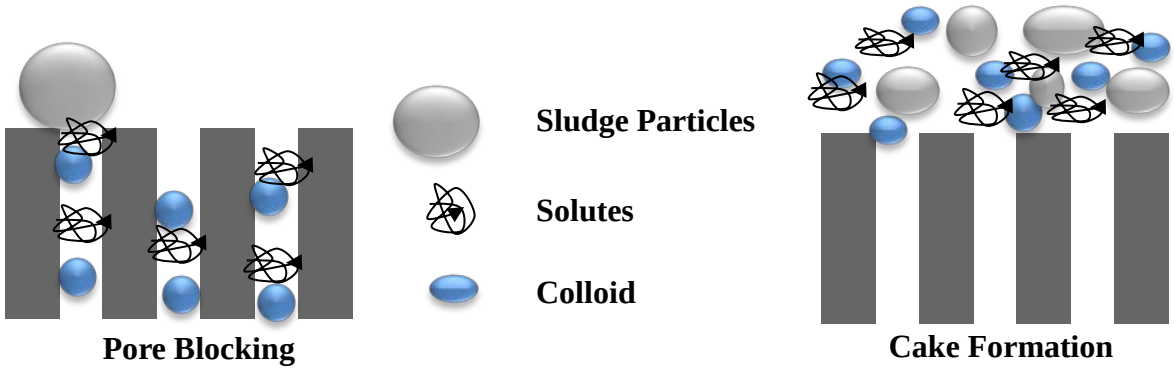

Figure 2.8 Fouling processes in MBR[8,49]

2.1.2.1 Nature and Key Influences

There are four mechanisms that can lead to fouling[8,50]:

- **Adsorption of particles within/on membrane:** Specific interaction occurs between the membrane and particles. A monolayer of particles, which can increase the hydraulic resistance, occur on the membrane even in low or no flux.

- **Deposition of particles on membrane surface:** Particles are deposited step by step on the membrane surface, which is known as cake layer (Figure 2.8).

- **Pore blockage:** Since particles may clog, even partially, the pores in the membrane, flux is decreased with time.

- **Gel formation:** Due to concentration polarization, certain macromolecules may lead to a gel formation in the immediate vicinity of the membrane surface.

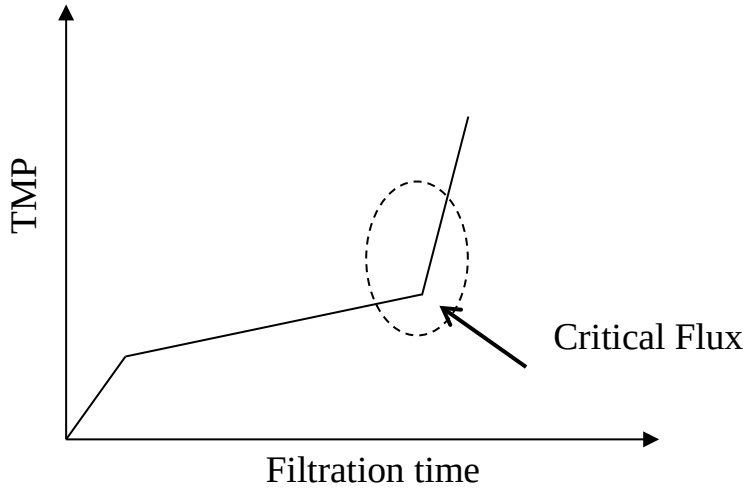

Figure 2.9 Typical stages of fouling[8]

Since the complex nature of activated sludge, fouling behavior for MBR is quite different from other membranes. Typically, fouling can be divided into three stages[51] (Figure 2.9):

- Stage 1: TMP increases rapidly at first, due to conditioning (short term)

- Stage 2: TMP increases slowly (long term)

- Stage 3: An immediate increase occurs in dTMP/dt, also known as TMP jump.

Concentration Polarization

Concentration polarization process, which takes place in all membranes, is another contributor to flux decline. In membrane separation process, some particles will permeate through the membrane while the others are retained. When retained components are accumulated on the feed side of the membrane surface, a concentration difference occurs. This filtration process will result in accumulation of the retained particles and depletion of permeated particles in the boundary layer, which is close to the surface of the membrane. This concentration difference will lead to precipitation and decrease in flux[52]. Also concentration polarization will create a back diffusion force from the boundary layer into the bulk[50].

2.1.2.2 Foulants

Foulants practically can be classified into 4 categories[50]:

- Particulates
- Organic precipitates: macromolecules, biological substances, etc.
- Inorganic precipitates: metal hydroxides, calcium salts, etc.
- Colloids

Large suspended solids may foul the membranes and create the cake layer. Small colloidal particles also can be the reason of fouling layers. Macromolecules can form gel or cake layer on the membrane. Small molecules have strong interaction with the membrane compared to

big molecules. So, they have more tendencies for adsorption. Moreover, if pH or concentration changes, precipitation of salts and hydroxides may occur. Extracellular polymer and bacteria growth may occur on the membrane surface called biological foulant[50].

2.1.2.3 Fouling Types

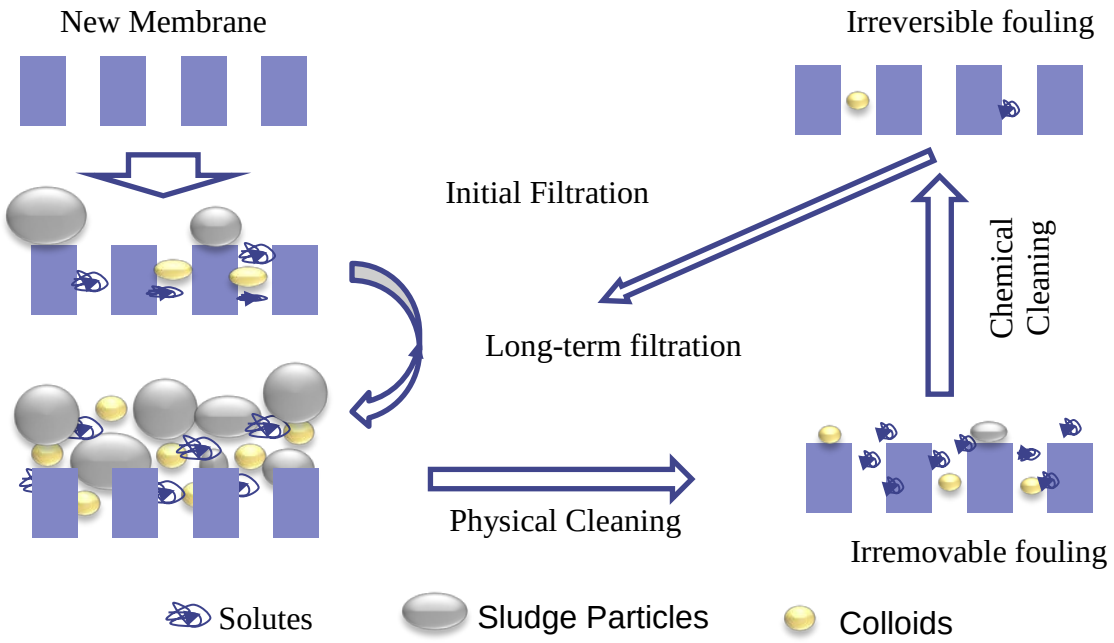

Figure 2.10 Schematic illustration of removable, irremovable and irreversible fouling[8]

Removable, Irremovable and Irreversible Fouling

There are different types of fouling in terms of recoverability (Figure 2.10). There are different definitions in the literature. Traditionally, removable (reversible) fouling means that it can be removed by physical means such as backwashing or relaxation under cross flow conditions. Loosely attached foulants result in removable fouling while pore blocking and strongly attached foulants result in irremovable fouling, which can be recovered by chemical

cleaning. Irreversible fouling refers to fouling that cannot be removed by any approach including chemical cleaning[8].

Control and investigation of irremovable fouling has great importance for long term and stable treatment processes.

Biofouling, organic fouling, and inorganic fouling

Fouling can be classified into three categories in terms of fouling components: biofouling, organic fouling and inorganic fouling. Biofouling can be defined as growth and deposition of bacteria cells or flocs on the membrane's surface. Biofouling may be the biggest concern for MF and UF because foulants in MBR are generally bigger than pores size of the membrane. When individual cells or cell clusters are deposited on the surface, biocake layer is formed. The biocake layer can be investigated by some techniques like scanning electron microscopy, atomic force microscopy, and direct observation through the membrane[8].

Organic fouling can be defined as the deposition of biopolymers such as proteins and polysaccharides onto the membrane's surface. Since biopolymers have smaller pore size, they can be easily deposited onto the surface[19]. Chemical and biological precipitations are the two means for forming inorganic fouling. Bioreactor systems can have huge number of cations and anions such as Ca^{2+}, Mg^{2+}, Al^{3+}, Fe^{3+}, CO_3^{2-}. If the concentration of chemicals surpasses the saturation concentration, chemical precipitation occurs. Biofouling and inorganic fouling are accepted as the main reason for membrane fouling[8].

2.1.2.4 Dynamic Membranes

Dynamic membrane formation, which was first investigated at Oak Ridge Laboratories in 1965 and reported by Marcinko et al in 1966, is another important phenomenon in MBRs. It could be formed by organic or inorganic materials. Briefly, it is defined as the newly formed membrane on top the original membrane[8].

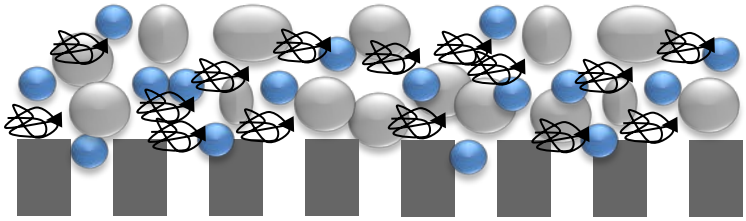

Figure 2.11 Formation of the dynamic membrane[8]

Dynamic membranes can be classified into two categories: precoated and self-forming. If a solution is passed through a porous support, precoated dynamic membrane can be fabricated. Self-forming dynamic membranes can be created by the particles in the solution, which is supposed to be filtered through the membrane. Self-forming dynamic membranes are directly related to MBR since biocake layer is a kind of self-formed dynamic membrane. In MBR, dynamic membrane including large sludge particles will be formed with time. Lee et al. (2001) reported that dynamic membrane protects the membrane surface like a barrier and prevents pores from being fouled. Besides, dynamic membranes behave as 2nd membrane, which improves the performance of the bioreactor (Figure 2.11). Removal efficiency depends on density, structure and components of the biocake layer[49].

2.1.2.5 Control of Fouling

Since fouling increases cost of the treatment, fouling control is crucial in water treatment plants. There have been several approaches to reduce or prevent the fouling. These can be categorized into two main categories: direct and indirect methods. Use of turbulence, pulse or reverse flow, using rotating or vibrating membranes, use of stirred cell with rotating blades close to the membrane, ultrasonic enhancement, chemical cleaning, hydraulic cleaning, mechanical cleaning, periodic backwash, and formation of a dynamic membrane layer are the some direct methods. Treatment of membrane's surface, preparation of more hydrophilic membranes, and optimizing wastewater processing may reduce the fouling indirectly[50]. Some of the fouling prevention and reducing techniques are discussed briefly below.

Air Scouring

Scouring is governed by the aeration which creates a shear stress on the membrane surface. Also scouring decreases cake formation. Aeration intensity should be optimum because excessive aeration may damage the membrane, and reduce the membrane's overall life. There are several different aeration flow rate types such as intermittent. If enough air scouring is not provided, localized dewatering (clogging, sludging, and plugging) may occur due to the fact that concentrated solids accumulate on the membrane surface[30].

Relaxation

Relaxation can be defined as the temporary pausing or stopping the membrane filtration. During relaxation, loosely attached foulants may leave from the membrane surface leading to flux increase[5]. However, the effect of relaxation is not significant compared to air scouring[30].

Adsorbent and Coagulant Addition

Powdered activated carbon, aluminum chloride, and ferric chloride are examples of the materials that reduce fouling, which means the improvement of the separation performance. Adsorbents and coagulants may increase flux. Adding extra chemicals to the wastewater is the worst part of this fouling control method[5]. Some chemicals may be added not only for reducing fouling but also for increasing removal of some specific materials in the wastewater. The most important parameter is the quantity of the adsorbent or coagulant[30].

Backwash Cleaning

It is also known as backflushing or backpulsing. Generally treated water is pumped in the reverse direction of permeate flow. Backwash liquid may include some chemicals in order to improve cleaning and fouling control. Efficiency of backwash process, which is a physical cleaning, depends on frequency, duration, and intensity[30].

Chemical Cleaning

It is also known as chemically enhanced backwash, regenerated cleaning, intensive cleaning and CIP (clean in place). Chemical cleaning is applied when any type of cleaning is not able to recover fouling. So, it is critical for long term operation. Generally sodium hypochlorite is used for removal of organic foulants, citric acid or oxalic acid is used for removal of inorganic foulants. Also some mineral acids, or caustic are required for stable chemical cleaning. The solution is charged in the reverse direction for a determined time. Process is longer than 2 hours and conducted in the absence of activated sludge. Typically intensive cleaning is applied every six months[30].

Mechanical Cleaning

Mechanical cleaning refers to cleaning by hand or spraying down with water. When other methods are not sufficient to remove debris or dewatered solids, mechanical cleaning could be applied. Mechanical limits should be considered in order not to break or damage the membrane. Manual cleaning, hand cleaning, or physical cleaning are referred as mechanical cleaning[30].

Innovative Cures for Fouling

Novel cures emerged recently: using new additives and carriers[53], sludge granulation[54],and membrane surface modification[55] are the some of the innovative cures for fouling. Moreover, some conventional techniques are optimized for fouling prevention[56].

2.2 Membrane Separation

Biological or natural membranes exist for centuries. On the other hand, synthetic membranes started to be used in applications nearly a hundred years ago. Nowadays membranes have been utilized for many applications such as separating gas and vapors, producing drinkable water from seas, and treating industrial wastewaters. Membranes are also used in energy applications such as li-ion batteries, fuel cells, solar cells and hydrogen storage. Another important usage of membranes is biomedical applications such as drug delivery systems, artificial organs, sensors and diagnostic devices[52].

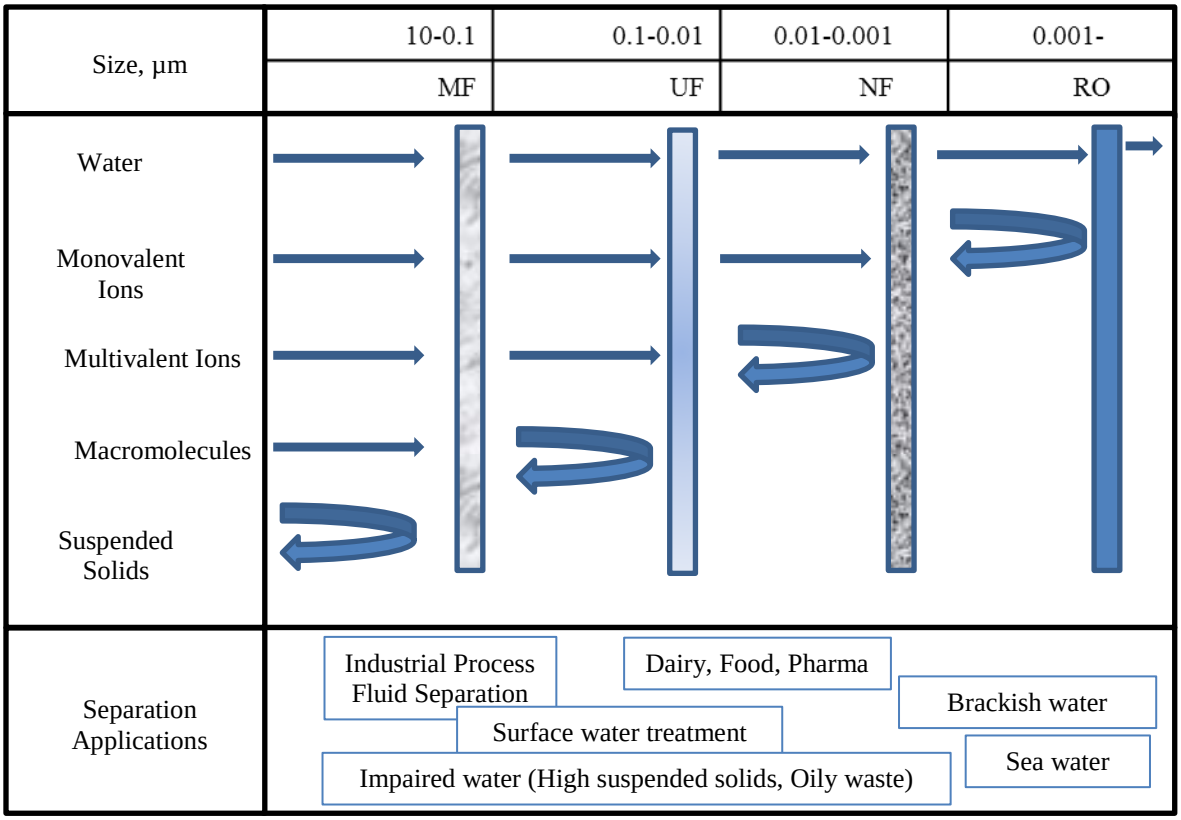

Figure 2.12 Functions of filtration processes[39]

Membrane is defined as a barrier which separates two phases and limits the transport of various materials in a selective matter. It can be driven by pressure, concentration, temperature, and electrical charge. Membranes can be thick/thin (may differ from 100 microns to nanometers), liquid/solid, symmetric/asymmetric, natural/synthetic, neutral/charged, and homogenous/heterogeneous[57]. Working mechanism of the membrane, which is called sieving, can be explained as follows: the pores on the surface form a barrier to impurities while allowing water molecules to pass. If the approaching particle has a diameter less than the pore diameter, the particle goes through the pore[39,58]. Membrane filtration process can be defined as a pressure or vacuum driven separation process in which

particulate matter larger than the medium's pore size is rejected by an engineered barrier primarily through a size exclusion mechanism[59–62].

Table 2.1 Commercial membranes[30]

Manufacturer	Type	Material	Nominal Pore Size (μm)	Filtration Type
GE	Submerged Hollow Fiber	Supported PVDF	0.04	UF
Siemens	Submerged Hollow Fiber	Unsupported PVDF	0.04	UF
Kubota	Submerged Flat Sheet	Unsupported Chlorinated PE	0.4	MF
Mitsubishi	Submerged Hollow Fiber	Unsupported PE	0.4	MF
Mitsubishi	Submerged Hollow Fiber	Supported PVDF	0.4	MF
Toray	Submerged Flat Sheet	Supported PVDF	0.08	MF
Koch	Submerged Hollow Fiber	Supported Polyethersulfone	0.05	UF
Dow	Submerged Hollow Fiber	Unsupported PVDF	0.1	MF
Norit	Tubular	Supported PVDF	0.03	UF
Huber	Submerged rotating flat sheet	Unsupported Polyethersulfone	0.04	UF
Pall	Submerged Hollow Fiber	Unsupported PVDF	0.1	MF

Technical usage of commercial scale membranes started five decades ago. In 1962 cellulose acetate based reverse osmosis membranes were developed. This was an important progress for gaining potable water from seas. It was produced as flat sheets then installed in spiral wound module. After that, membrane modules such as plate and frame, spiral wound, and capillary were constructed for various applications[52].

Microfiltration, ultrafiltration, nanofiltration, reverse osmosis and desalination are the typical types of pressure driven membrane processes[52]. In pressure driven filtration processes, solution with particles pass through the membrane. Larger particles are retained as retentate

while smaller particles pass through the barrier. These membranes are based on retentate dimension and pore size[39]. Functions of the processes are shown in Figure 2.12.

2.2.1 Membrane Filtration Processes

There are many types of materials for fabrication of membrane such as polymers, ceramics, and metals. Since polymers can meet specific necessities such as mechanical strength and biodegrability, they are the most adaptable material for membrane fabrication. However, since physical and chemical properties of the polymers differ so much, only few of them have commercial status. Generally, pore size of a membrane is the most critical parameter. As seen from the Table 2.1, commercial membranes' pore sizes changes from 0.03 to 0.4 μm.

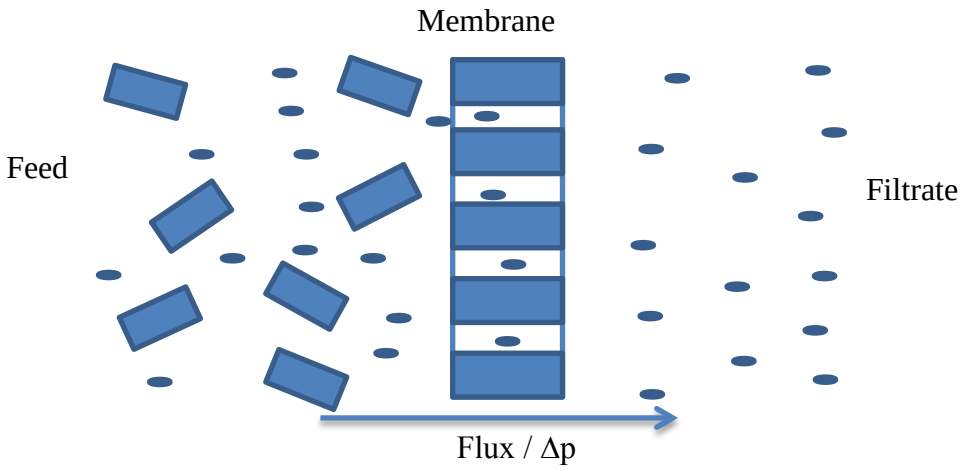

Figure 2.13 Microfiltration principle[52]

2.2.1.1 Microfiltration (MF)

Aerosols, viruses, bacteria, and dusts are removed by microfiltration, which was the first used membrane separation process. Membrane pore size ranges from 0.1 to 10 μm in diameter. Pressure ranges from 0.5 to 3 Bar. This process is suitable for retaining suspensions

and emulsions. Microfiltration (Figure 2.13) is commonly used for prefiltration and sterile filtration[39,52]. Because only larger particles are separated in microfiltration, osmotic pressure and diffusion of particles are so low that they are neglected. Figure 2.13 also depicts symmetric porous membrane, which means the pore size is almost identical over the entire cross-section.

2.2.1.2 Ultrafiltration (UF)

Pore size of the UF membranes is significantly smaller than MF membranes and ranging from 10 to 100 nm. The ultrafiltration is the process between nanofiltration and microfiltration. Typically, macromolecules and colloids are retained from a solution[51]. Retention properties of ultrafiltration are expressed in terms of molecular weight cutoff (MWCO) which is approximately 10,000 to 100,000 datons. This value corresponds to estimated molecular weight (MW) of a solution that is 90% retained by the ultrafiltration membrane. Mass transport is conducted by flux through pores and driving force is pressure like MF. Applied hydrostatic pressure ranges from 1 to 5 bar[52]. The main obstacle for UF processes is fouling of natural organic matter[63].

2.2.1.3 Nanofiltration (NF)

Pore sizes of the NF membranes, where they are used for water softening for two decades[63], are ranging from 1 to 10 nm and MWCO of 1,000 to 100,000 daltons [39]. Due to lower pore size, permeability of NF membranes is lower than UF membranes, but higher than reverse osmosis. Treatment is conducted by two different principles; one is pore sieving, the other is the surface charge. Therefore charged particles or ions can be filtered by nanofiltration

membranes via interaction between charged particles and charged or neutral membrane surface[39,52].

2.2.1.4 Reverse Osmosis (RO)

Even though RO membranes have no distinct pores, pore size of the RO membranes is accepted less than 1nm. Removal depends on a diffusive mechanism. When two solutions with different concentration are separated by a semi-permeable membrane, water flows from higher concentration to a lower concentration. Due to concentration difference, pressure difference called osmotic pressure is generated. In order to reverse the osmotic flow, larger pressure has to be applied to the side which has a lower concentration. Pressure applied to RO process is between 10 and 60 bars. Therefore enough mechanical strength is required[39,52,61].

Production of drinking water from seawater (desalination) is one of most successful applications of RO process[3]. However, RO desalination is not energy efficient. Therefore alternative processes have been studied for replacing RO desalination such as manipulated (forward) osmosis [63].

2.2.2 Theory of Membrane Separation

Membrane separation includes transportation of liquid and particles. Some of the particles will be filtered while some of the particles and liquid will pass through the membrane media during the process. So it would be better to explain the theory step by step. First, fluid

transportation mechanism is discussed. After that liquid filtration theory is explained with and without fouling in detail.

2.2.2.1 Theory Governing Fluid Transport through Membranes

Fluid transport through membrane can be written as[58]:

$$\overrightarrow{N_A} = \rho_A \vec{\vartheta} - D_{AB} \vec{\nabla} \rho_A \tag{2.1}$$

Where, N_A is the mass flux component A through membrane (mass per time per area), ρ_A is the mass density of component A, $\vec{\vartheta}$ is the average velocity of fluid through the membrane, D_{AB} is the effective diffusion coefficient of component A, $\vec{\nabla}\rho_A$ is the mass density gradient

Darcy's Law can be used to express the mass average velocity since pore flow contributes to flux[58]:

$$\vec{\vartheta} = -\frac{K}{\mu}(\overrightarrow{\nabla \rho} - \rho \vec{g}) \tag{2.2}$$

Where, K is the Darcy Law permeability of the medium, μ is the fluid viscosity, $\overrightarrow{\nabla \rho}$ is the pressure gradient, ρ is the solution density, $\vec{g}$ is the gravity vector.

If Eq 2.1 and Eq 2.2 are combined in the –x direction, which typically corresponds to transport direction (perpendicular to membrane surface with neglecting gravity), the following equation is obtained:

$$\overrightarrow{N_{Ax}} = \frac{K\ P_A}{\mu}\frac{dp}{dx} - \mathrm{D_{AB}}\frac{dP_A}{dx} \quad (2.3)$$

1st part of Eq 2.3 corresponds to mass flux because of pressure driven convection through pores. 2nd part corresponds to flux due to diffusion. It can be neglected when compared to convection (pressure driven force). Pressure gradient across the membrane is proportional to the flux for the Eq 2.3. Transmembrane pressure difference, which is the driving force governing transport of liquid through membrane, is the applied pressure difference across the membrane. [58].

2.2.2.2 Modeling Filtration in the Absence of Fouling

Because both microfiltration and ultrafiltration utilize porous membrane, the pore flow model can be used. Darcy's Law explains flux through unfouled membrane where flux is proportional to applied pressure difference[50]:

$$J = P.\left(p_f - p_p\right) = p.\Delta p \quad (2.4)$$

Where, J is volumetric flux, Δp is Transmembrane Pressure (TMP), P is the permeability constant.

Permeability constant depends on membrane characteristics such as pore size distribution, porosity, and viscosity of permeate. In order to describe P, the Carman-Kozeny equation can be applied if the membrane is compared to an arrangement of near-spherical particles (as is the case in ceramic membranes)[50]:

$$J = \frac{\varepsilon^3}{K.\mu.S^2(1-\varepsilon)^2}.\frac{\Delta p}{I_{pore}} \quad (2.5)$$

Where, ε is porosity, μ is dynamic viscosity of the permeate, K is a constant, I_{pore} is the thickness of the porous layer, S is the specific area (surface area per unit volume). Nature of the matter structure determines K and S.

However, when the structure of membrane is accepted as uniform capillaries, which can be formed via track etching, a different method is required. The Hagen- Poiseuille equation can be used not only for uniform capillary structures but also for majority of the membranes. Then, the equation can be expressed as[50]:

$$\mathrm{J} = \frac{\varepsilon.d_{pore}^2}{32.\mu.\tau}.\frac{\Delta p}{I_{pore}} \quad (2.6)$$

Where, τ is the tortuosity of the capillaries, d_{pore} is the diameter of the capillaries, μ is dynamic viscosity of the permeate, I_{pore} is the thickness of the porous layer.

It should be mentioned that viscosity of permeate is inversely proportional to the flux.

Equation 2.6 cannot describe the unfouled membranes' flux because the structure of the membranes is not ideal. In other words, pores are not cylindrical. Moreover, concentration polarization will occur in the presence of solute. Instead of these equations, flux is described as the following equation in the absence of fouling[50]:

$$J = \frac{\Delta p - \Delta \pi}{\mu . R_m} \quad (2.7)$$

Where, R_m is the membrane resistance (empirically measured), $\Delta\pi$ is zero if the feed is pure solvent, and $\Delta p - \Delta \pi$ is the driving force through the membrane. For a given structure, R_m is constant. R_{cp}, resistance of concentration polarization layer, can be added to equation 2.7:

$$J = \frac{\Delta p}{\mu(R_m + R_{cp})} \quad (2.8)$$

Since there is almost no osmotic effect in MF, osmotic effects are not included in the final equation in the absence of fouling[50].

2.2.2.3 Modeling Filtration in the Presence of Fouling

In the presence of fouling, additional terms have to be added to the equation due to accumulation of particles on/in the membrane which is known as fouling. Every type of fouling will affect the flux[50].

Flux of water without particles through the membrane can be expressed by Darcy's Law[64]:

$$J = \frac{\Delta p}{\mu . R_m} \quad (2.9)$$

Where, J is the permeation flux (m^3/m^2s), Δp is the transmembrane pressure (Pa), μ is the viscosity (Pa.s), and R_m is the clean membrane resistance (1/m).

Since fouling is going to take place in the separation process, the permeation flux will always be lower than the flux given by Eq. 2.9. Question is how membrane resistance can be calculated. Pore blocking, concentration polarization, and cake formation are the main contributors to the fouling. So, when all of effecting parameters are taken into account, total membrane resistance can be calculated as[64]:

$$R_t = R_m + R_p + R_c + R_{cp} \tag{2.10}$$

Where, R_m is the membrane resistance, R_p is the pore blocking resistance, R_c is the cake resistance, and R_{cp} is the concentration polarization resistance.

Eq 2.11 can be written as:

$$J = \frac{\Delta p}{\mu . (R_m + R_p + R_c + R_{cp})} \tag{2.11}$$

2.3 Use of Nonwoven Media in Membrane Bioreactors

2.3.1 Introduction

The membrane bioreactor (MBR) process is a wastewater treatment technology that matures over time with good effluent quality and small space requirement at reasonable cost[65–68]. It combines both activated sludge and membrane filtration processes[31]. Evaluating a filtration media depends on permeability, removal efficiency, filtration life (capacity), and filtration cost[69]. With regard to this evaluation, capital cost of the membrane bioreactors is high due to

expensive membrane unit, which is one of the obstacles for the widespread application of MBRs[6,66]. Also, cost for membrane replacement due to membrane failing still remains as long–term cost[70]. From the point of view of cost issues, researchers have considered the use of low-cost filters such as mesh[71–75], and nonwoven fabrics[76–79] as replacements of membrane in MBR applications.

Meshes with coarse pore size (thus better flow) are proposed as an alternative membrane material due to dynamic membrane formation on the surface[80–82]. However, bioreactor operation might be unstable due to high specific cake resistance even in the presence of a thin cake layer[83]. Also, insufficient sludge accumulation may occur in mesh filters[84,85]. Furthermore, biocake fouling in mesh filters can become irreversible due to clogging during long term operation, leading to periodical filter cleaning problems[86,87].

Nonwoven filter medium is a porous web composed of randomly overlapping fibers and whose specific role is to filter the components of a fluid being transported through the medium[88]. Nonwoven fabric filters have been used as support material for membranes frequently[89–95], recently many studies are being conducted where nonwovens are used as biomass carrier and separation medium in MBRs.

Table 2.1 Recent publications on usage of nonwoven media in MBRs

Nonwoven			MBR Design				Reference
Material	Pore size [μm]	Thic kness [mm]	MBR Configuration		Module Type	Driving Force	
PP	5	-	Submerged	Aerobic	Plate/Frame	Suction	Gander et al. (2000)[96]
PP	1.5 , 3 , 5	-	Submerged	Aerobic	Plate/Frame	Suction	Chang et al. (2001)[97]
PET	50-200	-	Submerged	Aerobic	Plate/Frame	Suction	Moghaddam et al.(2002)[98]
PET	10 , 30 , 50	-	Submerged	Aerobic	Tubular	Suction	Chang et al. (2003)[99]
PP	3, 5	-	Submerged	Aerobic	-	Suction	Zhi-Guo et al.(2005)[100]
PP	13.1, 25.2, 38.8	1	Submerged	Aerobic	Tubular	Suction	Chang et al. (2006)[101]
PP	20-30	-	Submerged	Aerobic	Tubular	Suction	Horng et al. (2006)[102]
PP	20	0.6	Submerged	Aerobic	Tubular	Suction	Chang et al. (2007) [103]
PP	12	-	Side-stream	Anaerobic	Plate/Frame	Suction	Ho et al. (2007)[104]
PET	0.64	-	Submerged	Anaerobic	Tubular	Suction	An et al. (2009)[105]
-	0.2, 2, 20	-	Submerged	Aerobic	Plate/Frame	Suction	Horng et al. (2009)[106]
PET	100	4	Submerged	Aerobic	Bag	Gravity	Ren et al. (2010)[107]
PA	0.4	0.12	Submerged	Aerobic	Plate/Frame	Suction	Bjorge et al (2009)[108]
PP	14	0.6	Submerged	Aerobic	Plate/Frame	Suction	Chuang et al. (2011)[109]
PA 6	0.21		Submerged	Aerobic	Plate/Frame	Suction	Bilad et al. (2011[110])
PP	20	0.6	Submerged	Aerobic	Plate/Frame	Suction	Chuang et al. (2011)[111]
PP	100	-	Submerged	Anaerobic -Aerobic	Bag	Gravity	Lee et al. (2012)[112]
PET	100	5	Submerged	Aerobic	Plate/Frame	Suction	Meng et al. (2013)[113]
PET	5, 10	-	Submerged	Aerobic	Bag	Gravity	He at al.(2014)[114]
PE	5, 10	2.3	Submerged	Aerobic	Bag	Gravity	He et al. (2014)[115]
-	38.1	-	Submerged	Aerobic	Plate/Frame	Suction	Wang et al. (2015)[116]

Anammox (anaerobic ammonium oxidation) -a wastewater game-changer is one of the world's most promising wastewater and trade wastewater technologies to replace activated sludge in removing nitrogen[117]. Enhancing retention of microorganisms on a medium increases the removal efficiency in a bioreactor[118]. Since culturing anammox bacteria is a long process, appropriate starter culture must be selected[119]. Fujii et al.(2002), and Liu et al. (2009) demonstrated that nonwoven fabrics keep high biomass retention during anammox process [118,120]. Porous nonwoven fabrics with different forms such as strip[121] and ring[122] are promising materials for starter culture of biomass due to high porosity and cost efficiency[123].

Nonwoven usage as separation medium attracts more attention than nonwoven usage as biomass carrier or support material due to enhanced flux, controllable fiber size, controllable pore size and thickness[12,112]. Many patents were issued on use of nonwoven fabrics in membrane bioreactor in the 2000s[124–130]. In spite of the fact that, dynamic membrane formation(cake layer or secondary membrane) contributes to produce better effluent quality for nonwovens[131], effluents obtained through conventional nonwovens were not as good as effluents from membranes in many MBR studies due to nonwovens' larger pore size[98,100,104,113]. A list of recent publications on use of nonwoven media in membrane bioreactor is shown in Table 2.1.

The scope of the present section is to critically review the literatures of membrane bioreactor where nonwovens are used as a separation medium. The main objective of this review is to identify the factors leading to better nonwoven filtration performances in terms of removal efficiency and flux/fouling behavior.

2.3.2 Performance Comparisons of Nonwoven and Other Separation Media

2.3.2.1 Comparison of Nonwovens and Meshes

Loderer et al. (2013) compared the MBR performances of meshes having 30 and 70 μm pore size and nonwovens having 30 and 70 μm pore size. Meshes showed better fluxes in the first 30 minutes. In a 24-hour period of filtering, nonwoven and mesh showed different filtration behavior. Transmembrane pressure (TMP) increased gradually in the first 16 hours for the nonwoven samples. After that, TMP of the nonwoven systems increased significantly. However, mesh filter showed no noticeable increase in TMP for 21 hours, after the 21st hour TMP had a sharp increase. In other words, filter clogging occurred for mesh filter suddenly (TMP jump) after 21 hours of operation[132].

2.3.2.2 Comparison of Typical Nonwovens and Membranes

Chang et al. (2001) compared the PP nonwovens having 1.5, 3, and 5 μm pore size with 0.3 μm PS membrane. Nonwovens' clean water fluxes were greater than 0.3 μm PS membrane. All membranes exhibited a rapid flux decline at the beginning of the treatment. After 20 days of operation, flux of the nonwovens were between 2 and 8 $lm^{-2}h^{-1}$where the flux of PS membrane was around 10 $lm^{-2}h^{-1}$. Effluent from the PS membrane showed a mean of 7-log reduction in total coliforms (TCs) while nonwovens showed only a 2-4-log reduction in total coliforms, which is quite low compared to PS membrane[97].

Zhi-Guo et al. (2005) compared the 3 and 5 μm PP nonwovens with 0.4 μm hollow fiber membrane. According to the results, there was a little difference in the effluent water quality

between the nonwoven and the membrane. Both nonwovens and hollow membrane bioreactor exhibited a high removal efficiency of COD, TOC on synthetic wastewater treatment with colorless, odorless, and no suspended solid in the effluent water[100].

Nonwoven fabric filter with 100 μm pore size and Polyethylene membrane with 0.25 μm pore size are compared in a bioreactor whose driving force was gravity. Even if the pore size of the nonwoven was 400 times larger than the Polyethylene membrane, SS concentration of the nonwoven was stable and below 2 mg/l where SS concentration of effluent from the membrane was 0.8 mg/l. The average COD concentration of effluent from the nonwoven was 7.5 mg/l where membrane's was 4.9 mg/l[112].

A glass-filled hydrophobic polypropylene membrane with 0.5 μm pore size, a Polysulfone membrane with 0.4 μm pore size and a meltblown polypropylene nonwoven with 5 μm pore size were compared in a submerged MBR treating domestic wastewater by Gander et al. Glass filled PP membrane did not allow a flow through the membrane. The nonwoven's initial flux was 162.5 $lm^{-2}h^{-1}$ while PS membrane's initial flux was 45 $lm^{-2}h^{-1}$. Nonwoven's flux rapidly declined to 8 $lm^{-2}h^{-1}$ in 3 hours where PS membrane's flux declined to 41.75 $lm^{2}h^{-1}$ in 3 hours. This indicates that the nonwoven had a rapid flux decline. After 57 days of operation, membrane cleaning is applied. The PS membrane demonstrated almost complete flux recovery, where the nonwoven showed relatively little flux recovery, indicating a great irremovable fouling for the nonwoven. In other words, flux of PS membrane is readily recoverable compared to the nonwoven. Effluent from PS membrane with 0.4 μm showed a

9-log reduction in total coliforms where the nonwoven with 5 μm showed a 5-log reduction. Both membranes showed very close COD and turbidity removal[96].

2.3.2.3 Comparison of Nanofibrous Nonwovens and Membranes

Bjorge et al. (2009) investigated the feasibility of PA (Polyamide) nanofibrous nonwovens (with and without silver addition) with 0.4 μm mean pore size by comparing with commercial PTFE membranes. Clean water flux of the nanofibrous nonwoven was higher than commercial membranes. Tensile strength of the nanofibrous nonwoven was quite close to the commercial PTFE membrane. However, nanofibrous nonwoven couldn't withstand the vacuum more than 5 days. The nonwoven media showed high fouling so that backwash frequency increased up to 10/hr where backwash frequency of the commercial flat sheet (Kuboto) membrane was 1/hr. Non-functionalized nanofibrous nonwoven's removal efficiency was not satisfactory in terms of water quality. Pathogen removal of functionalized nanofibrous nonwoven was better than the non-functionalized one but it was not as good as commercial membranes. Also nanofibrous nonwoven showed great irreversible fouling which resulted in a rapid decay of the flux. The authors stated that nanofiber nonwovens are not competitive with commercial membranes yet, and suggested further improvements to employ nanofibrous nonwovens in membrane bioreactor[108,133].

Kim et al. (2014) compared the PVDF-PMMA nanofibrous nonwoven (0.45 μm pore size) with the commercial PVDF membrane with the same pore size. Pure water permeability of the nanofibrous nonwoven was higher than the commercial PVDF cast membrane due to the nonwoven's greater porosity. In other words, intrinsic resistance of the nonwoven was lower

than the membrane. Contact angle of nanofibrous nonwoven was smaller than 10°, indicating a great hydrophilic character. Also AFM images demonstrated that the membrane's roughness was greater than nonwoven, which indicates more flux recovery efficiency for the nonwoven. However, significant initial fouling occurred for the nonwoven which is the main drawback for the nanofibrous nonwovens. Removal efficiencies (SS, COD, TN, and TP) were close to each other and both effluents were free from suspended solids[134].

2.3.3 Effects of Nonwoven Properties on Bioreactor Performance

Even if biological step and operating conditions have strongest influence on treatment performance[135],material characteristics such as material type, pore size, shape, pore size distribution, thickness, porosity, hydrophilicity, surface roughness, and surface charge offers flexibilities during preliminary time of the filtration (before cake formation)[136].

2.3.3.1 Nonwoven Structure

Structural elements of nonwovens such as fiber diameter have less effect on separation performance compared to characteristics of nonwovens, since the structural elements determine the nonwoven characteristics such as pore size, and its distribution.

Fiber Diameter

Bilad et al. (2011) produced a series of nanofibrous nonwovens with different fiber diameters (100-500 nm) to investigate the effects of nanofiber diameter. The authors demonstrated that nanofibrous nonwoven's pore size and porosity decreased as fiber size decreased. The results demonstrated that effect of nanofiber diameter on critical flux is insignificant because overall

porosities were close to each other. Hydraulic performances are related to porosity rather than fiber diameter[110].

Porosity

Porosity is the ratio of pore space to bulk material[137]. Since flux is proportional to porosity according to the Hagen-Poiseuille equation, it is more related to transport properties. Also surface porosity is critical since surface porosity may trigger local flux differences[138,139].

Basis Weight

Generally high basis weight gives a thicker nonwoven. According to the Hagen–Poiseuille equation, flux is inversely proportional to the thickness. Bilad et al. (2011) demonstrated that samples with different basis weights resulted in similar pore size and porosity. Only thickness of the nonwoven was changed. The authors showed that basis weight (10, 20, 60 and 100 g/m^2) did not affect critical flux significantly, since flux highly depends on pore characteristics in microfiltration processes[110].

Seo et al. investigated the effect of basis weight on MBR performance. Authors utilized PP nonwoven fabrics with 35, 50, 70 g/m^2. There was not much detailed information about the nonwoven properties such as pore size. In the first 20 min. nonwoven with 35 g/m^2 produced the highest flux where the nonwoven with 70 g/m^2 produced the lowest flux. Also particle size gradually decreased as sludge cake layer is formed for all samples. The lighter nonwoven produced effluent with bigger particles[140].

Pore Connectivity and Tortuosity

Tortuous pore path through the thickness and interconnected pore structure with multiple filtration layers are employed in nonwoven structures[141,142]. According to the Hagen-Poiseuille equation tortuosity is inversely proportional to flux. Ho and Zydney (2006) stated that highly interconnected membranes showed lower rates of flux decline due to lateral flow through alternate pores[143]. Bacchin et al. (2013) investigated the pore connectivity and tortuosity by creating a straight channel, connected channel and staggered formation with the help of pillars. Connected channel represented the pore connectivity where staggered pillars represented both pore connectivity and tortuosity. Rapid internal clogging occurred for staggered pillars where internal clogging stayed to a very low level with straight channel. And filtration efficiencies of connected and straight formation were close to each other and lower than staggered formation[144].

Pore Shape

Typically, pore shapes of nonwovens are more irregular than conventional membranes. Irregularly shaped pores have more selectivity against a round shaped pore with the same area[138]. Chandler and Zydney (2006) studied the effects of membrane pore geometry on fouling behavior. The membrane with slotted pore geometry showed slower flux decline than the membrane with circular pore. The membrane with circular pore shape showed an initial region of pore blockage followed by cake filtration however, the slotted pore membrane's cake layer was located directly over the pore entrance which was significantly more complex. The authors suggested that proper pore shape selection may reduce the fouling[145].

2.3.3.2 Nonwoven Characteristics

Pore Size

Hagen–Poiseuille equation describes the relation between the pore size and flux[146,147].

$$J = \frac{\varepsilon\, r^2}{8\,\mu\,\tau}\frac{\Delta p}{\Delta x} \tag{2.12}$$

Where, J is flux (m^3/m^2s), ε: surface porosity (%), r is pore radius (m), μ is water viscosity (Pas), τ is tortuosity, Δp is Transmembrane pressure (Pa), and Δx is membrane thickness (m).

The Hagen–Poiseuille equation considers pore shape as cylindrical. However, pore shapes are not always cylindrical[146]. According to the Hagen-Poiseuille equation, higher flux is expected when the pore size of the membrane is bigger. However, it is not the case for microfiltration where particles are trapped in the structure and reduce the flux. This is why large pore membranes like MF membranes have higher fouling propensity than UF membranes[32].

Chang et al. (2001) studied the effects of PP nonwoven pore size (1.5, 3, and 5 μm) on MBR performance. According to the results, 5 μm nonwoven gave the highest clean water flux followed by the 3 and 1.5 μm. All the nonwovens showed a very quick flux decline initially. After MBR operation, 1.5 μm nonwoven had the highest filtration resistance followed by the 3 and 5 μm respectively when the resistances were measured just after the MBR operation. Resistance results indicated that 1.5 μm nonwoven exhibited greater internal fouling and

required a more rigorous cleaning regime compared to the other nonwovens. Pore size of the nonwoven had little effect on reduction of total coliforms (TCs), probably due to the formation of a dynamic layer. Removal efficiencies indicated that nonwovens are efficient in treating wastewater[97].

Chang et al. (2003) compared the performances of 3 different PET nonwovens with 10, 30, and 50 µm pore size. Initial permeate flux of 50 µm nonwoven was the highest followed by 10 µm and 30 µm. After 20 days of operation, nonwoven with 30 µm showed insignificant flux reduction compared to the other nonwovens. Authors explained that when the size of the particles in wastewater is close to the membrane pore size, tendency of particle blocking is small[99].

Chang et al. (2006) compared three different nonwoven fabrics with 13.1, 25.2, and 38.8 µm pore size in MBR. COD concentrations were below 100 mg/l for all three nonwovens during 120 days of operation where the wastewater's COD was between 200-1000 mg/l. When the initial flux was set to 0.2 m^3/m^2d (below critical flux), almost constant identical fluxes were observed for all the three nonwovens. But, when the initial fluxes increased over the critical flux value, the lowest permeate flux decline was observed at the nonwoven with 25.2 µm pore size and the highest permeate flux decline was observed at the nonwoven with 13.1 µm pore size. The authors suggested that different mechanisms are led to the nonwoven's different flux decline behavior[101].

Pore Size Distribution

If a particle can penetrate into the membrane, it blocks the pore and reduces the flux. If a particle cannot penetrate into the membrane, it will be deposited on the surface and form a cake layer. Therefore effects of pore size and its distribution highly depend on feed water characteristics such as particle size distribution[33,101].

Pore size distributions of nonwovens are typically wider compared to membranes, which may result in high fouling and high flux decline locally. Also since nonwovens are composed of randomly overlapped fiber, pores may not be distributed homogeneously throughout the surface, which may lead to local fouling and flux differences. So, uniform surface pore distribution and narrow pore size distribution are required[148].

Surface Roughness

Because nonwovens have rougher surface than typical membranes, particles are easily deposited on the filter surface and form a cake layer[148]. Also, large contact area increases the chance of permanent particle fouling by increasing intermolecular forces. Many researchers stated that particles accumulate rough membranes' valleys, resulting in valley clogging which leads to more severe flux decline according to smooth membranes[138,149–151]. Therefore, antifouling property can be improved by decreasing the roughness[134].

Hydrophilicity

Even though hydrophobic membranes are more resistive against chemical, thermal, and biological conditions, hydrophilic membranes are preferred in filtration applications since they are less prone to organic fouling[152,153]. A hydrophilic membrane forms more hydrogen

bonds with water while a hydrophobic membrane forms no or less hydrogen bonds. When the surface of the membrane forms hydrogen bonds with water, foulants are not able to contact with the membrane's surface directly. Therefore foulants will have less area to attach on the surface. So that hydrophobic membranes have large tendency to foul especially for organic compounds[147]. In other words, rate of flux decline for hydrophobic membrane is greater than hydrophilic membrane[154].

Many attempts have been made to reduce fouling by modifying the surface with hydrophilic and functional polymers[155,156]. Yoon et al (2006) fabricated a high flux ultrafiltration membrane containing a thin layer of hydrophilic and water resistant chitosan coating, PAN nanofibrous web as mid-layer support, and PET nonwoven as substrate[157]. Zhang et al. (2007) modified polypropylene nonwoven fabric by dipping method to immobilize PVA on the surface. According to the results; antifouling property of modified nonwoven was improved, modified nonwoven had smaller flux decline in the treatment of pharmaceutical wastewater by MBR, and the modified nonwoven had lower fouling resistance compared to original the nonwoven fabric[158].Wang et al.(2009) modified the PP nonwoven by adsorption and cross-linking PVA-g-4VP (Vinyl pyridine) copolymer on both its outer and inner surface. The results demonstrated that modified nonwoven had hydrophilic and strong antifouling properties[159]. Wang et al. (2010) coated the both internal and external surface of the nonwoven fabric (0.5 μm pore size) by chitosan to prepare a high flux and antifouling membrane. The original nonwoven showed the highest loss of flux within the filtration time, because chitosan coating prevented foulants to deposit on the nonwoven surface. Also, the

results indicated that the chitosan modified membrane reduced the irreversible fouling. The permeate turbidity of all nonwovens were below 0.3 NTU, and SS concentrations were out of the lowest detection limit over the entire operation period[160]. He et al. (2014) reported the feasibility of diatomite/iron oxide modified PE nonwoven fabric in MBR application. Contact angle of untreated PE nonwoven was 122.66° where modified nonwoven's was 39.33°, indicating that modified nonwoven is more hydrophilic. The results showed that original nonwoven had shorter operation period, lower critical flux, and higher operation TMP[115]. In another study, He at al. (2016) firstly coated nonwoven surface with diatomite in order to enhance the retention capacity. Contact angle of modified nonwoven was 53.83° while original nonwoven's contact angle was 112.71°, which means that hydrophilic character was improved. Secondly, PVA modification was performed to improve hydrophilicity. Effluent produced via modified nonwoven had lower turbidity, higher removal efficiency of COD and nutrients. In other words, effluent of modified nonwoven had better water quality.Also, at 45^{th} - 51^{st} day, the original nonwoven's TMP increased significantly while modified nonwoven's TMP was stable throughout the filtration, indicating that the modified nonwoven had better antifouling behavior[114].

Surface Charge

Nonwovens' surface charge could be more useful than membranes since nonwovens have more specific surface area due to small fiber size. Surface charge is committed when a material came across with an aqueous solution by forming electrical double layer. Potential at the surface of shear between the charged surface and the solution is called zeta (ζ) or electro-kinetic potential[161]. An interaction occurs between membrane surface and nanoparticles due

to charge effects. Similar charges attract while opposite charges repulse. Ionic strength and pH have significant effect on colloidal fouling. Generally, membrane surface is negatively charged in order to increase the rejection of dissolved salts and minimize adsorption of negatively charged organic foulants and microorganisms[138,147].

2.3.4 Effects of Operating Conditions

2.3.4.1 MBR Configuration

Seo et al. (2007) compared the flat and tubular module where nonwovens are utilized as a separation medium in an aerobic reactor. Filtration pressures of the two modules were close to each other during the operation period where the initial fluxes were 0.5 and 1.11 m/d. But the pressures showed different patterns when the fluxes were increased to 1.73 m/d for the two modules. After 27 days of operation, tubular type module's filtration pressure was under 5 kPa, while flat type module's increased to 16 kPa rapidly. The authors compared two tubular module configurations as well where modules installed vertically and horizontally separately. The filtration pressure of the vertically installed module increased faster which might be due to hydraulic head loss inside the tube. Also the horizontal module demonstrated a relatively even distribution of cake layer while the vertically installed module had more sludge accumulation on the tip than the center at the end of the operation. Shape and particle size of the sludge particles were not different notably[162].

Daels et al. (2010) investigated the possible use of nanofibrous nonwovens in bioreactors at three different settings. Application of a flat sheet nanofibrous nonwoven in a typical MBR (AS-MBR) was the first configuration. Effect of dosing polymer (MPE50) on fouling was the

second. And the third one was the application of nanofibrous nonwoven in a trickling filter membrane bioreactor (TF-MBR). Material used was Polyamide 6 nanofibrous nonwoven with 0.4 µm pore size. Backwashing frequency at the AS-MBR was 2/hr due to high fouling while backwash frequency in trickling filter decreased to 1/hr since trickling removed some suspended solids. Also trickling filter MBR showed more stable and higher flux compared to other setups. The best removal efficiency was in the typical MBR with 99% turbidity, 99% TSS, and 94% COD. Only total nitrogen (NH_4^+ + NO_3^-) removal was not satisfying due to incomplete denitrification. For the typical MBR with the MPE50, the overall results were worse than the other two setups. The tests showed that the nanofibrous nonwoven is not competitive with the currently applied commercial membrane due to severe irreversible fouling. The authors recommended to use pre-filter and optimization of nanofibrous nonwoven structure for the application of nanofibrous membranes in MBR[163].

2.3.4.2 Aeration

Effects of aeration on nonwoven fouling have not been understood yet. High aeration intensity may reduce fouling, however flocs may be broken at the same time[8,164–166]. Chuang et al. (2011) reported that as aeration intensity increased, flux was declined more due to sharp turbulence and high shear force on the nonwoven's surface[111]. However Chang et al (2007) demonstrated that the lowest filtration resistance could be obtained by optimum aeration intensity. In other words, the filtration resistance was reduced as aeration intensity increased until a specific intensity, after that point the filtration resistance increased due to the floc breakage[103].

2.3.4.3 Influent Particle Size

Chuang et al. (2011) investigated the single-particle size effect on submerged nonwoven bioreactor. TiO_2 particles with 0.2-0.4 μm, 1-2 μm and 43 μm particle sizes were filtered separately via meltblown nonwoven with 20 μm pore size. The flux reductions were lower than 1% in 0.2-0.4 and 1-2 μm particles while the flux reduction was only 3.4% for 43 μm particle size in 6 hours. According to the flux decline results, small particles (0.2-0.4 and 1-2 μm) escaped from the nonwoven continuously indicating that cake layer was not formed. The authors stated that mixed particle conditions are useful for building cake layer (dynamic membrane) in nonwovens[111].

2.3.4.4 Other Operating Conditions

Chemical cleaning is more effective than flushing nonwoven surface with tap water in terms of flux recovery[100]. Chang et al. (2001) compared the air and water backwashing processes. After 30 days of operation, final flux of the nonwoven was higher when air backwashing was applied. The water backwash almost had no effect on recovering fouled nonwoven's flux. Also the results demonstrated that backwashing efficiency was free from nonwoven's pore size. Consequently, the authors indicated that air backwashing was more efficient than water backwashing[99].

Lee et al. (2012) found that the effect of MLSS concentration on filtration resistance was not considerable at the initial fluxes for nonwovens. However, the resistance increased with increasing MLSS concentration at higher fluxes[112]. Chang et al. (2007) demonstrated that the effect of MLSS concentration was not influential below 0.8 m^3/m^2s[103].

Chuang et al. (2011) investigated the effect of SRT on fouling behavior of nonwoven fabrics. There was no significant fouling in nonwoven during 1-77h filtration with SRT of 15 days. However, the non-fouling phase duration for SRT of 30 and 60 days were 31 and 13 hours respectively. Both reversible and irreversible fouling generated for nonwoven with different SRTs. The results showed that fouling and flux behavior were highly affected by SRT[109]. Also, Horng et al. (2006) demonstrated that suspended solid removal efficiency increases as hydraulic retention time (HRT) increases[102].

2.3.5 Fouling in Nonwovens

Nonwoven fabrics show a great internal fouling since typically pore size of the nonwovens are greater than MF membranes[97,100]. Due to overlapping fiber structure, different fouling behavior is expected from nonwovens compared to typical membranes. Severe fouling due to pore blockage may occur when pore size of the material is bigger than particle size[32]. At initial stage of fouling, flux decreases quickly because fouling resistance increases quickly due to deposition of particles on nonwoven's surface, pore absorption and clogging. Filtration is unstable at this initial stage. After a long time, cake layer forms on the surface due to more accumulation of particles. At this stable stage, fouling resistance increases slowly and flux decline is slow[64]. Pore size of the nonwoven decreases rapidly after being in touch with the activated sludge, which made the fabric into a relatively thick membrane[107]. In addition, Horng et al. (2009) reported that cake formation is the dominant mechanism leading to fouling compared to pore narrowing and pore blocking[106].

Gander et al. (2000) demonstrated that flux of a membrane is more readily recoverable with mechanical and chemical cleaning compared to a nonwoven. In other words, it is very difficult to remove the internal fouling of a nonwoven with cleaning[96].

An et al. (2009) investigated foulants in an anaerobic nonwoven bioreactor by several techniques such as GFC(Gel permeation chromatography), FT-IR, and SEM. EPS cut out from the fouling layer of nonwoven had broader molecular weight distributions and larger molecular weight compared to the membrane effluent and wastewater influent. Protein and clay materials were the major components of the nonwoven's fouling layer. Also SEM and EDX analyses showed that organic substances and inorganic elements such as Mg, Al, Ca formed the cake layer of the nonwoven[105]. Ren at al. (2010) detected bacterial colonies and excessive presence of organic matter in the cake layer of the nonwoven[107].

2.3.5.1 Nonwoven Fouling Analysis

Degree of nonwoven fouling can be quantified by the resistance-in-series model[109,167]:

$$R_t = \frac{\Delta p}{\vartheta . \mathrm{J}_{mbr}} \tag{2.13}$$

$$R_t = \mathrm{R_m} + \mathrm{R_c} + \mathrm{R_f} \tag{2.14}$$

Where J_{mbr} is permeation flux (m^3/m^2s); Δp is the transnonwoven pressure (Pa); ϑ is the viscosity of the permeate (Pa.s); R_t is the total filtration resistance (m^{-1}); $\mathrm{R_m}$ is the intrinsic

nonwoven resistance (m^{-1}), R_c is the cake layer resistance (m^{-1}), and R_f is the fouling resistance due to pore blocking and adsorption (m^{-1})

R_m ,R_c and R_f can be calculated using the following equations:

$$R_m = \frac{\Delta\rho}{\vartheta . J_w} \quad (2.15)$$

$$R_f = \frac{\Delta\rho}{\vartheta . J_{w'}} - R_m \quad (2.16)$$

$$R_c = \frac{\Delta\rho}{\vartheta . J_{AS}} - R_m - R_f \quad (2.17)$$

Where, J_w is initial clean water flux, $J_{w'}$ is the final water flux after removing cake layer, and J_{AS} is the flux of the MBR at steady state.

2.3.5.2 Nonwoven Fouling Control

There have been several conventional methods such as influent pretreatment[168,169], air scouring[170,171], relaxation[172,173], adsorbent[174,175] and coagulant addition[176,177], backwash cleaning[44,178], and chemical cleaning[179] in MBR that can be used to control nonwoven fouling. For a successful fouling control fluid mechanics (shear stress), sludge properties (particle size, extracellular polymeric substance, surface charge), module design, membrane material (hydrophobicity, roughness, pore size, packing density), and operating conditions (pH, HRT, SRT, backwash cycle, F/M) should be taken into account[180].

Controlling fouling via designing nonwovens could be more effective than controlling fouling with other techniques such as hydraulic parameters, because nonwovens had a great internal fouling potential, which is mostly irreversible due to depth filter structure. If the particles are captured before entering the nonwoven structure, irreversible fouling could be reduced. So, designing nonwovens as surface filter instead of depth filter is expected to reduce the fouling. Calendering process, which is a widespread bonding technique in textile industry, is a mean to produce surface filter structure from depth filter structure. Nonwoven web is passed between rollers at determined pressure and temperature in the calendering process where nonwoven characteristics such as thickness, pore size, pore size distribution, surface roughness, tensile properties, clean water flux, and solid volume fraction is controlled[181–184]. Calendering process may lead to reduced valley clogging on the nonwoven surface since it makes the nonwoven's surface smoother. Also narrowing pore size distribution and decreasing average pore size of the nonwoven by calendering process may result in less internal fouling.

Another important nonwoven fouling control technique is surface modification. Nonwovens are typically made of relatively hydrophobic polymers, leading to high fouling due to adsorption of particles, especially in case of organics such as proteins. Modifying nonwoven's surface results in less flux decline throughout the treatment process.

2.4 Summary

Nonwovens are unique materials for support layer use for conventional membranes due to high strength, low cost, and high flux. Recently, researchers started to use nonwovens as

biomass carrier due to nonwovens' superior properties such as high porosity, high strength, and rough surface. However, the most challenging application of nonwovens in water filtration is to use biomass separation medium.

This section reviewed the existing literature of membrane bioreactor where nonwovens were utilized as separation media. Although many progresses have been made for using nonwoven filters in MBR, nonwoven based MBR is still under development, and are not competitive with membranes yet according to the studies. The reasons why nonwovens cannot compete with typical membranes are relatively bigger pore size, wide pore size distribution, depth filter structure with tortuous pore path, and rough surface. Even if dynamic membrane (cake layer) formation contributes to increase removal efficiency, water quality of the effluent from conventional nonwovens is not as good as the effluent from commercial membranes due to nonwovens' coarse pore. Also pore size distributions of conventional nonwovens are wider than commercial membranes, which may result in severe fouling with regard to effluent particle size. This is because particles, smaller than nonwoven's pore size, are trapped within the structure due to sieving mechanism. If nonwovens are used as depth filter, particles will likely clog the structure. Furthermore, depth filter structure and tortuous pore path through the thickness lead to fast internal fouling which is mostly irreversible. Also, rough surface of conventional nonwovens may result in valley clogging on the surface. It is found out that majority of the fouling of a nonwoven media is due to cake formation.

Nonwoven's structural elements do not affect the MBR performance directly. However, those structure properties should be engineered to meet the specifications for low fouling.

With this point of view, designing the material, in addition to operating conditions, is the key point to produce low fouling nonwovens. Among the nonwoven properties, pore characteristics are likely the most important parameter affecting the MBR performance with respect to size-exclusive filtration. Besides, operating parameters always should be optimized to reach the best performance of nonwovens.

Design and production of nonwovens with given pore size is gaining importance in order to meet water quality requirements. Studies about the factors affecting the MBR performances can provide new and valuable insights for controlling the fouling and meeting water quality limits. Producing nonwovens in the form of surface filter instead of depth filter could increase removal efficiency and reduce fouling. Moreover, surface modifications have great contributions to reduce fouling of the nonwovens. Further investigations are inevitable to produce low fouling nonwovens by different methods.

3. Research Objectives

3.1 Motivation

The ability to design and produce nonwovens with given properties are desirable for many filtration applications such as microfiltration. For size-exclusion filtration, pore size is considered to be the most critical parameter of a medium to determine performance of the treatment. One of the motivations of this research is to develop a basis to predict the mean pore size of a nonwoven web.

There is a gap in the literature on particle separation performance of nonwovens for water treatment. One must collect critical information about the material, the web, and the process to establish a detailed knowledge base for fundamental understanding of the particle removal performance of nonwovens. This study mainly focuses on the effects of nonwoven characteristics, which have not been addressed yet in the literature. Moreover, nonwovens are frequently used as a support layer in MBR, but there is no commercially available nonwoven as separation medium for MBR yet.

After identifying the limitations and challenges of using nonwovens, the research strategy focused on addressing the limitations of nonwovens by using post-processing methodologies. The limitations of nonwovens in terms of microfiltration are discussed below:

- **Depth filter structure:** Generally, nonwovens have a high internal fouling potential due to their depth filter structure. Compared to membranes, nonwovens exhibit

tortuosity and depth filter structure, which can both result in irreversible pore blocking fouling.

- **Pore size:** Pore size is likely the most important parameter for membrane separation. The average pore size of conventional nonwovens tends to be larger than typical membranes. Therefore, further processing may be required to reduce the average pore size in order to meet the water quality limits. Furthermore, nonwovens with bigger pores may have a greater tendency for pore blocking fouling with regard to influent characteristics.

- **Wider pore size distribution:** Conventional nonwovens have wider pore size distributions compared to typical membranes. For example, pore size may range from 2 µm to 80 µm for meltblown fabrics while the PVDF membrane studied here has a pore size distribution of 0.5 µm to 1.5 µm.

- **Rough surface:** Generally, nonwovens have rougher surface compared to membranes. Foulants will have a higher tendency to be attached in case of rough surface. This attachment may result in higher cake layer fouling. Also, a rough surface may limit the air scouring.

- **High surface area:** Nonwovens tend to have higher specific surface area than membranes. Foulants attach to the surface of materials, so webs composed of high surface area fibers may lead to greater internal fouling.

Tailorability of nonwovens to meet the requirements is one of the driving forces behind this study.

3.2 Objectives

Nonwoven applications in filtration require a medium designed to a particular pore size specification within the 0.1 to 20 μm range. Commercial membranes used in MBR typically have pore size in the range of 0.1 to 0.4 μm. In order for a nonwoven to meet effluent quality requirements, the pore size range should be close to this range, because particle separation in MBR depends on size-exclusion filtration. Therefore, this study examines how pore size is controlled in nonwovens. The first objective is to develop a basis by which to design and construct nonwovens with given pore size specifications.

In order to fabricate membrane-like structures through nonwovens and meet the requirements of microfiltration filters, post-processing techniques are required. The second objective is to form a membrane-like structure from nonwovens through post-processing techniques.

Nonwoven pore structure is totally different from that of typical membranes. Consequently, the fouling process of nonwovens is expected to behave in a different way. Additionally, pore size characteristics govern the performance of the bioreactor system in size-exclusion filtration. The third objective is to investigate the effects of mean pore size of nonwovens on effluent quality and fouling behavior.

3.3 Approach

Nonwovens, which tend to be low-cost compared to membranes, are associated with enhanced flux due to larger porosity[100,185]. Characteristics of the nonwoven media such as pore size, and pore size distribution can be controlled during web formation and through post-processing techniques[99]. In other words, nonwoven media can be designed and engineered, and diverse functionalities can be added easily[186].

Almost all of the nonwoven characteristics have an impact on separation performance. Pore size, pore size distribution, porosity, surface charge, roughness and hydrophilicity are some of these parameters. With regard to size-exclusion filtration, the interest is in how we control the pore size by controlling structure properties during web formation and by solid volume fraction through post-processing. The structural parameters that we can control during meltblown process are fiber size, basis weight and solid volume fraction. These structural parameters are controlled through tuning operational parameters of the web formation technique (capillary size, throughput, collector speed, and air intensity).

With regard to size-exclusion filtration, a basis for producing nonwovens at given pore size is required. A series of meltblown fabrics are produced with different settings, and the relationships between processing conditions, structure properties and mean pore size are investigated.

Selecting the polymer is one of the key variables for fouling control. Polybutylene terephthalate (PBT) ($C_{12}H_{12}O_4$) is chosen as a raw material. PBT, which has good

mechanical and chemical resistance, crystallizes fast and is processed easily. It has low manufacturing cost. Also, modifying the surface of the PBT is easy compared to polyolefin (PP and PE) due to the higher number of functional groups in PBT. Furthermore, PBT-based products have been used in many water treatment applications.

Among the various nonwoven fabric production techniques, meltblowing is versatile for applications in liquid filtration. Fiber diameter of meltblown fabric varies from 0.1 to 30 µm where pore size range is 1- 30 µm. Also, there is no additional bonding step needed for fabricating a reliable medium.

Calendering is a widespread finishing process where the material is passed between rollers at determined temperature and pressure[187]. Normally, calendering is not required in the case of meltblown fabrics. However, it can be applied for specific purposes such as microporous membrane formation. Calendaring also addresses some limitations of the nonwovens such as rough surface, wide pore size distribution, bigger average pore size, and low strength.

4. Basis for Designing of Nonwovens with Given Pore Size

4.1 Introduction

Nonwovens have been generally regarded as cost effective substitutes for conventional textiles for more than half a century[188]. Nowadays nonwovens are used as substitutes for many technical materials such as filtering media, battery separators and insulation media. Each technical usage has its own requirements. In particular, size-exclusion filtration applications require a medium designed to a particular pore size. For example microfiltration membranes are designed to filter particles in the range of 0.1 μm to about 5 μm[189].

Nonwovens, which have a complex structure, are composed of fibrous materials and their volume is occupied by air and fibers. Mass per unit area of the nonwoven fabric is defined as fabric weight (or basis weight), which is usually measured in g/m^2 (or gsm). Fabric thickness is defined as the distance between the fabric surfaces under a specified applied pressure, which varies if the fabric is compressible (high-loft). Bulk density (or fabric density) is defined as the weight per unit volume of the nonwoven (kg/m^3), which is calculated by dividing measured weight per unit area (kg/m^2) by the measured thickness of the fabric (m)[190].

Fibers, whose geometry is characterized in terms of length, diameter, aspect ratio, cross-sectional shape, specific surface area, crimp, and orientation distribution, are the basic unit of a nonwoven structure[191]. Pores are defined as the void spaces between fibers, and are characterized in terms of total pore volume, pore size, pore size distribution, and pore

connectivity. A pore channel has a tortuous pore path and continuous void through the thickness. Then, size of the void at any location along this channel is called pore size[192]. There are three groups of pore size: the largest pore size (aka apparent opening pore size or opening pore size), the constriction pore size (aka pore-throat size), and the pore volume size[188,190]. The fraction of the total pore volume to the web volume is called porosity. Conversely, the ratio of volume occupied by the fibers to whole volume of the web is called SVF or packing density or solid volume fraction (SVF). Compactness of the web is indicated by the packing density, which affects many properties of the web such as pore size and has a great impact on liquid filtration and fluid permeability[12].

Producing nonwovens with a given pore size has always been of great interest because microfiltration performance is driven by the sieving mechanism. It is generally accepted that small fibers result in small pores. Since a decrease in fiber diameter leads to a large increase in the number of pores, average pore size decreases for a given fabric density. Analysis of the relationship between fiber diameter and number of pores presented here follows the approach developed by Abdel-Ghani and Davies (1985)[193]. If the free area of a layer is ε, then the following equation can be written:

$$n_p a_p = \varepsilon A \tag{4.1}$$

Where, n_p is the number of pores, a_p is the mean area of a pore, ε is the free area of a layer, and A is the total area where fibers are deposited.

Deposited fibers will occupy an area A_f:

$$A_f = n_f d_f l_f - \omega \tag{4.2}$$

Where, ω is the area of fiber crossings per unit area, d_f is the mean fiber diameter, and l_f is the mean fiber length. ω can be expressed as:

$$\omega = \frac{n_{fc}\, n_f d_f}{2} \tag{4.3}$$

Where, n_{fc} is the number of fiber crossings. In a nonwoven structure, where $\varepsilon > 0.9$, and $\omega \ll A_f$. Then the following equation is obtained:

$$1 - \varepsilon = \frac{n_f d_f l_f}{A} \tag{4.4}$$

Abdel-Ghani and Davies (1985) also showed that the mean length of a fiber in area A is $l_f = K\sqrt{A}$ by. When the constant K is determined as $\pi/4$ by considering the randomness (method of simulation), then l_f becomes$\sqrt{A}\pi/4$. If we use $l_f$in Eq.4.4, the following equation is obtained:

$$n_f = \frac{1 - \varepsilon\, \sqrt{A}\, 4}{\pi\, d_f} \tag{4.5}$$

The number of pores is expressed by Abdel Ghani and Davies (1985) as:

$$n_p = \frac{\pi \, {n_f}^2}{16} \tag{4.6}$$

Following the above equations, the number of pores in a unit area can be written in terms of structure properties by using Eqs. 4.5, and 4.6:

$$n_p = \frac{(1-\varepsilon)^2 \, A}{\pi \, {d_f}^2} \tag{4.7}$$

Eq. 4.7 suggests that the number of pores in the unit area is inversely proportional to the square of fiber diameter. In other words, as fiber size decreases, the number of pores in the given area increases exponentially.

Another structural parameter affecting the mean pore size is SVF, which can be controlled either during web formation or by post-processing techniques such as calendering. It has been reported by many researchers that calendering decreases the thickness of the nonwoven and increases the SVF, resulting in a significant decrease in mean pore size[182,184,194]. Calendering also narrows the pore size distribution.

Even if the fiber size and SVF are identical, pore size of the nonwoven may be different due to the influence of another structure property: fiber orientation distribution (FOD). Fiber orientation angle, which is the relative directional position of individual fibers in the structure, is used to measure the FOD. Statistical function (the frequency distribution) of these fiber orientation angles in a nonwoven structure determines the FOD. The ratio of number of fibers falling within a series of predetermined ranges of orientation angle to total

counted fibers is used to determine frequency distributions[195]. Rawal et al. (2010) stated that the random (air-laid) structure exhibits a larger mean pore size compared to directional (parallel or cross-laid) structures[196].

Another additional factor, crimp, which is a term to describe waviness, twistiness, or curliness of a fiber along the length, may have an impact on pore size[197,198]. Kim and Pourdeyhimi (2000) found that an increase in fiber crimp results in smaller pores in highly anisotropic structures while crimp has little or no effect on pore size in isotropic structures[199].

4.2 Theoretical Studies on Predicting Nonwoven Pore Size

Lombard et al.[200] and Faure et al.[201] utilized Poissonian line network theory to determine a theoretical model for pore size distributions of nonwoven fabrics. Rawal[202] developed an analytical model based on gamma distribution of circles inscribed in the convex polygons formed between the straight lines.

Wrotnowski developed a mathematical model where the fiber cross section is circular; fibers are parallel, straight and aligned in a square pattern. It is assumed that the pore is generated between four fibers[203,204]. The equation is given in the Table 4.1.

Giroud proposed a theoretical equation based on porosity, basis weight, fiber diameter, and a coefficient for calculating the constriction pore size (the pore-throat diameter) of nonwovens (Table 4.1). In that equation, γ is a coefficient to be obtained by calibration with test data. γ is taken 10 for some experiments which was quite satisfactory, considering the difficulty of measurement of nonwoven pore size[205].

Table 4.1 Summary of the mean pore size models

Equation	Notation	Reference
$d_p = \left(\frac{42.5\sqrt{F/\rho_f}}{cos\,45}\right) - d_f$	d_f : Fiber diameter ρ_{fabric}: Fabric density g/cm3, F : Fiber linear density(denier)	Wrotnowski (1962) [204]
$d_p = (\frac{1}{\sqrt{(1-\varepsilon)}} - 1 + \frac{\gamma\varepsilon}{G/(\rho_f . d_f)})d_f$	d_f : Fiber diameter, ε: Porosity, G :Basis Weight, γ :Unknown parameter, ρ_f:Fiber density	Giroud (1996) [205]
$d_p = \frac{d_f}{1/\left(\frac{1}{2(\varepsilon)^2\,(1-\varepsilon)^{1.5}\,(1+56(1-\varepsilon)^3)}\right)^{0.5}}$	d_f :Fiber diameter ε : Porosity	Tsai (1999) [206]
$d_p = \frac{1}{\sqrt{2}}\sqrt{\frac{\varepsilon}{1-\varepsilon}}d_f$	d_f : Fiber diameter ε : Porosity	Neckar and Ibrahim (2003) [207]
$d_p = 32.26{d_f}^{0.2354}\,(\frac{4G}{\pi\,\rho_f\,{d_f}^2})^{-0.526}$	d_f : Fiber diameter G : Mass per unit area ρ_f : Fiber density	Lifshutz (2005) [208]
$d_p = \frac{\pi\,d_f}{8\,(1-\varepsilon)}$	d_f : Fiber diameter ε : Porosity	Simmonds et al. (2007) [209]

Tsai modified Hagen-Poiseuille law to obtain average circular capillary equivalent pore size[12,206]. According to derivation of this equation, the average circular equivalent pore size becomes:

$$d_p = (\frac{32\,\alpha\,v_0 T}{\Delta P\,\varepsilon^2})^{0.5} \qquad (4.8)$$

Where α is air viscosity, v_0 is face velocity, T is web thickness, ε is porosity, ΔP is pressure difference.

When pressure difference is written in terms of fabric properties:

$$\Delta P = \frac{\alpha\, v_0\, T\, f(\mu)}{{d_f}^2} \tag{4.9}$$

Where $f(\mu) = 64\,(1 + 56\mu^3)\,\mu^{1.5}$. This equation is derived through an experimental correction done by Davies (1976) [210] where solid volume fraction was between 0.006 and 0.3. Substituting ΔP in Eq. 4.8 using Eq. 4.9 gives:

$$d_p = \frac{d_f}{g(\mu)} \tag{4.10}$$

Where

$$g(\mu) = 1/\left(\frac{1}{2(\varepsilon)^2\,(1-\varepsilon)^{1.5}\,(1 + 56(1-\varepsilon)^3)}\right)^{0.5} \tag{4.11}$$

Then Eq. 4.10 turns into by using Eq. 4.10 and 4.11:

$$d_p = \frac{d_f}{1/\left(\frac{1}{2(\varepsilon)^2\,(1-\varepsilon)^{1.5}\,(1 + 56(1-\varepsilon)^3)}\right)^{0.5}} \tag{4.12}$$

Where, ε is porosity. So, the mean pore size of the nonwovens can be predicted by porosity and fiber diameter.

Neckar et al. described the pores between fibers in general assembly by treating fibers as air fibers surrounded by fictional borders. The space between the fibers is called pores. Since the

contact area between fibers is very small, the authors assumed that pore surface area is equal to the fiber surface area. Equivalent pore diameter is expressed as[207,211];

$$dp = \frac{1 + q_p}{1 + q} \frac{\varepsilon}{1 - \varepsilon} d_f \tag{4.13}$$

Where q is cross-sectional shape factor of a real fiber, q_p is shape factor of pore, d_f is fiber diameter, and $\boldsymbol{\varepsilon}$ is porosity. The model is derived according to the assumptions that fibers have round cross-sectional shape with equivalent fiber diameter. Eq 4.13 takes different forms with constant pore shape factor, with the constant pore length and for generalized pore. The authors assumed that fibers are arranged in a hexagonal structure, and suggested the following equation for pores in hexagonal structure with round shaped fibers:

$$d_p = \frac{1}{\sqrt{2}} \sqrt{\frac{\varepsilon}{1 - \varepsilon}} d_f \tag{4.14}$$

Lifshutz[208] found a correlation between mean flow pore size and total fiber length per unit area, and fiber diameter. Lifshutz's model is free from porosity in case of highly porous structures (<3% SVF). Area and perimeter of each of the polygonal regions generated by the intersection of all the fibers are calculated through image analysis software. From the perimeter and area of polygonal regions, "hydraulic diameter" is calculated. After that a relationship between hydraulic pore diameter and the mean flow pore diameter is established depending on whether one assumes that the pores in a real nonwoven take the form of an orifice or a capillary. For the orifice model:

$$d_{mf} = 1.337\ d_h \tag{4.15}$$

For the capillary model:

$$d_{mf} = 2.336\ d_h \tag{4.16}$$

Where d_{mf} is mean flow pore size, d_h is hydraulic diameter.

Lifshutz defined the basis length as the total length of fiber per unit area of the web (Δ):

$$\Delta = \frac{4\ G}{\pi\ {d_f}^2 \rho} \tag{4.17}$$

Where, G is the mass per unit area of the web, and ρ is fiber material density. Lifshutz conducted a set of experiments resulting in statistical correlation:

$$d_{mf} = 32.26\ {d_f}^{0.2354} \Delta^{-0.5260} \tag{4.18}$$

The approach of Simmonds et al. (2007) was first to determine the open pore area and number of pores. Then mean pore area was calculated, and then the wetted perimeter of polygon pore size was determined by length of sides. The mean pore area and perimeter were used to calculate hydraulic radius of polygon pore from which the mean pore size was calculated. The authors also found that maximum pore size was approximately three times the size of mean pore size. Mean pore size of the web is given as[209]:

$$d_p = \frac{\pi\, d_f}{8(1-\varepsilon)} \tag{4.19}$$

Where, d_f is fiber diameter, ε is porosity.

4.3 Experimental Validation

4.3.1 Materials

Two sets of meltblown fabrics were produced with a lab-size Biax Fiberfilm (WI, US) meltblown line under various conditions. The length of the meltblown die was 38 cm with 368 capillary holes in 2 rows for polymer extrusion, and 1128 holes of air in 6 rows.

In the first set (group 1), Dupont™ Crastin® PBT resin was used as raw material. The capillary size was 508 μm. Die temperature was set to 310°C, where die air temperature was 293°C. Throughput rates were 0.156, 0.245, and 0.336 gram per hole per minute. Die air pressures were set to 58, 73, 83, and 97 kPa. Nonwovens were deposited onto a rotating drum collector with three die-to-collector distances that varied from 20 to 40 cm. Fabrics were produced at four different basis weights ranging from 60 to 160 g/m^2. Then, these webs were calendered through a laminator at 600 kN/m^2 and 200 °C. The calendered webs were named with –C after the sample names in group 1.

In the second set (group 2), Lanxess™ Pocan® PBT resin was used as the raw material, and the capillary size was 228.6 μm. Die temperature was set to 265°C, while die air temperature was 260°C. Throughput rates were 0.03, 0.05, 0.07, and 0.09 gram per hole per minute. Die

air pressures were set to 57, 69, 83, and 97 Pa. Nonwovens were deposited onto a rotating drum collector where die-to-collector distance was fixed to 30 cm. Fabrics were produced at four different basis weights ranging from 20 to 120 g/m^2. Then, these webs were calendered through a steel roller with 0.1 mm gap and at 170 °C. The calendered webs were named with –C after the sample names in group 2.

Table 4.2 Basic web characteristics of group 1 meltblown fabrics

Sample ID	Characteristics				
	Fiber Diameter (µm)	Basis Weight (g/m^2)	Thickness (µm)	SVF	Mean Flow Pore Diameter (µm)
S2-B-A	11.2(±2.5)	121(±1.3)	671.1(±15)	0.14	17.51
S2-B-A-C	12.4(±2.3)	125.7(±1.26)	519(±18)	0.18	17.12
S2-B-B	11.6(±2.5)	121.1(±1.04)	694.5(±24)	0.13	19.71
S2-B-B-C	13.8(±2.4)	125.8(±1.07)	557.8(±31)	0.17	19.33
S2-B-C	13.7(±2.1)	120.1(±1.37)	712.0(±17)	0.13	23.03
S2-B-C-C	15.1(±2.4)	125.2(±1.07)	550(±30)	0.17	20.80
S2-B-D	15.1(±1.9)	120.4(±3.32)	749.1(±17)	0.12	41.10
S2-B-D-C	15.8(±2.4)	124.6(±2.28)	557.2(±31)	0.17	31.12
S2-B-E	11.8(±2.1)	121.1(±4.98)	702.2(±19)	0.13	27.34
S2-B-E-C	13.2(±2.8)	129.1(±2.46)	519.8(±20)	0.19	20.10
S2-B-F	9.4(±1.8)	125.5(±4.86)	703.6(±22)	0.14	24.11
S2-B-F-C	11.1(±2.4)	131.6(±4.43)	573.4(±48)	0.18	18.86
S2-B-G	14.9(±1.9)	158.7(±2.19)	825.7(±27)	0.15	28.84
S2-B-G-C	15.8(±2.1)	164.5(±2.9)	664.6(±15)	0.19	24.35
S2-B-H	15(±2.2)	78.9(±2.84)	682.1(±14)	0.09	47.18
S2-B-H-C	15.9(±2.4)	81.6(±1.74)	441.5(±35)	0.14	38.90
S2-B-I	15.6(±2.1)	58.6(±0.91)	658.1(±16)	0.07	63.45
S2-B-I-C	16(±3.7)	61(±1.13)	372.7(±19)	0.12	42.02
S2-B-J	14.9(±2.2)	127.6(±1.9)	780.2(±17)	0.12	37.30
S2-B-J-C	15.7(±3.6)	133.6(±1.3)	571.7(±14)	0.18	29.79

In addition to webs produced through the meltblown technique mentioned above, existing mean pore size models of nonwovens have been validated with 18 commercial nonwoven

separation media (group 3). These separation media include both calendered and uncalendered samples.

4.3.2 Analytical Methods

The fabric characterizations include fiber diameter, basis weight and thickness measurement as well as pore size and porosity calculation.

Table 4.3 Basic web characteristics of group 2 meltblown fabrics

Sample ID	Characteristics				
	Fiber Diameter (μm)	Basis Weight (g/m^2)	Thickness (μm)	SVF	Mean Flow Pore Diameter (μm)
S3-C-B	1.75(±1.1)	32(±1.5)	256.4(±19.6)	0.09	10.8
S3-C-B-C	2.1(±1.2)	33(±0.6)	177(±7)	0.14	9.2
S3-C-C	2.26(±0.8)	30(±0.6)	264.2(±3.1)	0.09	13.8
S3-C-C-C	2.23(±1.1)	31(±1.8)	164(±4)	0.15	11.9
S3-C-D	2.9(±1.1)	30(±0.6)	283.4(±3.9)	0.08	15.4
S3-C-D-C	3.34(±1.2)	32(±2.7)	168(±7)	0.14	13.7
S3-C-E	2.12(±1.2)	29(±1.6)	260(±5.2)	0.09	13.6
S3-C-E-C	2.13(±1.2)	32(±1.6)	170(±8.4)	0.14	10.5
S3-C-F	3.26(±1.3)	31(±0.6)	279.1(±4.6)	0.08	17.4
S3-C-F-C	3.3(±1.3)	31(±1.6)	171(±12)	0.14	13.3
S3-C-G	3.43(±1.5)	30(±1.5)	258.3(±3.5)	0.09	19.4
S3-C-G-C	3.67(±1.4)	31(±1.6)	174(±6.2)	0.14	13.6
S3-C-I-	2.29(±1)	40(±1.2)	355(±10)	0.09	13.9
S3-C-I-C	2.39(±0.9)	42(±2.1)	108(±8.9)	0.30	4.62
S3-C-K	2.82 (±1.4)	119(±2.5)	1003(±14)	0.09	15.92
S3-C-K-C	3.1(±1.4)	130(±3.2)	211(±13.5)	0.47	3.02

Fiber Diameter and Morphology

Nonwoven samples were coated with a thin layer of gold and analyzed by two scanning electron microscopes (Phenom ProX at The Nonwovens Institute and JEOL 7600F at AIF, NCSU) in order to examine the fiber morphology. Fiber diameters were measured using

Adobe Acrobat Pro software with at least 100 individual fiber diameter measurements. The results were expressed as average, and ± indicates the standard deviations.

Table 4.4 Basic web characteristics of the commercial nonwoven membranes (group 3)

Sample ID	Characteristics				
	Fiber Diameter (μm)	Basis Weight (g/m^2)	Thickness (μm)	SVF	Mean Flow Pore Diameter (μm)
1	1.34	84	188	0.47	0.80
2	1.57	100	203	0.52	1.00
3	1.94	96	229	0.44	2.20
4	2.38	95	127	0.57	2.40
5	1.40	20	66	0.32	2.70
6	2.27	45	102	0.47	3.10
7	1.82	45	152	0.31	5.00
8	2.24	40	71	0.43	5.10
9	1.69	100	813	0.13	5.50
10	1.81	32	109	0.31	5.70
11	2.44	25	229	0.12	9.60
12	2.35	40	330	0.13	9.80
13	2.54	80	508	0.17	10.10
14	1.21	10	86	0.12	10.20
15	2.89	100	508	0.15	11.00
16	2.76	80	457	0.13	11.80
17	2.42	40	254	0.12	13.30
18	2.32	20	152	0.14	15.00

Web Thickness

Thickness measurement was carried out according to ASTM D1777 by Precision Thickness Gauge-FT3 (Hanatek Instruments). Ten measurements were taken in units of micrometer (μm) and the average was taken. The results were expressed as average, and ± indicates the standard deviations.

Basis Weight

Basis weight measurement was carried out according to ASTM D3776 with three measurements in units of gram/m^2. The results were expressed as the average, and ± indicates the standard deviations.

Solid Volume Fraction

Solid volume fraction (SVF) was obtained from measured basis weight and thickness, and was calculated by using the following equation:

$$\mathrm{SVF} = \left(\frac{\mathrm{G}}{T\,\rho_f}\right)100 \tag{4.20}$$

Where ε is the percent porosity, G is the fabric basis weight in g/m^2, T is the nonwoven's thickness in μm, and ρ_f is the density of the polymers (fiber) in g/cm^3.

Pore Size

Pore structure analysis was carried out using a PMI Capillary Flow Porometer (model CFD-1100-AEL), based on the principle of the liquid extrusion porometry technique[212]. In a typical CFP experiment, the material is filled with a wetting solution (Galwick ™ with surface tension of 15.9 dynes/cm), and is subject to gas pressure. The pressure on the material is increased in controlled fashion while the flow rate of gas through the material is simultaneously monitored. In this technique, it was assumed that the sample is wetted completely by the wetting solution and therefore contact angle of 0° was taken for

calculations. Pore size measurements were carried out according to the following equation[213,214]:

$$d_p = \frac{4\gamma \cos\theta}{p} \tag{4.21}$$

Where $d_p$is the pore diameter, γ is the surface tension of the wetting liquid, θ is the contact angle of the wetting liquid, p is the extrusion pressure. Pore throat diameter, average pore diameter, and bubble point (largest pore diameter) are provided with this technique. Three specimens of each nonwoven media were tested the average was calculated.

4.3.3 Validations of Mean Pore Size Models

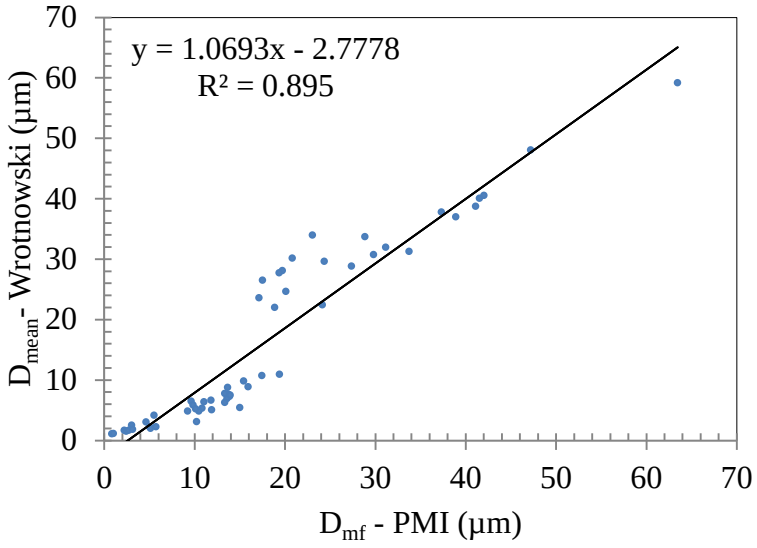

Figure 4.1 PMI data versus Wrotnowski model for mean pore diameter

Table 4.2 shows the basic web characteristics of the group 1 fabrics. Fiber diameters were in the range of 9.4 and 15.9 µm. Standard deviations are less than 30% of average fiber diameter. Thicknesses and solidities of the samples are consistent with a reasonable range.

Mean flow pore sizes were in the range of 17.12 and 63.45 µm. A slight increase in basis weight has been observed for calendered samples, and SVF of calendered samples was higher than uncalendered samples due to thickness decrease.

Table 4.3 shows the basic web characteristics of the fabrics in group 2. Fiber diameters are in the range of 1.75 and 3.67 µm. Standard deviations are less than 50% of average fiber diameter, and thicknesses and solidities of the samples are consistent with a reasonable range. Mean flow pore sizes were in the range of 3.02 and 19.37 µm. As with the fabrics in group 1, a slight increase in basis weight was observed for calendered samples. Again, SVF of calendered samples was higher than uncalendered samples.

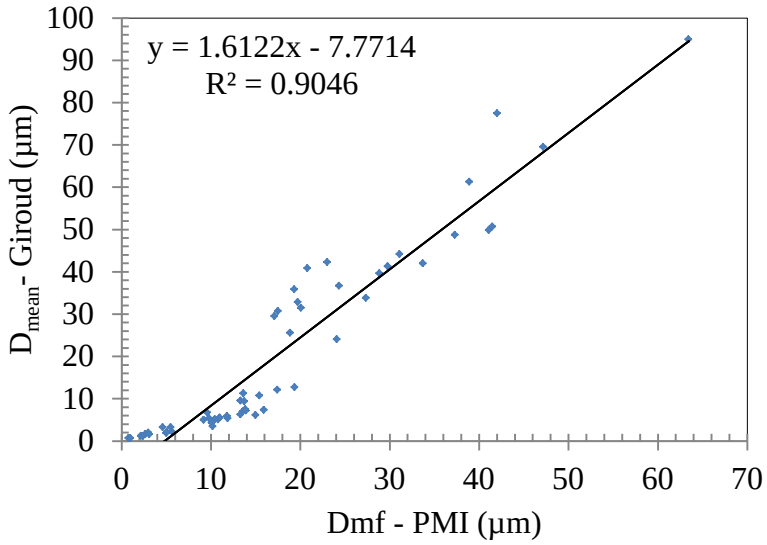

Figure 4.2 PMI data versus Giroud model for mean pore diameter

Basic web characteristics of the commercial nonwoven media are shown in Table 4.4. The data corresponding to the characteristics are based on the data sheet of the commercial membranes, which did not include standard deviations. Pore sizes of these nonwovens, made

of PP or PBT, were in the range of 0.8 and 15 µm. Fiber diameters were in the range of 1.34 µm and 2.89 µm where solidities were in the range of 0.12 and 0.57.

Mean pore diameters are calculated for the three series of webs: group 1 webs and group 2 webs produced through meltblowing and commercial nonwoven separation media.

Generally, a model fits the data well when the measured and predicted values are close to each other. Therefore, straight line (regression line) equations are provided. R-squared values are also calculated because it is the indication of how close the data are to the regression line.

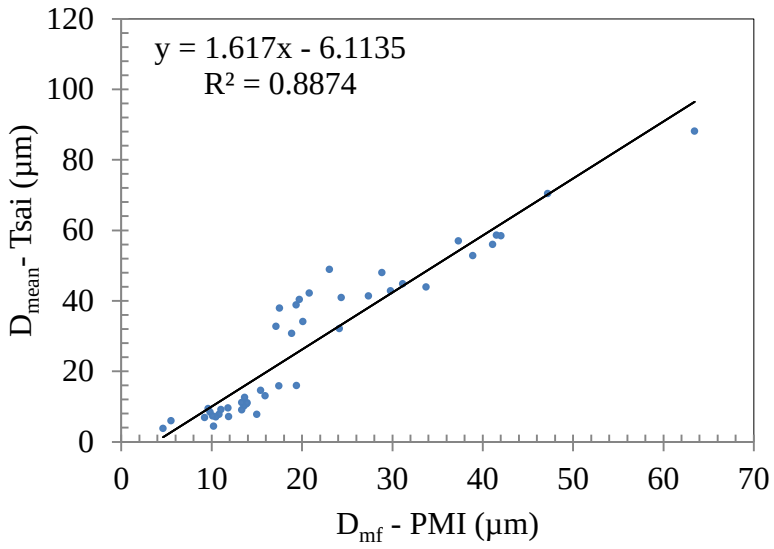

Figure 4.3 PMI data versus Tsai model for mean pore diameter

Figure 4.1 shows the correlation between the PMI data and the results predicted by Wrotnowski. In this model it was assumed that the fiber cross section is circular; fibers are parallel, straight and aligned in a square pattern. Also, it was assumed that the pore is generated between four fibers. The regression line fit is good, and the R-squared value is also quite satisfactory. Generally, it was observed that when the fiber diameter is smaller than 4

μm, predicted pore diameters are smaller than measured pore sizes (for group 2 and 3). However, when the fiber diameter is larger than 10 μm, predicted pore diameters are larger than measured pore sizes (for group 1).

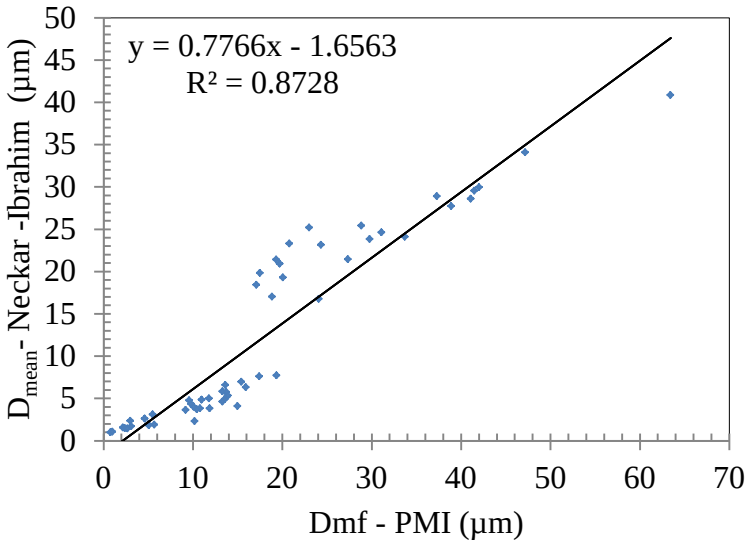

.

Figure 4.4 PMI data versus Neckar and Ibrahim model for mean pore diameter

Figure 4.2 shows the correlation between the PMI data and the results predicted by Giroud for all samples. The unknown dimensionless parameter has been taken as 10 because in Giroud's study, an excellent agreement between the curve and the experimental data was obtained for needle-punched nonwovens. The regression line fit is not good compared to Wrotnowski; however the R-squared value is satisfactory. Generally, it was observed that when the fiber diameter is smaller than 4 μm, predicted pore diameters are smaller than measured pore sizes (for group 2 and 3). However, when the fiber diameter is larger than 10 μm, predicted pore diameters are larger than measured pore sizes (for group 1).

Figure 4.3 shows the correlation between the PMI data and the results predicted by Tsai. The samples which have SVF between 0.006 and 0.3 have been used to plot the graph, because the model includes an experimental correction where the SVF is between 0.006 and 0.3. The regression line fit and the R-squared are not good compared to Wrotnowski. Generally, it was observed that when the fiber diameter is smaller than 4 μm, predicted pore diameters are smaller than measured pore sizes. However, when the fiber diameter is larger than 10 μm, predicted pore diameters are larger than measured pore sizes.

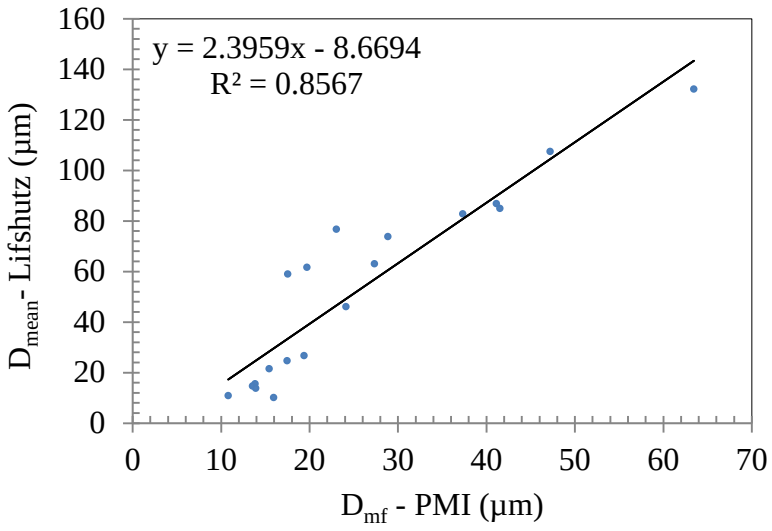

Figure 4.5 PMI data versus Lifshutz model for mean pore diameter

Figure 4.4 shows the correlation between the PMI data and the results predicted by Neckar and Ibrahim. The model is derived according to the assumptions that fibers have round cross-sectional shape with equivalent fiber diameter, and fibers are regularly arranged in a hexagonal structure. The regression line fit and R-squared value are not as good as Wrotnowski model.

Figure 4.5 shows the correlation between the PMI data and the results predicted by Lifshutz. Lifshutz used very open structure structures (SVF<0.03) to verify his model. According to the model, mean flow pore size is independent of SVF as long as the nonwoven maintains a low SVF. As a result, only the uncalendered samples have been used to plot Figure 4.5. The regression line fit and the R-squared value are not good compared to Wrotnowski model.

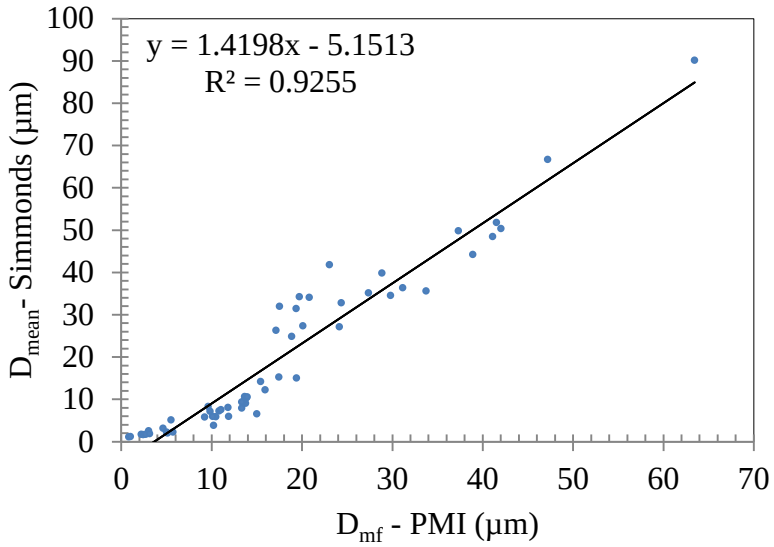

Figure 4.6 PMI data versus Simmonds model for mean pore diameter

Figure 4.6 shows the correlation between the PMI data and the results predicted by Simmonds et al. The regression line does not fit well compared to Wrotnowski, however R-squared value is better than Wrotnowski model. Generally, it was observed that when the fiber sizes are smaller than 4 µm, predicted pore diameters are smaller than measured pore sizes. However, as the Tsai model, when the fiber sizes are bigger than 10 µm, predicted pore diameters are larger than measured pore sizes.

4.4 Model Development: A Unified Approach

Three assumptions have been made before carrying out the following theoretical analyses: fibers are cylindrical and have equal density and size, fibers are randomly oriented on elemental plane of the nonwoven, and liquid can only flow in a vertical direction. Basically, the approach of Simmonds et al. (2008) has been followed in this unified model. The primary difference in the two models is that the mean pore perimeter has been determined in a different way in this model.

Mean Pore Area

Simmonds et al. (2008) rearranged the study of Kallmes and Corte (1960) and found that the mean pore area (α_p) is inversely proportional to the square of the total length of fiber in elementary plane[209,215]:

$$\alpha_p = \frac{\pi}{(n_f\ l)^2} \tag{4.22}$$

Where n_f is number of fiber, l is fiber length.

Mean Pore Perimeter

In a nonwoven structure, most of the fiber surface area is shared with pores, however at some locations fibers contact with each other, and form small junctions[211]. If these fiber-fiber junctions are neglected, total fiber surface area in nonwoven assembly will be roughly equal to the total pore surface area (A_p):

$$A_p = \pi \ d_f \ L \tag{4.23}$$

Where, L is total length of fibers in the nonwoven structure. Total length can be written as $L = 4.G/\rho.\pi.{d_f}^2$, where G is basis weight and ρ is density of the fiber. Then, Eq. 4.23 turns into:

$$A_p = \frac{4\ G}{\rho\ d_f} \tag{4.24}$$

If the total pore surface area is divided by pore length (l_p) and number of pores (n_p), mean perimeter of a pore (P_p) is obtained as:

$$P_p = \frac{A_p}{l_p\ n_p} \tag{4.25}$$

A pore's length can be written as:

$$l_p = T\ \tau \tag{4.26}$$

Where τ is tortuosity. Eq. 4.6, 4.24, and 4.26 are integrated into Eq. 4.25 so that the mean pore perimeter is obtained as:

$$P_p = \frac{64\ \mathrm{G}}{\rho\ d_f \quad T\ \tau \quad \pi\ {n_f}^2} \tag{4.27}$$

Hydraulic radius is defined as the ratio of pore area to pore perimeter:

$$r_h = \frac{\alpha_p}{P_p} \tag{4.28}$$

Then hydraulic radius is obtained by using Eq. 4.22 and 4.27, where SVF $(1-\varepsilon)$ is expressed as: $(1-\varepsilon) = \frac{G}{T.p}$ and if average fiber length is accepted as $l = \frac{\pi}{4}$ in the unit area[193], hydraulic radius becomes:

$$r_h = \frac{\tau\, d_f}{4\,(1-\varepsilon)} \tag{4.29}$$

Hydraulic diameter is four times the hydraulic radius for polygon tubes and channels[216]. So Eq. 4.29 turns into:

$$d_h = \frac{\tau\, d_f}{(1-\varepsilon)} \tag{4.30}$$

Tortuosity can be defined as the ratio of actual flow path length average to the thickness of the nonwoven[217]. Koponen et al. (1998) modeled the tortuosity as a function of porosity[218]:

$$\tau = 1 + \sigma \frac{(1-\varepsilon)}{(\varepsilon - \varepsilon_p)^m} \tag{4.31}$$

Where ε is porosity, ε_p is the percolation threshold (0.33), the constant $\sigma = 0.65$, and the constant $m = 0.19$.

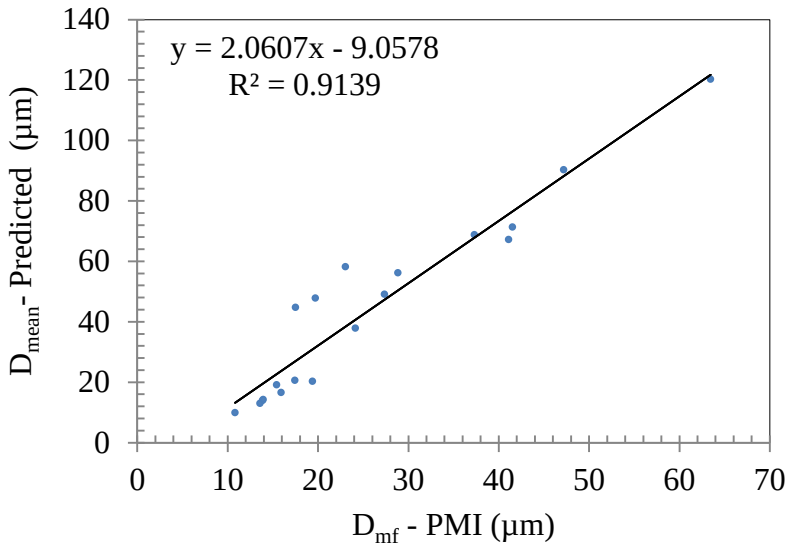

Figure 4.7 PMI data versus the developed model for mean pore diameter

Eq. 4.30 is derived for an elemental plane, however as more layers are deposited, mean pore size decreases. Simmonds et al. (2007) stated that at least two elemental planes always interact to determine the effective pore size in three-dimensional structure[209]. As a result, mean pore size of three-dimensional structures can be written as $d_p = d_{p-elemental}/n_l$. Where n_l is number of layers, $d_{p-elemental}$ is the mean pore size in elemental plane. If the interaction of layers is assumed to be minimal and equal to 2, mean pore size is obtained by combining Eq. 4.30 and Eq. 4.31:

$$d_{p,mean} = \frac{1 + \sigma \frac{(1-\varepsilon)}{(\varepsilon - \varepsilon_p)^m}}{2\,(1-\varepsilon)}\; d_f \tag{4.32}$$

Where ε is porosity, ε_p is percolation threshold (0.33), $\sigma = 0.65$, and $m = 0.19$ are constants. In this model, fiber-fiber junctions are neglected in order to calculate mean pore

perimeter. Since fiber-fiber crossover increases as SVF increases, this model is expected to be more useful for those nonwovens with low solidities.

Table 4.5 Experimental and predicted mean pore diameters

Sample ID	Measured Mean Flow Pore Diameter (µm)	Predicted Pore Diameter (µm)	Error %
S2-B-A	17.51	44.79	156
S2-B-B	19.71	47.82	143
S2-B-C	23.03	58.20	153
S2-B-D	41.10	67.24	64
S2-B-E	27.34	49.13	80
S2-B-F	24.11	37.96	57
S2-B-G	28.84	56.25	95
S2-B-H	47.18	90.34	91
S2-B-I	63.45	120.34	90
S2-B-J	37.30	68.87	85
S3-C-B	10.81	9.91	-8
S3-C-C	13.85	14.00	1
S3-C-D	15.42	19.19	24
S3-C-E	13.56	13.07	-4
S3-C-F	17.44	20.61	18
S3-C-G	19.37	20.37	5
S3-C-I	13.91	14.31	3
S3-C-K	15.92	16.63	4

4.5 Validation of the Developed Model

Figure 4.7 shows the correlation between the PMI data and the results predicted in this study. Since the model is valid for only highly porous webs, only uncalendered samples have been used to draw the Figure 4.7. The regression line does not fit well compared to Wrotnowski, however the R-squared value is better than Wrotnowski model. Generally, it was observed that when the fiber sizes are bigger than 10 µm, predicted pore diameters are larger than measured pore sizes.

Table 4.5 shows the measured and predicted mean pore diameter values with % relative errors. Fiber diameters of S2-B webs are between 9.4 and 15.7 μm, while fiber diameters of S3-C webs are between 1.74 and 3.67 μm. Relative error values of the S2-B samples are greater than 64%, while relative error values of the S3-C samples are lower than 24%. This indicates that the developed model works better for fiber diameters around 3 μm compared to big fibers around 13 μm.

4.6 Comparison of the Mean Pore Size Models

In this study, validations of 7 different mean pore size models have been investigated. The regression line fit of the Wrotnowski model is better compared to other models, and the R-squared value of the Wrotnowski model is 0.89. In the Giroud model, the unknown dimensionless parameter has been taken as 10 because it was mentioned that an excellent agreement between the curve and the experimental data was obtained for needle-punched nonwovens. The regression line fit of Giroud model is not good compared to Wrotnowski model; however the R-squared value (0.90) is better than Wrotnowski model. If a new unknown dimensionless coefficient is determined for meltblown webs, the regression line fit can be improved in the Giroud model. In the Tsai model, the samples which have SVF between 0.006 and 0.3 have been used to validate the model, because the model includes an experimental correction in that specific SVF range. The regression line and R-squared value of the Tsai model were not good compared to Wrotnowski model. The regression line fit and R-squared value of the Neckar and Ibrahim model were not as good as Wrotnowski model either. Lifshutz used very open structures (SVF<0.03) to verify his model. According to the

model, mean flow pore size was independent of SVF as long as the nonwovens preserve low SVF. This was the main drawback of the Lifshutz model. Although the R-squared value of Lifshutz model is 0.85, the regression line does not fit well compared to the Wrotnowski model. Generally, predicted pore size values were greater than measured mean low pore size in Lifshutz model. The R-squared value of the Simmonds model is the best among all models, yet the regression line fit is not good compared to the Wrotnowski model. The regression line of the developed model does not fit well compared to Wrotnowski, however R-squared value is better than Wrotnowski model. The developed model is valid for highly porous webs. This is why the developed model is validated only for uncalendered samples. When the fiber diameters were between 9.4 and 15.7 µm, relative error values of the samples are greater than 64%. However, when the fiber diameters were between 1.75 and 3.67 µm, relative error values of the samples are lower than 24%. This indicates that the developed model works better for small fibers (around 3 µm) compared to big fibers (around 13 µm) for highly porous webs.

4.7 Conclusions

Validations of the existing and the developed mean pore size models showed that Wrotnowski's model has the best agreement with the experimental data in the range studied here. The models also revealed that mean flow pore diameter of nonwovens mainly depends on the diameter of the fiber and the SVF, with the exception of Lifshutz's model.

5. Formation of Nonwoven Membrane

5.1 Experimental

5.1.1 Materials

Two series of meltblown fabrics were produced at Biax Meltblown line by using two different PBT resins: Dupont™ Crastin® Polybutylene terephthalate (PBT) FG6134 and Lanxess™ Pocan® B-600. The glass transition temperatures (T_g) and melting temperatures (T_m) were determined by DSC (Tzero™ Discovery DSC, TA Instruments®) during heating at a rate of 20°C/min. T_g of Crastin® PBT FG 6134 and Pocan® B-600 PBT were 65°C and 60°C, respectively, where T_m of Crastin® PBT FG 6134 and Pocan® B-600 PBT were ~225°C for both of them.

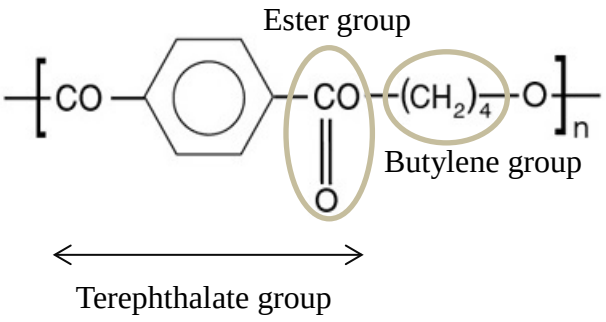

Figure 5.1 Chemical structure of PBT

Degradation temperatures (T_d) were determined by TGA technique (Discovery TGA, TA Instruments®). The resins heated up to 800°C. On-set degradation temperatures of Crastin® PBT FG 6134 and Pocan® B-600 PBT were 325°C and 315°C, respectively. TGA and DSC results of both resins are given in the Appendices. Chemical structure of PBT can be seen at Figure 5.1.

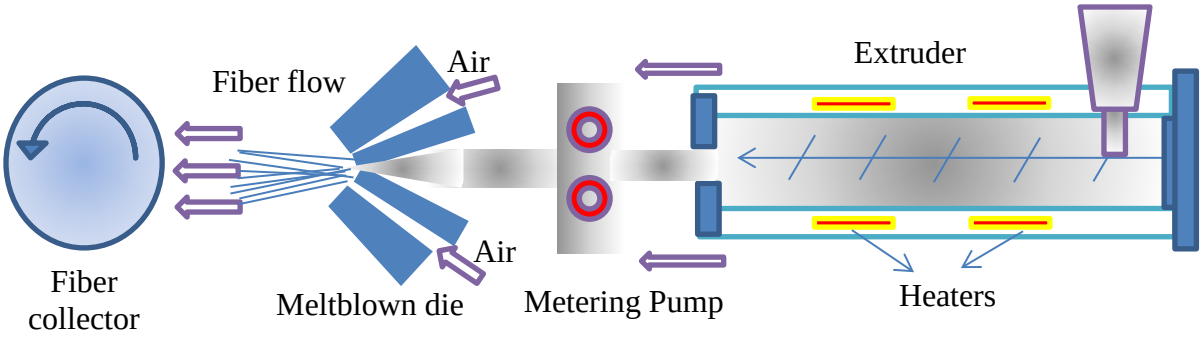

Figure 5.2 Schematic view of the meltblown technique

Prior to spinning, PBT resins were dried at least 4h to reduce the moisture content. Also, melt flow rates were measured by Instron® CEAST, 7026 Melt Flow Tester according to the ASTM 1238. MFRs of Crastin® FG 6134 and Pocan® B-600 PBT were 51 g/10 min, and 335 g/10min at 260°C, respectively. MFR results indicate that Pocan® B-600 has ultra-low viscosity where Crastin® FG 6134 has medium viscosity.

5.1.2 Web Formation

Two sets of meltblown fabrics were produced with a Lab-size Biax Fiberfilm (WI, US) meltblown line under various conditions. Length of the meltblown die was 38cm with 368 capillary holes in 2 rows for polymer extrusion, and 1128 holes of air in 6 rows. Schematic view of the meltblown technique can be seen in Figure 5.2.

In the first set (group 1), Dupont™ Crastin® PBT resin was used as raw material. The capillary size was 508 µm. Processing conditions of the web formation can be seen in Table 5.1 Nonwovens were deposited onto a rotating drum collector with three die-to-collector distances (DCD) that varied from 20 to 40 cm. Fabrics were produced at four different basis weights varying from 60 to 160 g/m^2.

Table 5.1 Meltblown processing conditions for group 1

Sample ID	Throughput (gram/hole/min)	DCD (cm)	Air (kN/m^2)	Basis Weight (g/m^2)
S2-B-A	0.336	20	97	120
S2-B-B	0.336	20	83	120
S2-B-C	0.336	20	73	120
S2-B-D	0.336	20	58	120
S2-B-E	0.245	20	58	120
S2-B-F	0.156	20	58	120
S2-B-G	0.336	20	58	160
S2-B-H	0.336	20	58	80
S2-B-I	0.336	20	58	60
S2-B-J	0.336	30	58	120
S2-B-K	0.336	40	58	120

In the second set (group 2), Lanxess™ Pocan® PBT resin was used as raw material, The capillary size was 228.6 µm. Die temperature was set to 265°C, where die air temperature was 260°C. The processing conditions can be seen in Table 5.2. Nonwovens were deposited onto a rotating drum collector where die-to-collector distance was fixed to 30 cm. Fabrics were produced at four different basis weights varying from 20 to 120 g/m^2.

In addition to meltblown webs produced through Biax meltblown line, another set of meltblown webs, used for membrane formation, were produced through one-meter-wide Reifenhauser REICOFIL™ Meltblown Pilot Line. Line speed varying from 10 to 100 m/min and the die to collector distance varied from 100 mm to 500 mm in this single beam machine. Max die temperature is 310 °C while max air temperature is 350°C. During production of

meltblown webs, DCD varied from 100 to 200 mm where air intensity varied from 600 to 1800. Throughput rates were 0.3, and 0.6 gram per hole per minute. Also, the basis weight varied from 40 to 100 g/m^2.

Table 5.2 Meltblown processing conditions for group 2

Sample ID	Throughput (gram/hole/min)	Air (kN/m^2)	DCD (mm)	Basis Weight (g/m^2)
S3-C-B	0.05	83	300	30
S3-C-C	0.07	83	300	30
S3-C-D	0.09	83	300	30
S3-C-E	0.07	97	300	30
S3-C-F	0.07	69	300	30
S3-C-G	0.07	57	300	30
S3-C-H	0.07	97	300	20
S3-C-I	0.07	97	300	40
S3-C-J	0.07	97	300	60
S3-C-K	0.09	97	300	120

5.1.3 Post-processing

Normally, it is not required to calender meltblown fabrics. But in this study, calendering was utilized to fabricate nonwoven membranes. Three different setups were used for post-processing. First post-processing was carried out through heat press, second post-processing was conducted through lamination device, and third post-processing technique was performed through heated calendar rollers.

5.1.3.1 Through Heat Press

First attempt for formation of membrane was made via heat press (Figure 5.3). Nonwovens used in this setup were produced through REICOFIL™ Meltblown Pilot Line. Throughput, airflow rate, and basis weight were 0.6 ghm (gram per hole per minute), 1600 (m^3/hr), 40, and 60 g/m^2, respectively. Temperature was varied among 180, 200, and 220 °C, while the pressure was kept constant as 6894 kN/m^2, the lowest limit on this setup. Also, residence time was set to 5, 10, and 15 seconds.

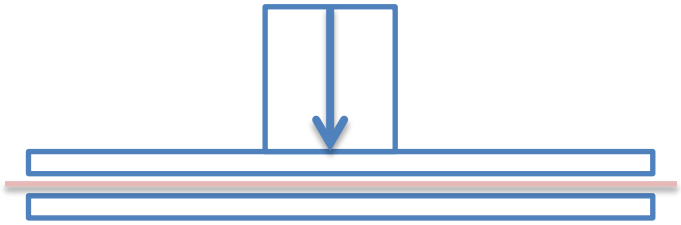

Figure 5.3 Schematic view of the heat press

5.1.3.2 Through Laminator

Two different laminator devices were utilized in this setup. A schematic view of the lamination devices can be seen in Figure 5.4. One of the two laminators was the Stork laminator located at Pilot Plant Lab in College of Textiles. A rubber surface was circulating around a metal cylinder, which was heated by oil in this setup (setup 2-a). The other setup was Klieverik™ heat press calendar located at Coating Lab in College of Textile. Nonwoven fabric was circulating between two rubber surfaces in this setup (setup 2-b).

Setup 2-a

Nonwovens used in Stork laminator machine were produced through REICOFIL™ Meltblown Pilot Line with two different DCD settings (150 and 225 mm). Throughput was

0.6 grams per hole per minute while air intensities were 800, 1300, and 1800 m^3/hr. Post-processing temperature was set to 155, 188, and 215°C, while the pressure was set to 275, 345, and 413 kN/m^2. Cylinder speed was set to 1, 5, and 8 m/min. Maximum pressure was 413 kN/m^2 for this setup.

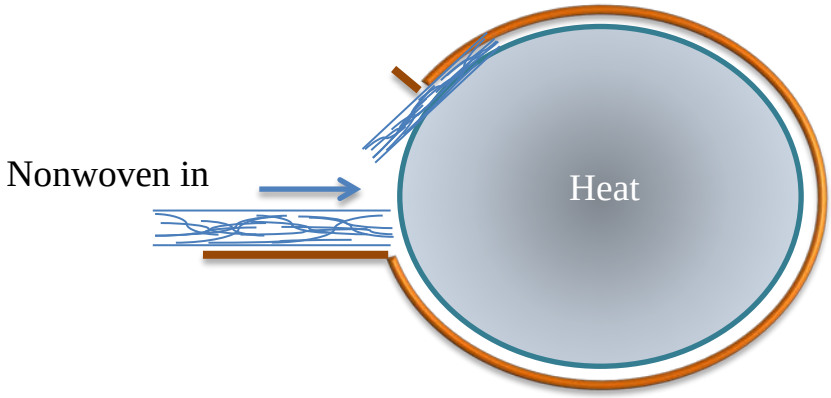

Figure 5.4 Schematic view of the laminator

Setup 2-b

Other used setup was the Klieverik™ heat press calender (setup 2-b) where the nonwovens circulating between two rubber surfaces. In setup 2-b, nonwovens produced through Biax meltblown line (group 1) were used as material. Post-processing temperature was set to 200°C (highest temperature before melting at this setup) while the pressure was 600 kN/m^2 (max limit). Cylinder speed was 2 m/min.

5.1.3.3 Through Heated Calender Rollers

The last setup was heated roller calendering (Figure 5.5) where the nonwovens pass between heated rollers at pre-determined pressure and temperature. Diameters of the rolls were equal to each other (35 cm). Three different sub-configurations have been used for this setup: steel-

steel rollers (setup3-a), rubber-steel rollers (setup 3-b), and steel-steel rollers where the gap between the rollers was pre-determined (setup 3-c).

Setup 3-a

In setup 3-a (steel-steel rollers), nonwovens produced through REICOFIL™ Meltblown Pilot Line have been used as raw material. Throughput was 0.3 gram per hole per minute while air intensity was 1000 m^3/hr. Basis weight was 60 gr/m^2. In this setup, temperature was set to 180°C, 200°C, and 220°C, where pressure was set to 1378, 2068, kN/m^2 2757 kN/m^2. The roller speed was kept constant as 5 m/min.

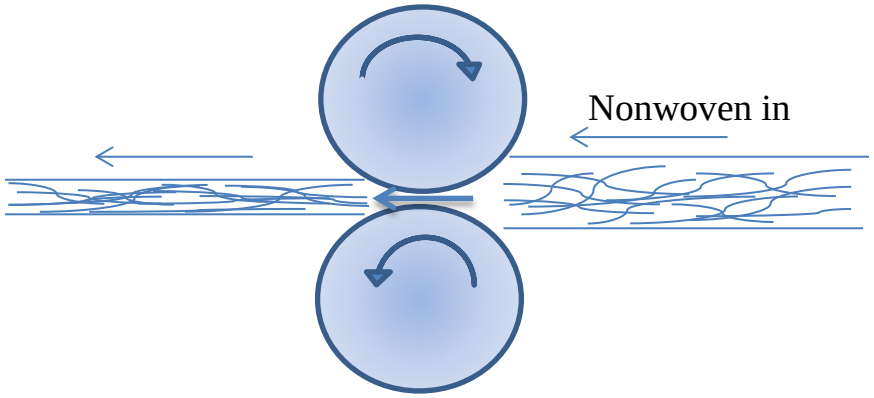

Figure 5.5 Schematic view of calendering

Setup 3-b

Another attempt was made via rubber-steel rollers. One of the rollers was made of steel with smooth surface while the other was made of rubber. Four different meltblown fabrics were used for this experiment. Throughput was 0.6 ghm (gram per hole per minute) for all samples. Airflow rate was 800 and 1200 (m^3/hr), where DCD was between 100 and 200 mm. Basis weight was 100 g/m^2 for all samples. For rubber-steel roller configuration, maximum temperature was 135°C due to decomposition of the rubber. As a result, calendering

temperature was set to 100, 120, and 135 °C. Pressure was set to 1378, 2757, and 4163 kN/m^2. Roller speed was set to 2, 5, and 8 m/min.

Furthermore, the effects of calendering processing conditions on nonwoven characteristics such as pore size and distributions, porosity, and air and water permeability were investigated through this setup.

Setup 3-c

Setup 3-c is a special configuration of heated calender steel rollers (setup 3-a). In this setup, the gap between the smooth steel rollers was set to 75 and 100 µm. The nonwovens produced through Biax Meltblown line (group 2) were calendered at this setup. Temperatures were set to 160°C and 170°C while the roller speed was 5 and 10 m/min.

5.1.4 Producing Nonwovens with Given Pore Size

To reach to a target pore size, model of Wrotnowski was chosen as the basis model. Final pore size was tried to reach by decreasing porosity through calendering. After the web was produced through meltblown technique, characteristics of the nonwoven (fiber size, thickness, and basis weight) were measured. Then, new thickness was calculated according to target pore size with the help of the model. In this calculation, fiber size and basis weight were assumed to remain constant after the post-processing.

Case 1

With regard to this approach, a PBT meltblown nonwoven was produced with 119 g/m^2. Average fiber diameter of this web was 2.82 µm. Fabric's thickness was 1003 µm. Measured

mean flow pore size was 15.92 µm. Targeted pore size was chosen as 2.5 µm. Then, in order to decrease pore size to 2.5 µm, final SVF and thickness were calculated. According to this calculation, SVF and thickness were supposed to be 0.44 and 207 µm, respectively. The calculated thickness was tried to reach through calendering where the gap between rollers was set to 75 µm at 170°C.

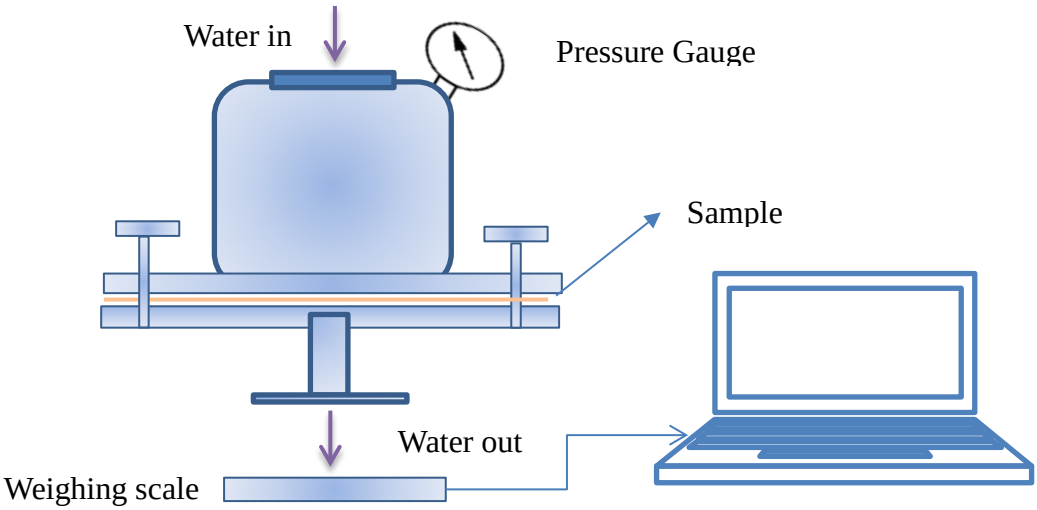

Figure 5.6 Schematic view of the water flux meter

Case 2

Another PBT meltblown web was produced with 40 g/m^2. Average, fiber diameter of this web was 2.29 µm. Fabric's thickness was 355 µm. Measured mean flow pore size was 13.91 µm. Targeted pore size was chosen as 3.5 µm. Then, in order to decrease the mean flow pore size to 3.5 µm, final SVF and thickness were calculated. According to this calculation, SVF, and thickness were supposed to be 0.24 and 125 µm, respectively. The calculated thickness was tried to reach through calendering where the gap between rollers was set to 75 µm at 170°C.

5.1.5 Analytical Methods

Fiber Diameter and Morphology

Nonwoven samples were coated with a thin layer of gold and analyzed by two scanning electron microscopes (Phenom ProX at The Nonwovens Institute and JEOL 7600F at AIF, NCSU) in order to examine the fiber morphology. Fiber diameters were measured using Adobe Acrobat Pro software with at least 100 individual fiber diameter measurements.

Web Thickness

Fabric thickness is one of the most important parameter determining the nonwoven properties such as fabric density. Measurement of thickness was performed at a constant pressure. But surface roughness and variation in basis weight may result in variations. Thickness measurement was carried out according to ASTM D1777 by Precision Thickness Gauge-FT3 (Hanatek Instruments). Ten measurements were taken in units of micrometer (μm). The results were expressed as average, and ± indicates the standard deviations.

Basis Weight

Basis weight measurement was carried out according to ASTM D3776. Three measurements were taken in the unit of gram/m^2. The results were expressed as average, and ± indicates the standard deviations.

Solidity (Solid Volume Fraction)

SVF, was obtained from measured basis weight and thickness, was calculated by using the following equation:

$$\mathrm{SVF} = \left(\frac{\mathrm{G}}{T\,\rho_f} \right) \tag{5.1}$$

Where SVF is the solid volume fraction, G is the fabric basis weight in g/m^2, T is the nonwoven's thickness in μm, and ρ_f is the density of the polymers (fiber) in g/cm^3.

Pore Size and Distribution

Pore structure analysis was carried out using a PMI Capillary Flow Porometer (model CFD-1100-AEL), based on the principle of the liquid extrusion porometry technique[212]. In a typical CFP experiment, the material is filled with a wetting solution (Galwick ™ in this study) whose surface tension is known, and is subject to gas pressure. The pressure on the material is increased in controlled fashion while the flow rate of gas through the material is simultaneously monitored. Closed and blind pores do not allow fluid to pass through; therefore fluid can only pass through open pores. Pore throat diameter, and bubble point (largest pore diameter) are provided with this technique. Pore size distribution measurements were carried out according to the following equation[213,214]:

$$d_p = \frac{4\gamma \cos\theta}{p} \tag{5.2}$$

Where $d_p$is the pore diameter, γ is the surface tension of the wetting liquid, θ is the contact angle of the wetting liquid, p is the extrusion pressure. In this technique, it was assumed that the sample was wetted completely by the wetting solution and therefore contact angle of 0°

was taken for calculations. Three specimen of each nonwoven media were tested. The results were expressed as average.

Air Permeability

Air permeability, mainly depends on pore characteristics such as pore volume, pore size and its distribution, is an important characteristic of nonwoven structures. Air permeability analysis was carried out according to ASTM D 737 with FX-3300 LabAir air permeability tester produced by Textest Instruments (Germany) through a fixed area of 38 cm^2. Ten specimens of each media were tested. The results were expressed as average, and ± indicates the standard deviations.

Table 5.3 Basic web characteristics of group 1 meltblown fabrics

Sample ID	Characteristics				
	Fiber Diameter (µm)	Thickness (µm)	SVF	Mean Flow Pore Diameter (µm)	Largest Pore Diameter (µm)
S2-B-A	11.2(±2.5)	671.1(±15)	0.14	17.51	42.04
S2-B-B	11.6(±2.8)	694.5(±24)	0.13	19.71	47.86
S2-B-C	13.7(±2.1)	712.0(±17)	0.13	23.03	55.88
S2-B-D	15.1(±1.9)	749.1(±17)	0.12	41.10	67.72
S2-B-E	11.8(±2.1)	702.2(±19)	0.13	27.34	51.63
S2-B-F	9.4(±1.8)	703.6(±22)	0.14	24.11	36.65
S2-B-G	14.9(±1.3)	825.7(±27)	0.15	28.84	58.61
S2-B-H	15(±2.2)	682.1(±14)	0.09	47.18	103.00
S2-B-I	15.6(±2.1)	658.1(±16)	0.07	63.45	111.78
S2-B-J	14.9(±2.2)	780.2(±17)	0.12	37.30	76.25
S2-B-K	14.9(±2.1)	810.2(±31)	0.11	41.50	77.90

Clean Water Permeability (CWP)

Clean water permeability was measured through the water flux meter located at the College of Textiles, NCSU. The device measures how much water passes in unit time through the medium at predetermined pressure (Figure 5.6). Area of the circular specimen was 45 cm^2. Clean water poured into the vessel where pressured gas was added into. Subsequently, the quantity of water passes through the nonwoven was measured on a weighing scale. Three specimens of each media were tested and results were obtained in the unit of g/sec per 45.5 cm^2 at 0.2 Bar.

5.2 Results and Discussion

5.2.1 Basic Characteristics of Meltblown Webs

The webs in group 1 were produced shot-free for all cases. However, few shots were observed for sample S3-C-K in group 2. It was likely due to the low molecular weight PBT resin. Pocan B-600 PBT resin had ultra-low viscosity which was the result of low molecular weight. For size-exclusive membranes, not only mean pore diameter but also largest pore diameter (bubble point) affects the water quality. This is why largest pore diameters also provided in addition to mean flow pore diameter.

Table 5.3 shows the basic web characteristics of group 1 meltblown fabrics. Standard deviations are given in parentheses in the Table 5.3. Fiber diameters were in the range of 9.4 and 15.6 μm. Standard deviations of fiber diameters were less than 30% of average fiber diameter. Thicknesses and solidities of the samples were consistent in a reasonable range.

Mean flow pore sizes were in the range of 17.51 and 63.45 µm. Pore size characteristics also shows that these webs had wide pore size distributions compared to the PVDF membrane.

Table 5.4 Basic web characteristics of group 2 meltblown fabrics

Sample ID	Characteristics				
	Fiber Diameter (µm)	Thickness (µm)	SVF	Mean Flow Pore Diameter (µm)	Largest Pore Diameter (µm)
S3-C-B	1.75(±1.1)	256.4(±19)	0.09	10.8	20.5
S3-C-C	2.26(±0.8)	264.2(±3.1)	0.09	13.8	22.8
S3-C-D	2.9(±1.1)	283.4(±4.1)	0.08	15.4	29.5
S3-C-E	2.12(±1.2)	260(±5.2)	0.09	13.6	18.9
S3-C-F	3.26(±1.3)	279.1(±4.7)	0.08	17.4	28.5
S3-C-G	3.43(±1.5)	258.3(±3.2)	0.09	19.4	29.6
S3-C-H	2.37(±1.2)	181(±3.6)	0.08	14.4	32.2
S3-C-I	2.29(±1)	355(±7.5)	0.09	13.9	22.2
S3-C-J	2.32(±0.9)	530.8(±7.8)	0.09	12.9	20.9
S3-C-K	2.82(±1.4)	1003(±14)	0.09	15.9	27.9

Table 5.4 shows the basic web characteristics of group 2 meltblown fabrics. Standard deviations are given in parentheses in the Table 5.4. Fiber diameters were in the range of 1.75 and 3.43 µm. Standard deviations of the fiber diameters were less than 50% of average fiber diameter. Thicknesses and solidities of the samples were consistent in a reasonable range as in the group 1. Mean flow pore sizes were in the range of 10.8 and 19.4 µm. Pore size characteristics are a priority for separation media. Pore size characteristics indicate that these webs have narrower pore size distributions compared to group 1 samples. Smaller

fibers resulted in not only smaller mean flow pore sizes, but also narrower pore size distributions.

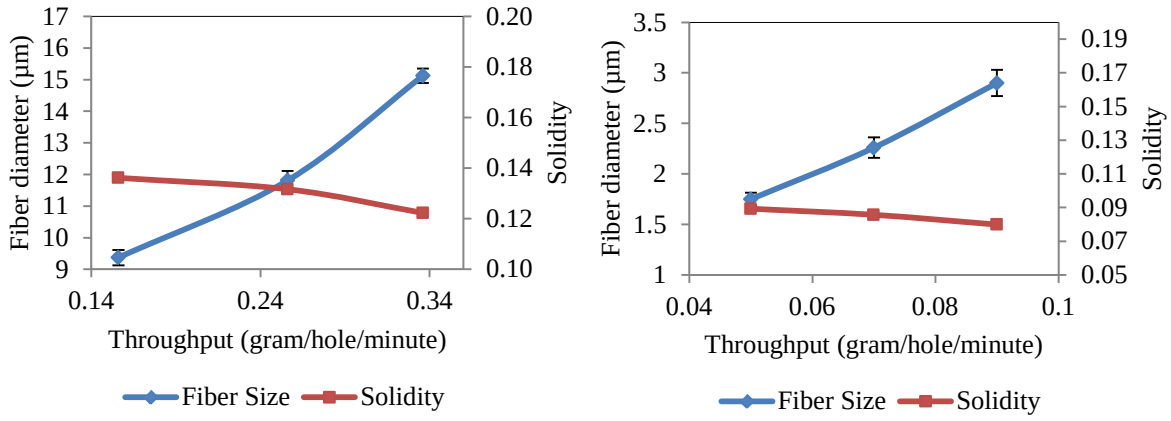

Figure 5.7 Effects of throughput on fiber size and SVF for group 1 (left) and group 2 (right) meltblown webs

5.2.2 Effects of Operating Parameters on Structure Properties

Structure properties determine the characteristics of nonwovens such as permeability and pore size. Pore models proved that there are two critical parameters determining mean pore diameter: fiber size and SVF. In other words, controlling mean pore size of nonwovens requires controlling fiber size and SVF. Therefore, how meltblown processing parameters affect the fiber size and SVF was studied.

Figure 5.7 shows the effects of polymer throughput on average fiber diameter. It was observed that as polymer throughput decreased, average fiber diameter decreased. Decreasing polymer flow rate decreased average fiber diameter because same drag force from the air jet acted on a smaller polymer mass.

Throughput

Throughput 0.05 ghm	Throughput 0.07 ghm	Throughput 0.09 ghm
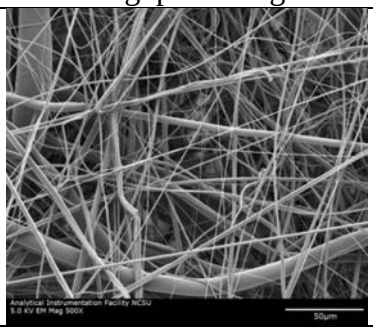	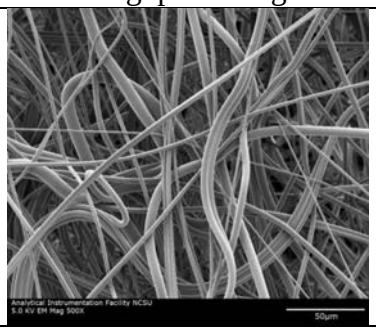	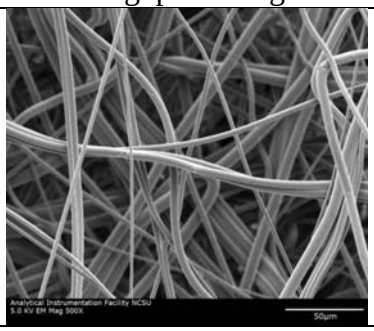
d_f= 1.75 µm	d_f= 2.26µm	d_f= 2.9 µm

Figure 5.8 SEM images of the samples: S3-C-B (left), S3-C-C (middle), and S3-C-D (right)

Figure 5.7 also shows the effect of polymer throughput on SVF. As seen from Figure 5.7, SVF change was so small for both series. SVF tends to decrease while polymer throughput increased. A small decrease in SVF was thought to occur due to fact that small fibers can result in better compactness.

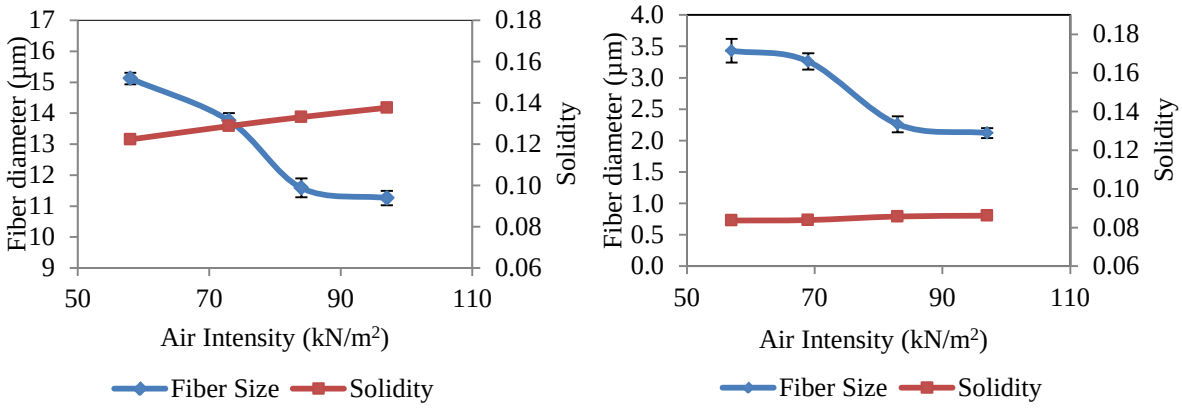

Figure 5.9 Effects of air flow on fiber size and SVF for group 1 (left) and group 2 (right) meltblown webs

Figure 5.8 shows the SEM images of the nonwovens from group 2 with different throughputs. As seen from the Figure 5.8, as polymer throughput increased, fiber size was getting bigger.

Air Flow

Figure 5.9 shows the effect of air flow rate on average fiber size. It was observed that as air flow rate increased, average fiber diameter decreased. Increasing air flow rate decreased average fiber diameter because more drag force from the air jet acted on the same polymer mass.

Air flow 57 kN/m^2	Air flow 83 kN/m^2	Air flow 97 kN/m^2
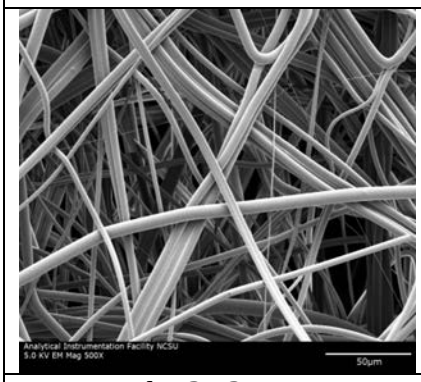	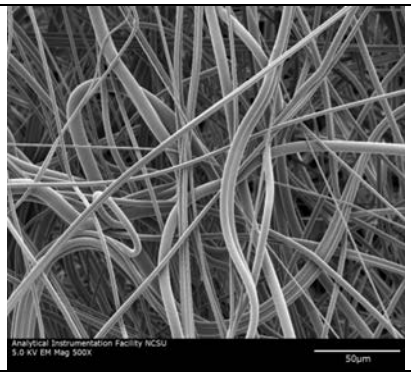	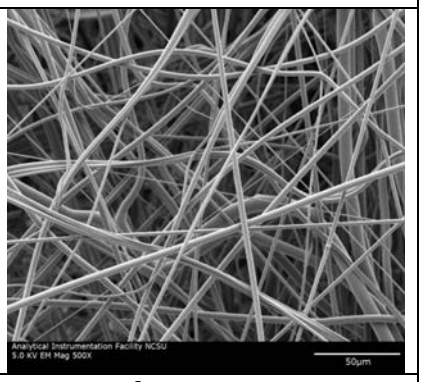
d_f= 3.43 µm	d_f= 2.26 µm	d_f= 2.12 µm

Figure 5.10 SEM images of the samples: S3-C-G (left), S3-C-C (middle), and S3-C-E (right)

Figure 5.9 also shows that the effect of air flow rate on SVF. As seen from the Figure 5.9, SVF change was so small. However, there was a slight increase in SVF as air flow rate increased. A slight increase in SVF is thought to occur due to the fact that, small fibers can result in better compactness.

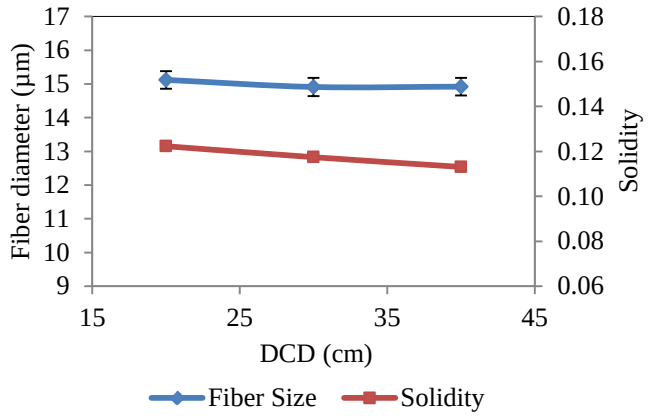

Figure 5.11 Effects of die to collector distance on fiber size and SVF for group 1 meltblown webs

Figure 5.10 shows the SEM images of the nonwovens from group 2 with different air flow rates. As seen from the Figure 5.10, as air flow rate increased, fiber size decreased.

DCD 200 mm	DCD 300 mm	DCD 400 mm
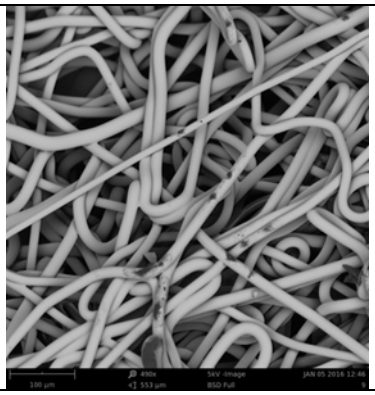	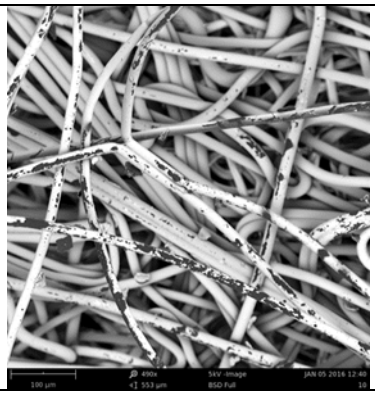	
d_f= 15.12 µm	d_f= 14.91	d_f= 14.92 µm

Figure 5.12 SEM images of the samples : S2-B-D (left), S2-B-J (middle), and S2-B-K (right)

Die to Collector Distance

Figure 5.11 shows the effect die to collector distance on fiber size and SVF. It was observed that as DCD increased, average fiber diameter did not change considerably. It is well-known that die to collector distance has more effect on compactness of the web. Increasing DCD

decreased SVF slightly (less compact structure) because air drag force gradually decreased as the distance from die to collector increased.

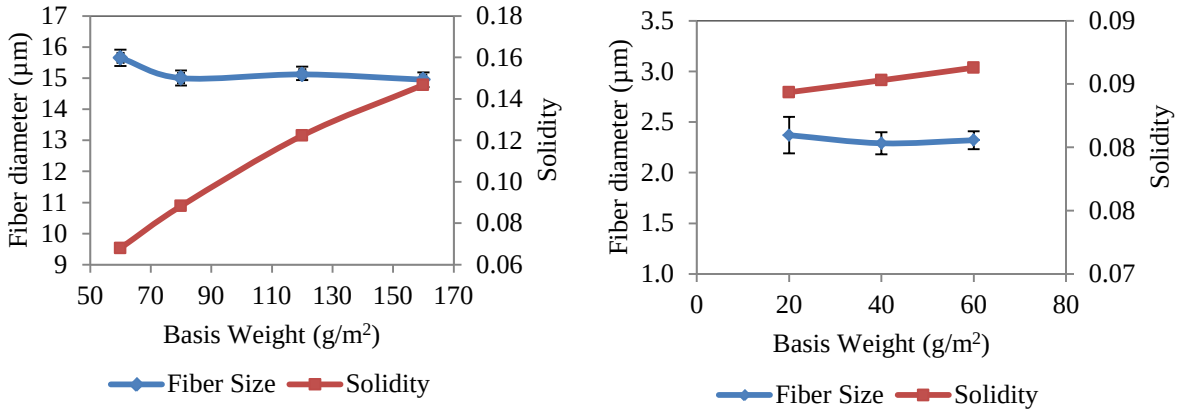

Figure 5.13 Effects of basis weight on fiber size and SVF for group 1 (left) and group 2 (right) meltblown webs

Figure 5.12 shows the SEM images of the nonwovens from group 1 with different DCDs. As seen from the Figure 5.12, as die to collector distance increased, average fiber diameter did not change considerably.

Basis Weight

Figure 5.13 shows the effect of basis weight on fiber size and SVF. It was observed that as basis weight increased, average fiber diameter did not change considerably. Since basis weight was determined by collector speed, no effect on fiber size was observed. Increasing basis weight increased SVF because as more layers deposited onto the web, compactness of the web increased.

5.2.3 Effects of Operating Parameters on Pore Size

Pore size models showed that mean pore size is the function of structure properties such as fiber size, SVF, and basis weight. In other words, structure properties determine the nonwoven characteristics such as mean flow pore size. Therefore, the relation between meltblowing operating parameter and pore size characteristics provides insights for controlling pore size during web formation.

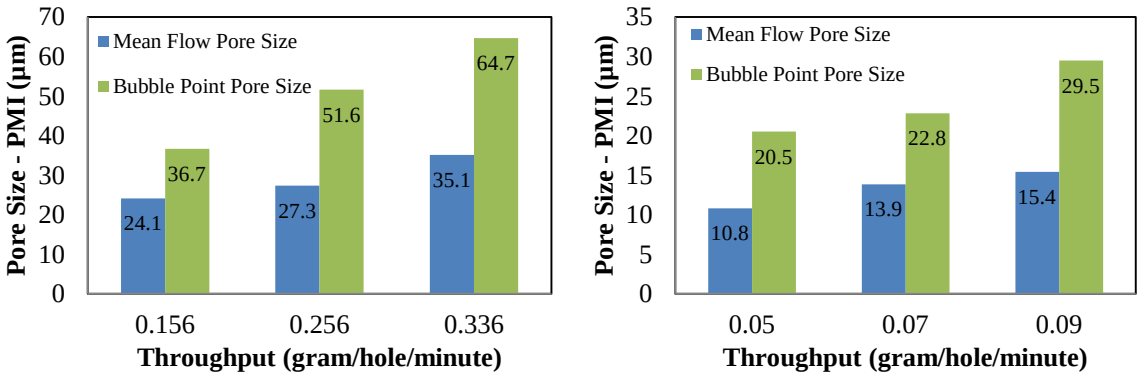

Figure 5.14 Effects of throughput on pore size for group 1 (left) and group 2 (right) meltblown webs

Figure 5.14 shows the effects of throughput on pore size characteristics. It was observed that as throughput increased, mean flow pore size increased. Since increasing the throughput increased the average fiber diameter and number of pores in unit area decreased. As a result, increasing the throughput resulted in bigger mean flow pore size. In like manner, largest pore sizes increased with increasing throughput.

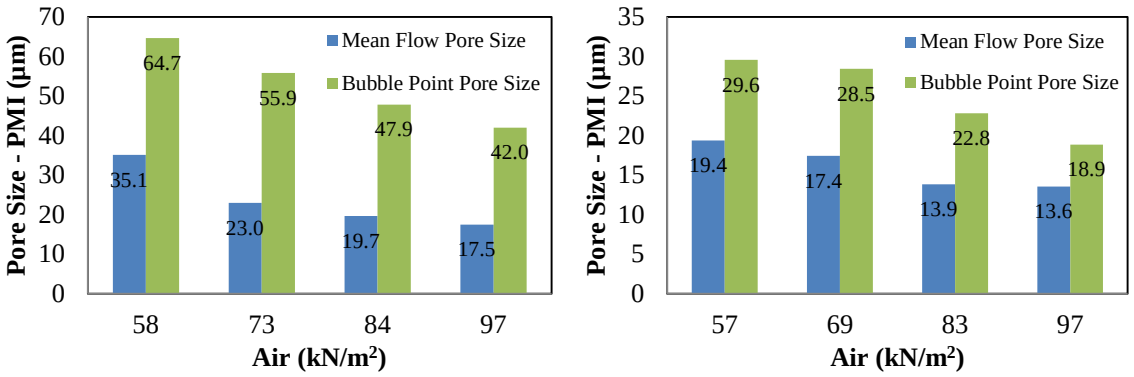

Figure 5.15 Effects of air flow on pore size1 (left) and group 2 (right) meltblown webs

Figure 5.15 shows the effects of air flow on pore size characteristics. It was observed that as air flow increased, mean flow pore size decreased. Since decreasing the air flow increased the average fiber diameter, and consequently number of pores in unit area decreased. Therefore, decreasing the air flow resulted in bigger mean flow pore size. Also, largest pore sizes decreased with increasing air flow.

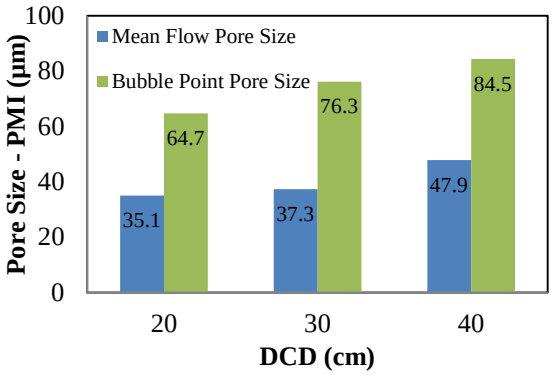

Figure 5.16 Effects of die to collector distance on pore size for group 1 meltblown webs

Figure 5.16 shows the effects of die to collector distance on pore size characteristics. It was observed that as DCD increased, mean flow pore size increased. Since decreasing the DCD increased the SVF, total pore volume in unit area decreased. As a result, decreasing the DCD

resulted in lower mean flow pore size. In addition, largest pore sizes increased with increasing DCD.

Figure 5.17 shows the effects of basis weight on pore size characteristics. It was observed that as basis weight increased, mean flow pore size decreased. Increasing the basis weight increased the SVF. Hence, increasing the basis weight resulted in lower mean flow pore size. Moreover, largest pore sizes decreased with increasing basis weight.

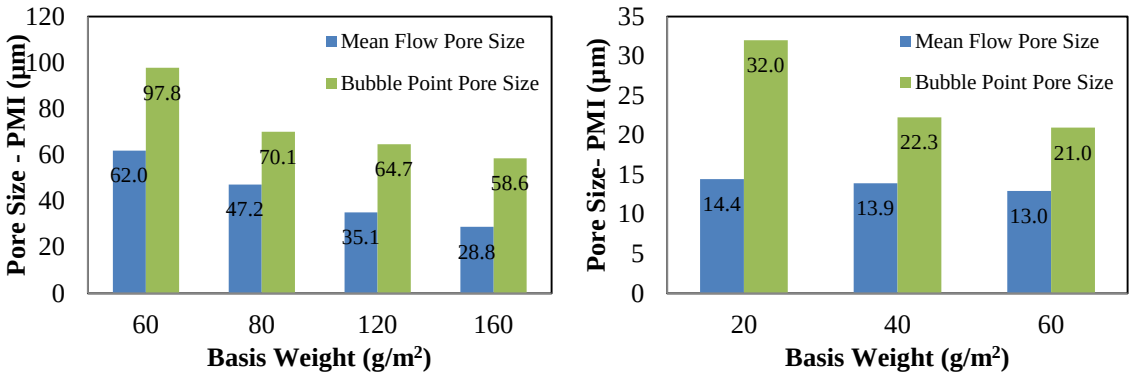

Figure 5.17 Effects of basis weight on pore size for group 1 (left) and group 2 (right) meltblown webs

5.2.4 Basic Web Characteristics after Post-processing

5.2.4.1 Post-processing through Heat Press

Highest temperature was 200°C for this setup. The nonwoven samples melted above 200°C. Lowest pressure was 6894 kN/m^2. Fabric damage in addtion to the adhesion of the samples to the plates was observed due to excessive pressure.

Table 5.5 shows the web characteristics after the heat press process. The percentage of the fiber diameter increase was from 5 to 20%. Thickness compression increased with increasing

dwell time. This was also expected because as dwell time increased, more compression occurred due to more heat transfer. The percentage of the nonwoven thickness compression was from 48 to 58%. Basis weights after the post-processing did not increase significantly (from 0 to 4 %). The percentage of the mean flow pore size decrease was around 30%.

Table 5.5 Web characteristics after post-processing through heat press

Sample ID	Post-Processing Parameters			Characteristics				
	Pressure (kN/m^2)	Temperature (°C)	Time (sec)	Fiber Diameter (µm)	Basis Weight (g/m^2)	Thickness (µm)	SVF	Mean Flow Pore Diameter (µm)
S1-A	Uncalendered			6.03(±3.1)	47(1.1)	350(±41)	0.10	18.66(±7.41)
S1-A1	6894	200	5	6.62(±2.9)	49(±0.6)	182(±18)	0.21	12.87(±6.05)
S1-A2	6894	200	10	7.11(±2.9)	49(±1.2	150(±17)	0.24	12.68(±6.06)
S1-A3	6894	200	15	7.13(±4.9)	47(±0.6)	148(±14)	0.24	12.98(±6.15)

Figure 5.18 shows the images of the uncalendered and calendered samples post-processed through heat press. More compact structures were expected after the post-processing. However, this change was not observed through the SEM images.

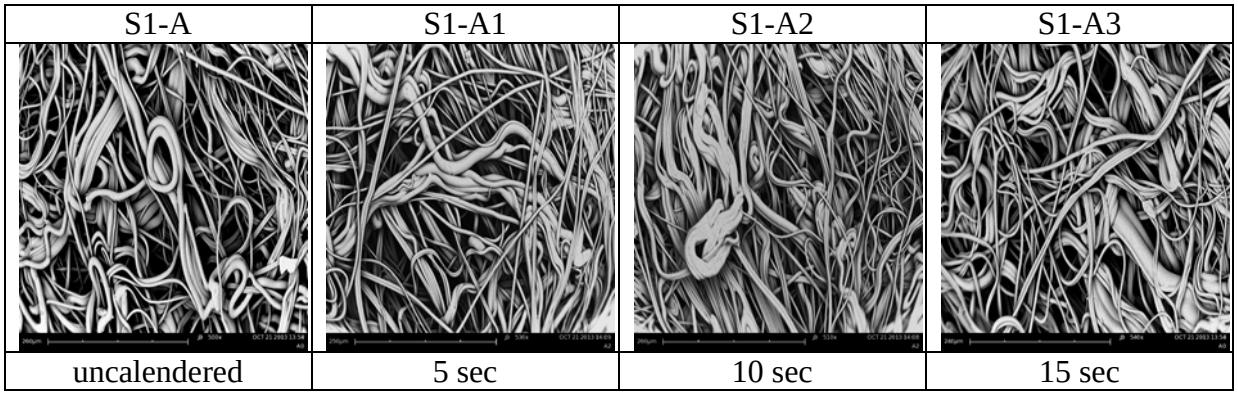

Figure 5.18 SEM images after post-processing through heat press

As a result, the basic web characteristics and the SEM images indicate that desired microporous membrane-like structure was not formed after the post-processing through heat press. Because, the pressure was excessive for membrane formation. Moreover, mean flow pore sizes still had large standard deviations compared to the PVDF membrane used in this study.

5.2.4.2 Post-processing through Laminator

Lamination devices utilize heat and pressure like heated calendering rollers. However, lamination is operated at low pressures compared to calendering. Therefore, lamination devices can be regarded as light calendering due to lower pressure.

Stork Laminator (Setup 2-a)

344 kN/m^2 was the highest pressure, while 0.1 m/min belt speed was the lowest in this setup.

Table 5.6 Web characteristics after post-processing through laminator (setup2-a)

Sample ID	Post-Processing Parameters			Characteristics				
	Pressure (kN/m^2)	Temperature (°C)	Belt Speed (m/min)	Fiber diameter (µm)	Basis Weight (g/m^2)	Thickness (µm)	SVF	Mean Flow Pore Diameter (µm)
S2-A-C	**Uncalendered**			7.93(±2.1)	112(±7.4)	735(±42)	0.12	14.37(±8.7)
S2-A-C1	344	155	0.1	8.36(±1.9)	110(±12.4)	622(±18)	0.13	11.24(±8.4)
S2-A-C2	344	185	0.1	8.30(±2.1)	110(±6.9)	619(±17)	0.14	11.2(7.4)
S2-A-C3	344	215	0.1	8.7(±2.3)	114(±9.8)	545(±33)	0.16	10.58(±8.3)

Table 5.6 shows the web characteristics after post-processing through Stork laminator. Fiber diameter increase was observed after this post-processing. The percentage of the fiber diameter increase was from 4 to 9%. Thickness compression increased with increasing

temperature. This is also expected because as temperature increases, more compression occurs due to more heat flow. The percentage of the nonwoven thickness compression was from 15 to 26%. With regard to small compression ratios, SVFs did not increase considerably. Additionally, basis weights after the post-processing did not increase significantly. The percentage of the mean flow pore size decrease is from 21 to 26%.

S2-A-C	S2-A-C1	S2-A-C2	S2-A-C3
	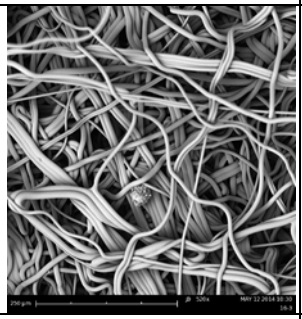		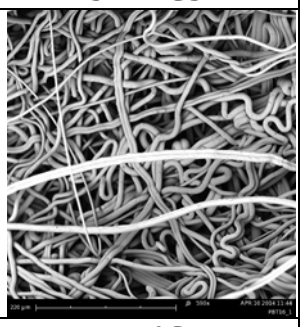
Uncalendered	155°C	185°C	215°C

Figure 5.19 SEM images after post-processing through laminator (setup 2-a)

Figure 5.19 shows the images of the uncalendered and calendered samples post-processed through Stork laminator. More compact structures and smooth surfaces were expected after the post-processing. However, only a small change was observed with increasing post-processing temperature. Desired structure was not formed on the surface of the nonwovens after the post-processing through Stork laminator.

SVF increase and mean flow pore size decrease were not significiant. Moreover, mean flow pore sizes still had large standard deviations. The basic web characteristics and the SEM images indicate that desired microporous membrane structure was not formed after the post-processing through Stork laminator. Because, the pressure was not sufficient to form membrane-like structure.

6Klieverik Laminator (Setup 2-b)

600 kN/m^2 was the highest pressure while 200°C was the highest temperature in this setup. Above 200°C, the nonwoven samples melted. In this setup, desired microporous web structure could not be formed due to unsufficienct pressure (same reason for the other lamination device).

Table 5.7 Web characteristics after post-processing through laminator (setup2-b)

Sample ID	Post-Processing Parameters			Characteristics				
	Pressure (kN/m^2)	Temperature (°C)	Speed (m/min)	Fiber diameter (µm)	Basis Weight (g/m^2)	Thickness (µm)	SVF	Mean Flow Pore Diameter (µm)
S2-B-F	Uncalendered			9.37(±1.9)	125.5(±4.8)	703(±22)	0.14	24.11(±9.9)
S2-B-F-C	600	200	2	11.05(±2.3)	131.6(±4.4)	573(±88)	0.18	18.86(±9)
S2-B-G	Uncalendered			14.95(±2)	158.7(±2.2)	825(±27)	0.15	28.84(±14.6)
S2-B-G-C	600	200	2	15.81(±2.1)	164.5(±2.9)	664(±16)	0.19	24.35(±13)
S2-B-H	Uncalendered			15(±1.9)	78.9(±2.8)	682(±14)	0.09	47.18(±24.3)
S2-B-H-C	600	200	2	15.97(±2.4)	81.6(±1.7)	441(±35)	0.14	38.90(±18.9)
S2-B-I	Uncalendered			15.65(±2.1)	58.6(±0.9)	658(±16)	0.07	61.95(±37)
S2-B-I-C	600	200	2	16.03(±2.2)	61(±1.1)	372(±19)	0.12	42.02(±24)

Table 5.7 shows the web characteristics after post-processing through Klieverik laminator. Fiber diameter increase was observed after the post-processing. The percentage of the fiber diameter increase was from 5 to 22%. Thickness compression was consistent for all samples. The percentage of the nonwoven thickness compression was from 18 to 43%. In spite of the thickness compression, SVF decrease was not significant for all samples. Basis weights after the post-processing increased slightly. The percentage of basis weight increase was from 3 to 4%. The percentage of the mean flow pore size decrease was from 16 to 32%.

S2-B-F	S2-B-G	S2-B-H	S2-B-I
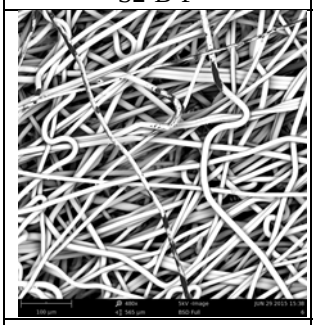	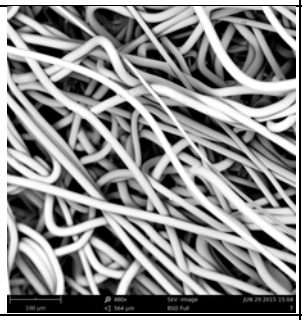	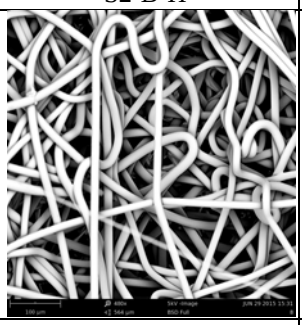	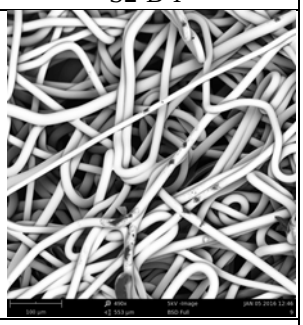
Uncalendered	Uncalendered	Uncalendered	Uncalendered
S2-B-F-C	S2-B-G-C	S2-B-H-C	S2-B-I-C
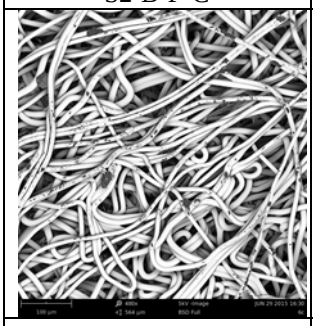	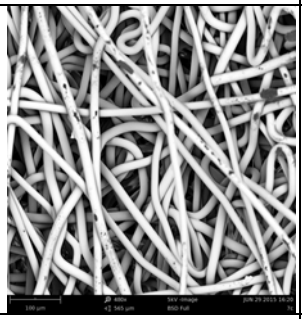		
Calendered	Calendered	Calendered	Calendered

Figure 5.20 SEM images after post-processing through laminator (setup 2-b)

Figure 5.20 shows the images of the uncalendered and calendered samples post-processed through Klieverik laminator. More compact structure and smooth surfaces were expected after the post-processing. However, almost no change was observed after the post-processing through the Klieverik Laminator. Desired structure was not formed on the surface of the nonwovens after this setup.

The basic web characteristics and the SEM images indicate that satisfactory membrane-like structure was not formed after the post-processing through Klieverik laminator. Because, SVF increase and mean flow pore size decrease were not significant. Furthermore, mean flow pore sizes still have large standard deviations.

5.2.4.3 Post-Processing through Heated Calender Rollers

Steel-steel rollers (Setup 3-a)

2757 kN/m^2 was the highest pressure while 200 °C was the highest temperature before melting. Even if the pressure decreased to 1378 kN/m^2, Fabric damage, in addition to adhesion of the samples to the cylinder rollers, was observed. Because of the partial melting, nonwoven fabrics turned into a film-like structure.

Table 5.8 Web characteristics after post-processing through calender rollers (setup3-b)

Sample ID	Post-Processing Parameters			Outputs				
	Pressure (kN/m^2)	Temperature (°C)	Speed (m/min)	Fiber Diameter	Basis Weight (g/m^2)	Thickness (µm)	SVF	Mean Flow Pore Diameter (µm)
S3-B-A	**Uncalendered**			10.8(±2.4)	104(±3.8)	894.80 (±13)	0.11	23.31 (±20.9)
S3-B-A1	2757	100	5	12(±2.7)	96(±1)	534.40(±17)	0.16	12.19 (±11.1)
S3-B-A2	2757	120	5	12.6(±2.6)	99(±2.1)	492.60(±26)	0.18	10.78 (±10.1)
S3-B-A3	1378	135	5	11.6(±2.1)	98(±3.2)	482.00(±9)	0.18	10.82 (±9.3)
S3-B-A4	2757	135	2	11.5(±2.2)	93(±1.7)	423.40(±11)	0.20	9.42 (±9.2)
S3-B-A5	2757	135	5	12.7(±3.2)	92(±2.6)	439.00(±21)	0.19	10.45 (±9.6)
S3-B-A6	2757	135	8	12.3(±2.5)	94(±4)	442.40(±10)	0.19	11.17 (±10.1)
S3-B-A7	4136	135	5	12.4(±2.1)	91(±3.6)	321.00(±11)	0.26	8.93 (±8.22)

Steel-Rubber rollers (Setup 3-b)

Main advantage of using rubber roller was that no fabric damage occured compared to steel rollers. Elasticity of the rubber prevented this damage. However, 135°C was the highest temperature before the rubber degrade. It was quite low for memrbane formation considering the melting point of PBT (~224°C).

Table 5.8 shows the web characteristics after the post-processing through heated calender roller setup. The percentage of the fiber diameter increase was from 6 to 11%. Thickness compression increased with decreasing roller speed. This was also expected because as dwell time increases, more compression occurs due to more heat transfer. The percentage of the nonwoven thickness compression was from 40 to 64%. At this time, contrary to previous setups, basis weights after the post-processing through this setup decreased slightly (5 to 12%). Percentage of the mean flow pore size decrease was from 47 to 61%.

S3-B-A	S3-B-A1	S3-B-A2	S3-B-A5
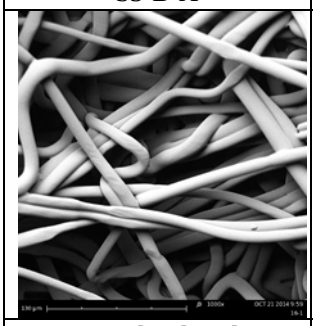			
Uncalendered	100 °C	120 °C	135 °C

Figure 5.21 SEM images after post-processing through calender rollers (setup 3-b) with different temperatures

Figure 5.21 shows the images of the uncalendered and calendered samples post-processed through setup 3b with different temperatures. More compact structures occurred after the post-processing. This is why fibers are tightly packed as a result of calendering. Therefore, more compact structure can be seen as the temperature increased, because more heat was transferred as temperature increased.

S3-B-A	S3-B-A3	S3-B-A5	S3-B-A7
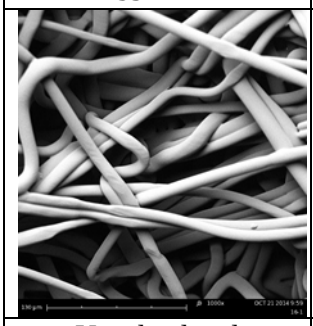		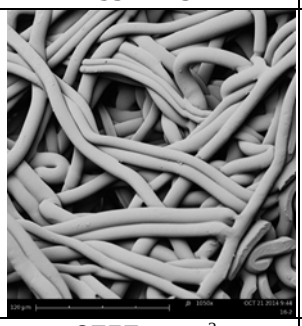	
Uncalendered	1378 kN/m^2	2757 kN/m^2	4136 kN/m^2

Figure 5.22 SEM images after post-processing through heated calender rollers (setup 3-b) with different pressures

Figure 5.22 shows the images of the uncalendered and calendered samples post-processed through setup 3b with different pressures. More compact structures were expected as the pressure increased. Consequently, fibers were tightly packed as pressure increased due to more heat transfer.

S3-B-A	S3-B-A4	S3-B-A5	S3-B-A6
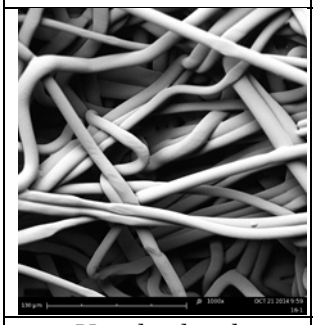			
Uncalendered	2 m/min	5 m/min	8 m/min

Figure 5.23 SEM images after post-processing through heated calender rollers (setup 3-b) with different dwell times

Figure 5.23 shows the images of the uncalendered and calendered samples post-processed through setup 3b with different dwell times. Dwell time increases as roller speed decreases. Therefore, more compact structures were expected as dwell time increased. Fibers were

tightly packed as dwell time increased as result of calendering. Because, more heat was transferred as dwell time increased.

Table 5.9 Web characteristics after post-processing through calender rollers (setup3-c)

Sample ID	Post-Processing Parameters			Characteristics				
	Temperature (°C)	Speed (m/min)	Gap between rollers (µm)	Fiber Diameter (µm)	Basis Weight (g/m^2)	Thickness (µm)	SVF	Mean Flow Pore Diameter (µm)
S3-C-B	Uncalendered			1.75(±1.1)	32(±1.5)	256.4(±19)	0.09	10.81(±4.2)
S3-C-B-C	170	10	100	2.1(±1.2)	33(±0.6)	177(±7)	0.14	9.2(±3.2)
S3-C-C	Uncalendered			2.26(±0.8)	30(±0.6)	264.2(±3.1)	0.09	13.8(±5.2)
S3-C-C-C	170	10	100	2.23(±1.1)	31(±1.8)	164(±4)	0.15	11.9(±3.9)
S3-C-D	Uncalendered			2.9(±1.1)	30(±0.6)	283.4(±3.9)	0.08	15.4(±5.7)
S3-C-D-C	170	10	100	3.34(±1.2)	32(±2.7)	168(±7)	0.14	13.7(±4.9)
S3-C-E	Uncalendered			2.12(±1.2)	29(±1.6)	260(±5.2)	0.09	13.6(±5)
S3-C-E-C	170	10	100	2.13(±1.2)	32(±1.6)	170(±8.4)	0.14	10.5(±3.1)
S3-C-F	Uncalendered			3.26(±1.3)	31(±0.6)	279.1(±4.6)	0.08	17.4(±6.5)
S3-C-F-C	170	10	100	3.3(±1.3)	31(±1.6)	171(±12)	0.14	13.32(±4.1)
S3-C-G	Uncalendered			3.43(±1.5)	30(±1.5)	258.3(±3.5)	0.09	19.4(±7.4)
S3-C-G-C	170	10	100	3.67(±1.4)	31(±1.6)	174(±6.2)	0.14	13.6(±4.7)
S3-C-I	Uncalendered			2.29(±1)	40(±1.2)	355(±10)	0.09	13.9(±5.5)
S3-C-I-C	170	10	75	2.39(±0.9)	42(±2.1)	108(±8.9)	0.30	4.6(±2)
S3-C-K	Uncalendered			2.82(±1.4)	119(±2.5)	1003(±14)	0.09	15.9(±7.2)
S3-C-K-C	170	10	75	3.1(±1.4)	130(±3.2)	211(±13.5)	0.47	3.02(±2.2)

Even if the surface of the nonwovens after calendering looked smoother compared to previous techniques, desired microporous membrane-like structure was not formed through

setup 3-b. SVF increase and mean flow pore size decrease were not significant. Furthermore, mean flow pore sizes still had large standard deviations.

Steel-Steel rollers where the gap is predetermined (Setup 3-c)

Main advantage of this setup was the more control on final thickness compared to previous setups. Even if some of the thickness compression recovered after the pressure was released, desired thickness can be reached with this setup.

Table 5.9 shows the web characteristics after the post-processing through setup 3-c. The percentage of the fiber diameter increase was from 1 to 20%. Thickness compression was observed for all samples. The percentage of the nonwoven compression was around 30% when the gap between rollers was 100 µm. The compression was around 80% when the gap between the rollers was 75 µm. Basis weights after the post-processing increased slightly (3 to 9%). Basis weight increase was greater for the sample S3-C-K due to its greater basis weight (119 g/m^2) compared to other samples. SVF increase was significant when the gap between the rollers were set to 75 µm (from 0.09 to 0.30 and 0.47). Also when the gap distance was 0.75 µm, the percentage of pore size decrease was from 67 to 81 % (from 13.91 µm to 4.62 µm, and from 15.92 µm to 3.02 µm).

Figure 5.24 shows the images of the uncalendered and calendered samples post-processed through steel rollers, where the gap between rollers was predetermined. As a result, more compact structures were expected after the post-processing. As seen from Figure 5.24, fibers were tightly packed as a result of calendering. Very smooth surface with tightly packed fibers was observed for the sample S3-C-K compared to the uncalendered sample.

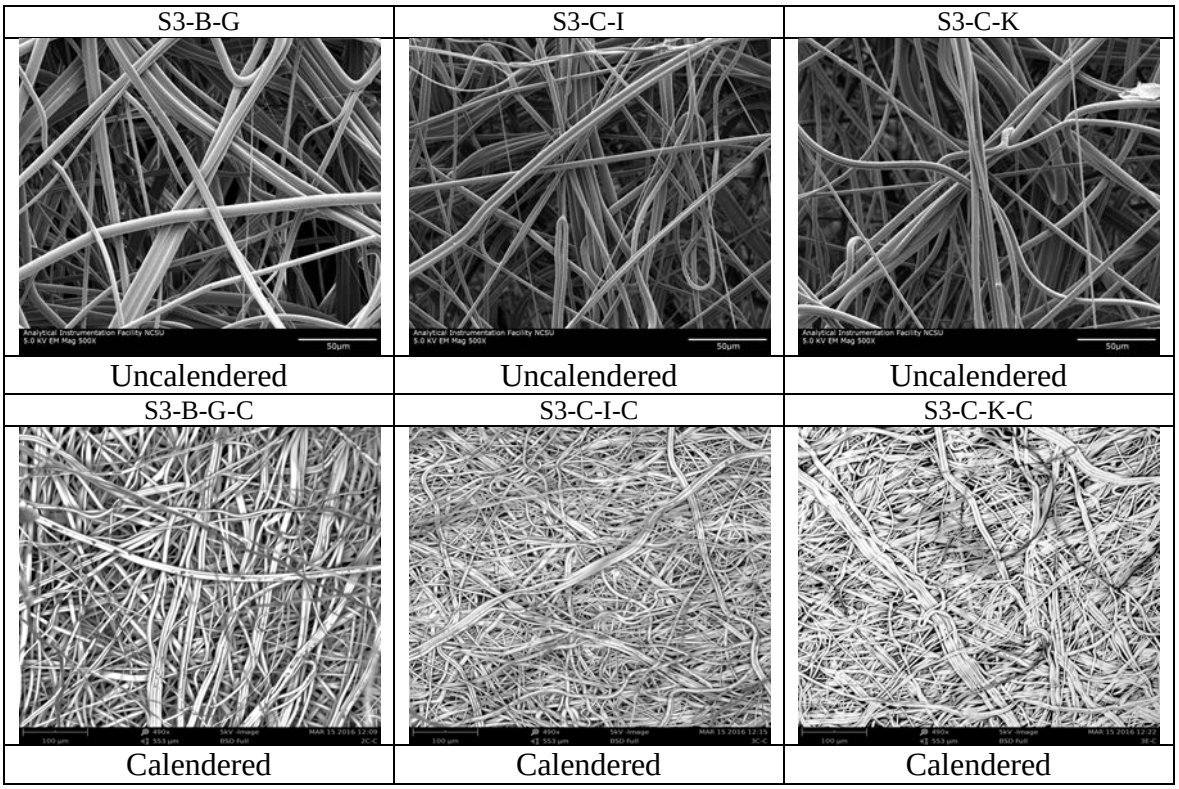

Figure 5.24 SEM images after post-processing through heated calender rollers (setup 3-c)

Figure 5.25 shows the cross-section images of the sample S3-C-K before and after calendering. As seen from the figure, fibers were tightly packed after calendering. Some of fibers' cross-section was non-round shaped for uncalendered sample. Many fibers with round cross-sectional shape were observed after calendering. Therefore, we can assume that, changes on cross-sectional shape of the fibers have not been observed for the fibers inside the web. However, cross-sectional shape of the fibers near to the surfaces of the web may have changed because; there was a direct contact between the heated rollers and the fibers near to the surface.

S3-C-K	S3-C-K-C
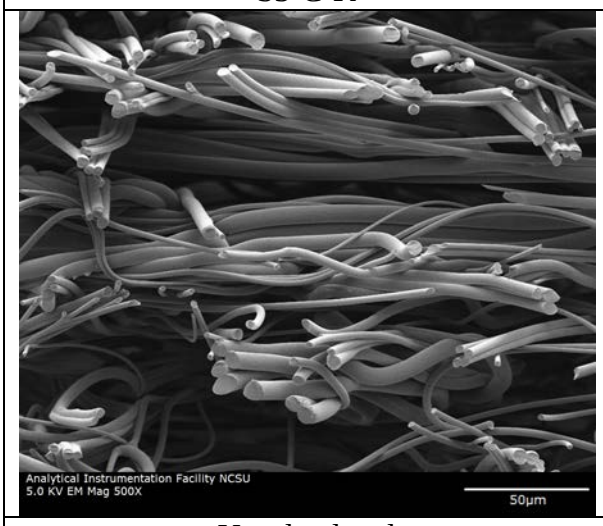	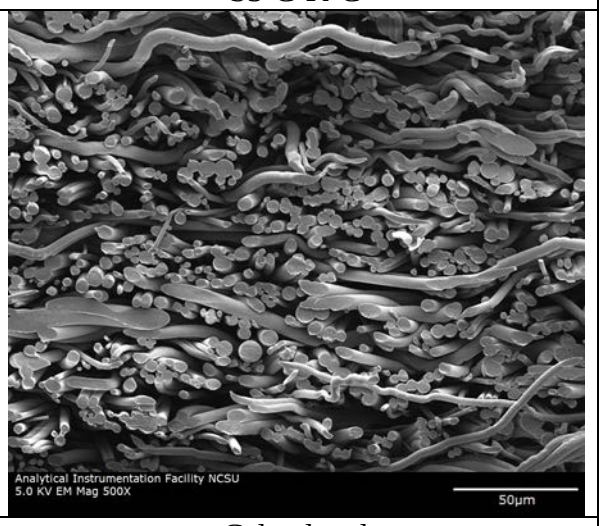
Uncalendered	Calendered

Figure 5.25 Cross section images of the samples: S3-C-K (uncalendered) and S3-C-K-C (calendered)

To sum up, this setup gives the closest structure that looks like microporous membrane. Surface of the nonwovens (after calendering) was smoother compared to previous techniques. Additionally, SVF increase and mean flow pore size decrease were significant. Standard deviations of mean flow pore size for calendered nonwovens in this setup were smaller compared to previous setups.

5.2.5 Effects of Process Parameters of Calendering

The nonwoven membranes mentioned in this section were post-processed through setup 3b. Both rubber and steel rollers had smooth surface. Therefore, it was assumed that a uniform heat transfer was generated.

5.2.5.1 Effects of Temperature

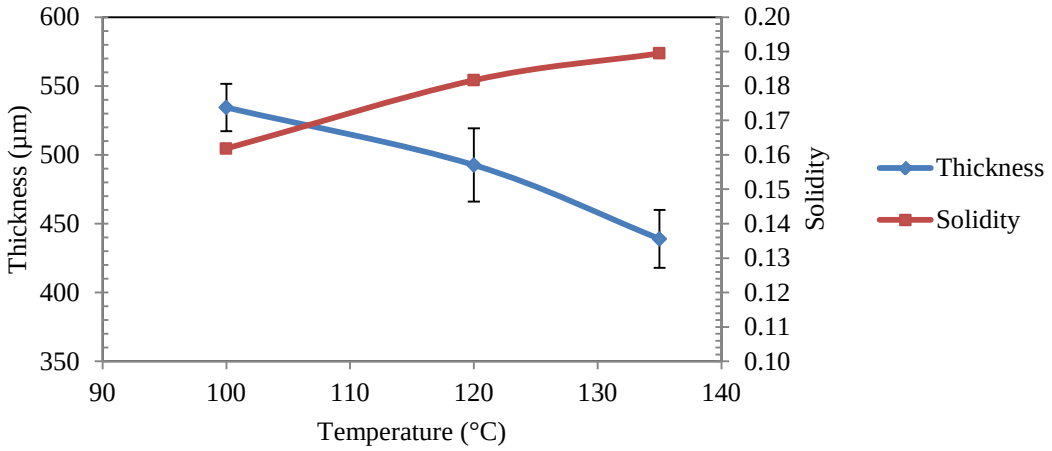

Figure 5.26 Effects of temperature on thickness and SVF

The temperature here refers to the temperature of the heated calender steel roll. A heat profile through the nonwoven was generated from the rolls to the nonwoven. This profile depends on the consolidated nonwoven's thermal characteristics.

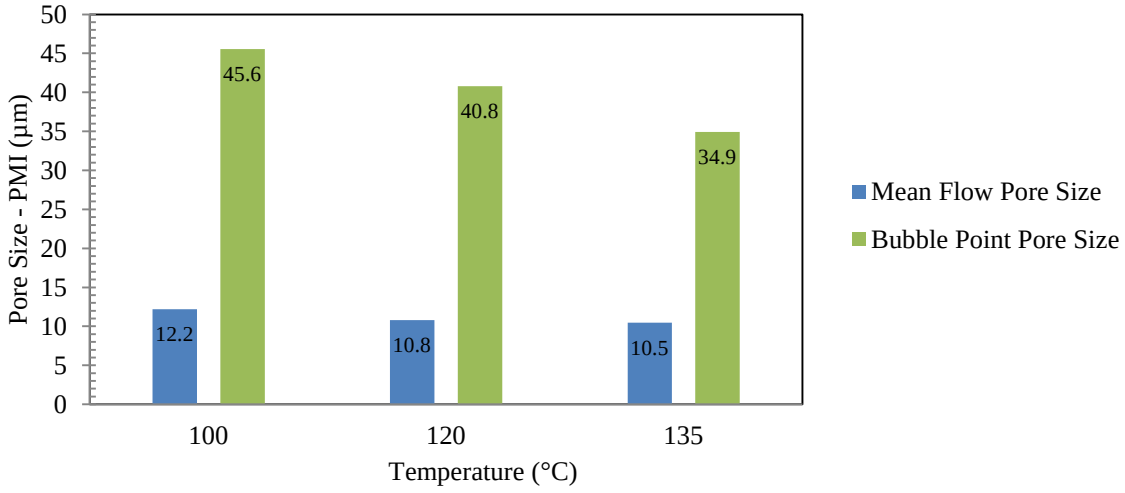

Figure 5.27 Effects of temperature on pore size characteristics

The uncalendered sample's thickness was 897 µm while SVF was 0.11. As seen from Figure 5.26, as temperature increased, thickness of the nonwoven decreased because higher temperature leads to better compaction at the same pressure and dwell time. Also, SVF increased gradually as a result of thickness compression.

Pore size characteristics especially mean flow and bubble point pore size, and pore size distribution determines the water filtration perofrmance. larger pores may result in decrease in filtration efficiency beacuse particles smaller than the larger pores may pass through the nonwoven. So that, pore size distribution should be as narrow as possible. In other words, too large pores are undesirable.

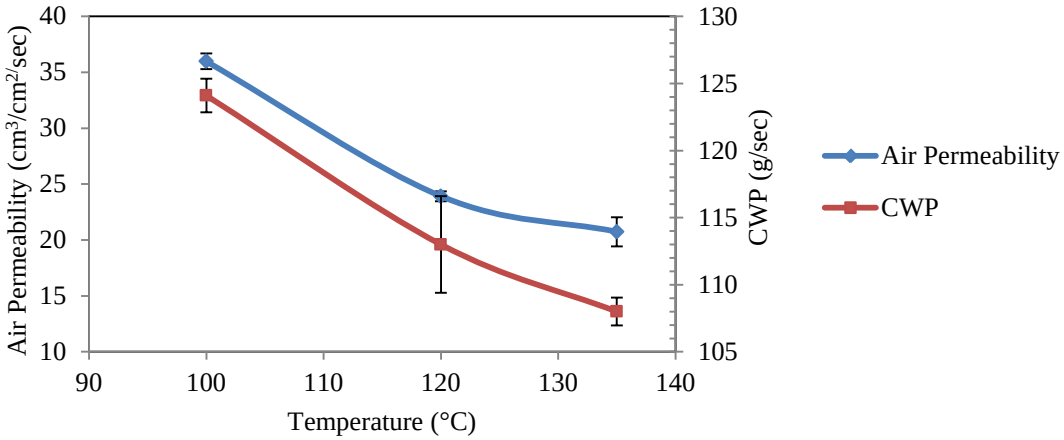

Figure 5.28 Effects of temperature on air permeability and clean water permeability

Figure 5.27 shows the effects of temperature on pore size characteristics. Uncalendered sample's mean flow pore size and bubble point pore size were 23.31 µm and 71.27 µm, respectively. As temperature increased, mean flow pore size decreased, because more heat was transferred. As a resuls, the SVFs were increased due to more thickness compression.

This is why mean flow size is expected to decrease with increasing temperature. Moreover, bubble (largest) point pore size decreased as temperature increased.

Figure 5.28 shows the air permeability values for the fabrics calendered at different temperatures. Air permeability is one of most important properties of nonwovens in filtration applications. Lower air permeability values prove that less air is able to penetrate through the nonwoven in unit time, while higher air permeability values prove that more air is able to penetrate through the nonwoven per unit time. Air permeability mainly depends on pore characteristics such as fabric density, pore size and its distribution, and porosity.

The air permeability value of the uncalendered sample was 91.06 ($cm^3/cm^{2/}sec$). The reasons why air permeability decreased while increasing the calendering temperature, are that SVF increased due to thickness compression, and mean flow pore size decreased due to SVF increase (Figure 5.28). In other words, air permeability decreased as the fabric density increased because resistance to air flow caused by consolidated web increased.

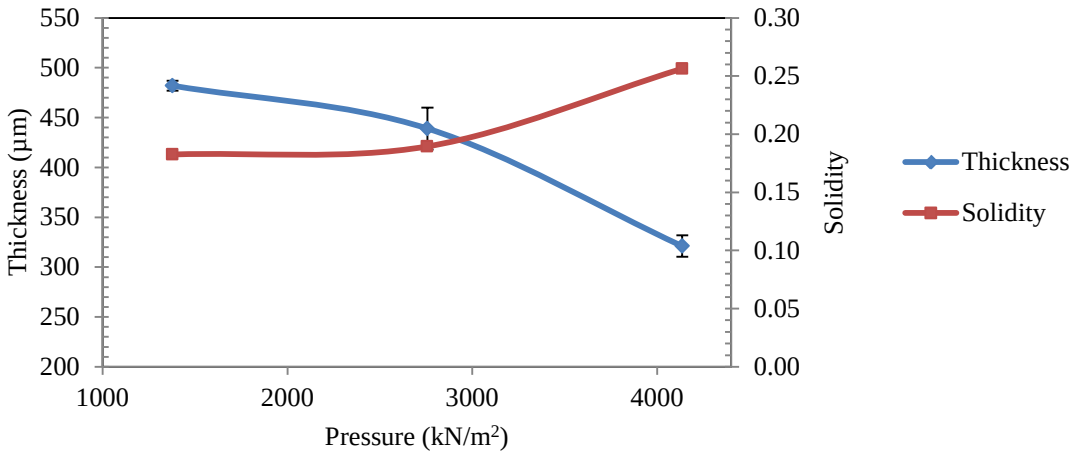

Figure 5.29 Effects of pressure on thickness and SVF

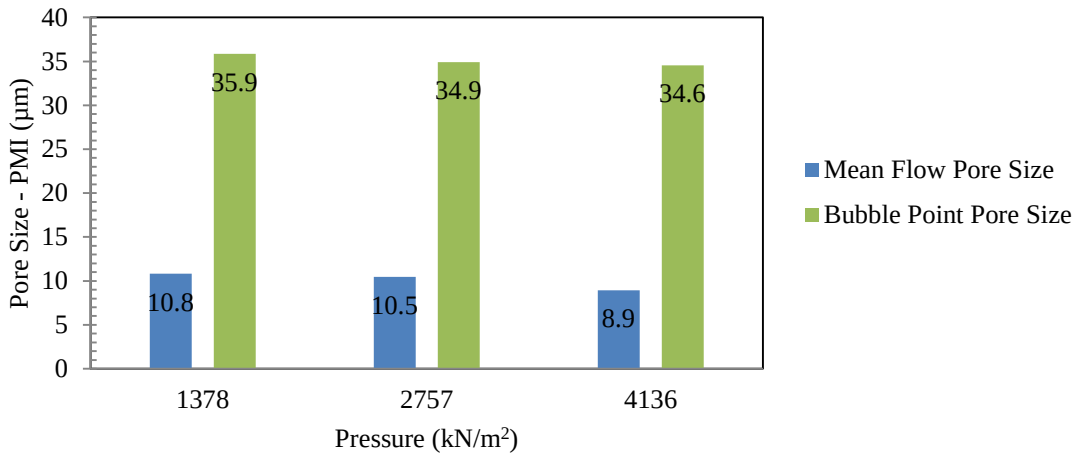

Figure 5.30 Effects of pressure on pore size characteristics

Figure 5.28 also shows the clean water permeability values for the fabrics calendered at different temperatures. The results are given in the unit of g/sec per 45.5. cm^2 at 0.05 Bar. Clean water permeability is another important property of nonwovens in water filtration applications. Lower clean water permeability values prove that less water is able to penetrate through the nonwoven per unit time, while higher clean water permeability values prove that more water is able to penetrate through the nonwoven per unit time. Water permeability mainly depends on pore characteristics such as pore size and its distribution, and porosity. The clean water permeability value of the uncalendered sample was 145 g/sec per 45.5 cm^2 at 0.05 Bar. The reasons why CWP decreased while increasing the calendering temperature, are that SVF increased due to thickness compression, and mean flow pore size decreased due to SVF increase. In other words, clean water permeability decreased as the fabric density increased because resistance to water flow caused by consolidated web increased with increasing temperature.

5.2.5.2 Effects of Pressure

The pressure refers here to the pressure between the calender rolls. The pressure is a critical parameter because it affects the heat transfer to and through the nonwoven. Generally, heat is transferred by conduction. Therefore, there will be almost no heat transfer if the pressure would be zero.

Figure 5.29 shows the effects of pressure on SVF and thickness. The uncalendered sample's thickness was 897 µm while SVF was 0.11. Thickness of the nonwoven decreased as pressure increased (Figure 5.29) because higher pressure resulted in more compaction at the same temperature and dwell time. Also, SVF increased gradually as a result of more thickness compression. Figure 5.30 shows the effects of pressure on pore size characteristics. Uncalendered sample's mean flow pore size and bubble point pore size were 23.31 µm and 71.27 µm respectively. Mean flow pore size decreased as pressure increased, because more heat flow was transferred as pressure increased. More heat flow increased the SVF due to more thickness compression. This is why mean flow size was expected to decrease with increasing pressure. However, effect of pressure on bubble (largest) point was not significant. Figure 5.31 shows the effect of pressure on air permeability. The air permeability value of the uncalendered sample was 91.06 ($cm^3/cm^{2/}sec$). The reasons why air permeability decreased while increasing the calendering pressure, are that SVF increased due to thickness compression, and mean flow pore size decreased. In other words, air permeability decreased as the fabric density increased because resistance to air flow caused by consolidated web increased.

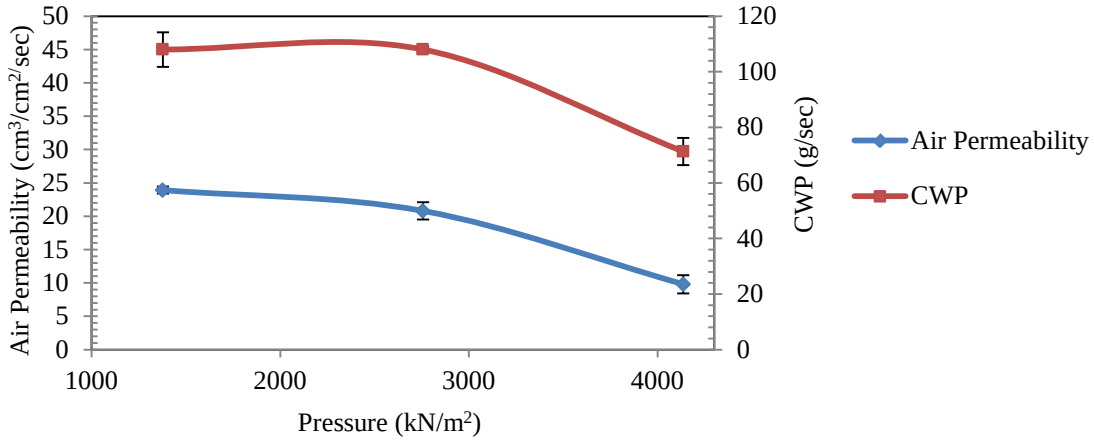

Figure 5.31 Effects of pressure on air permeability and clean water permeability

Figure 5.31 also shows the clean water permeability values for the fabrics calendered at different pressures. The results are given in the unit of g/sec per 45.5 cm^2 at 0.05 Bar. The clean water permeability value of the uncalendered sample was 145 g/sec per 45.5 cm^2 at 0.05 Bar. The reasons why CWP decreased while increasing the calendering pressure are that SVF increased due to thickness compression and mean flow pore size decreased due to SVF increase. In other words, clean water permeability decreased as the fabric density increased because resistance to water flow caused by consolidated web increased with increasing pressure.

5.2.6 Nonwovens with Given Pore Size

Case 1

After the post-processing, final thickness was measured as 211 µm. Calendered sample's basis weight was measured as 130 g/m^2. Using the final thickness and basis weight, final SVF was calculated as 0.47. It was greater than the target SVF (0.44), because basis weight of the web increased slightly. Mean flow pore size of the final web was 3.02 µm. Target

mean flow pore size (2.5 µm) was lower than measured mean flow pore size (3.02 µm) with the relative error of –21%.

Case 2

Final thickness was measured as 108 µm. Calendered sample's basis weight was measured as 42 g/m^2. Using the final thickness and basis weight, SVF was calculated as 0.30. It was greater than the target SVF (0.24), because basis weight of the web increased slightly, and final thickness (108 µm) was lower than the target thickness (125 µm). Mean flow pore size of the final web was 4.62 µm. In spite of the fact that final SVF (0.30) was greater than the target SVF (0.24), measured mean flow pore size (4.62 µm) was greater than the target pore size (3.5 µm) with the relative error of –32%.

5.3 Conclusions

Three different setups were investigated for formation of nonwoven membrane. Generally, post-processing techniques resulted in more compacted and yet permeable structures. The morphology and basic web characterisrics showed that steel-steel roller configuration, where the gap between the rollers has been predetermined, gave the most promising results. Smooth and membrane-like yet permeable structures were observed after this type of post-processing. Moreover, there was more control on thickness compression (compared to previous setups) in this setup by setting the gap between the rollers.

6. Wastewater Treatment

6.1 Experimental

6.1.1 Material

After the nonwoven membranes were fabricated, performance of the selected nonwoven separation media was investigated in terms of water quality and fouling. Each nonwoven used for separation had an effective membrane area of 0.1 m^2. Commercial hydrophilic PVDF membrane material with 0.65 µm pore size was purchased from EMD Millipore (MA,US). 4 different nonwoven membranes were produced through the meltblown technique with a Biax meltblown line. The material denoted as NW0 was post-processed through steel rollers at 170 °C where the gap between the rollers was 0.075 mm. NW1 and NW2 were post-processed through steel rollers at 160 °C where the gap between the rollers was 0.12 mm. NW3 was post-processed through the laminator (setup 2-b) at 600 kN/m^2 and 200 °C. The characteristics of these membranes are given in Table 6.2. A polyester mesh fabric with 500 µm mean pore size was used as the support layer. Prior to the treatment, all membranes were cut according to the module's size and attached from the edges with the help of a strong adhesive.

6.1.2 Experimental Setup

A bench-scale membrane bioreactor (Figure 6.1) was customized by Forever Pure®, ZYI™ Corporation, Santa Clara CA. This is a submerged and aerobic membrane bioreactor. The main tank volume is 0.05 m^3. The unit includes 5 flow meters, three pumps, one air

compressor, one pressure gauge and a flat sheet module. The MBR unit is capable of doing both air and water backwash.

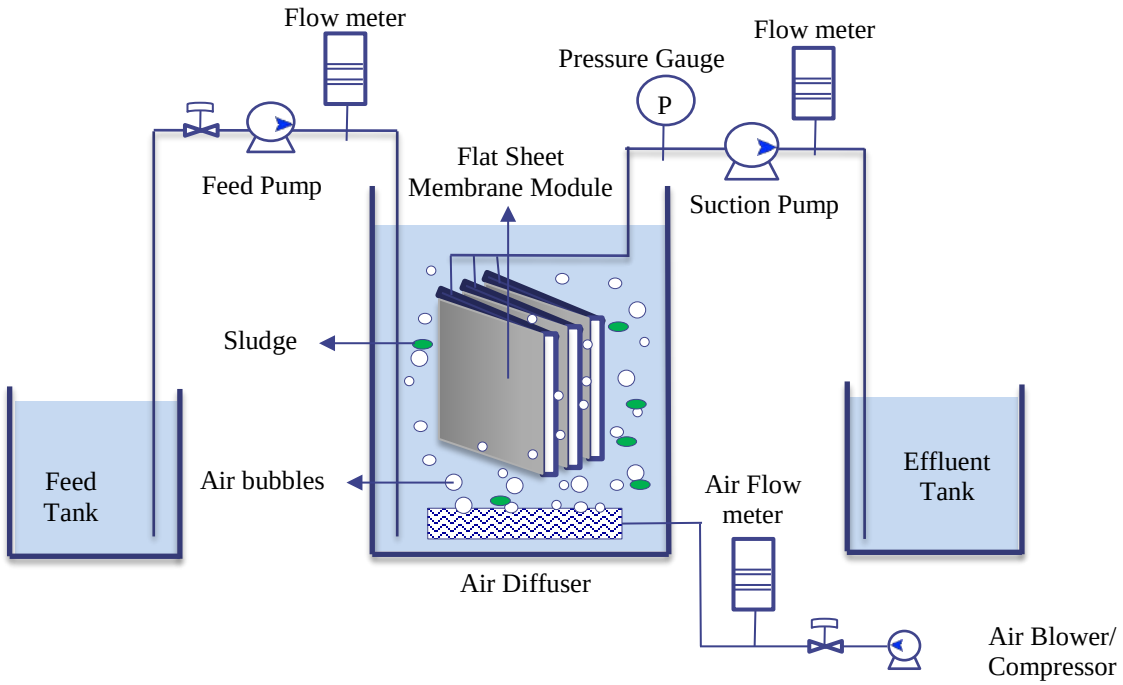

Figure 6.1 Schematic view of the lab-size membrane bioreactor

Transnonwoven pressure (TNP) range is 0-101 kN/m^2. TNP is measured regularly to track the membrane resistance throughout the filtration process. Air backwashing and aeration intensity can be increased up to 5.66 m^3/h. The water backwashing and influent flow rate range is 0 - 1.1 m^3/d.

The flat sheet membrane module, with dimensions of 16 x 28 x 45 cm was purchased from SINAP®, China. There are 5 plates in total with an effective membrane area of 0.1 m^2. One of them is used in the filtration experiments. A schematic view of the module can be seen in Figure 6.2. The bioreactor has an effective volume of 0.052 m^3.

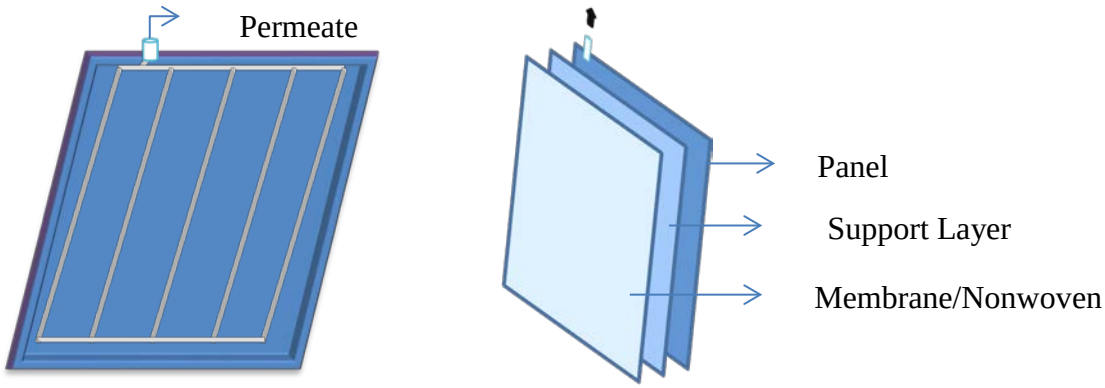

Figure 6.2 Shemaric view of the module (left) and the layers of the module (right)

6.1.2.1 Synthetic Wastewater

In order to keep the wastewater quality constant, a synthetic wastewater solution is used. The composition of the synthetic wastewater, which is shown in Table 6.1, is gathered from a well-known wastewater treatment company.

Alginate, dissolved in the water, leads to irreversible fouling rapidly due to the occurrence of adsorption at an early stage of filtration[219]. Yeast can grow fast on a medium containing a carbon source (as well as under anaerobic conditions), and is proposed for microbial activity. Yeast can double its population in 90 min[220]. Microcrystalline cellulose, a naturally occurring fraction of cellulose, is insoluble and chemically inert[221]. Bovine serum albumen is the protein, identical to blood serum albumin[222]. Calcium chloride is highly soluble in water[223]. Stearic acid floats on water due to its lower density compared to water[224]. Potassium chloride, which is readily soluble in water, is the most common potassium fertilizer in the market[225]. Calcium carbonate is insoluble in the water[226], however it is soluble in acids such as carbonic acid resulting from naturally occurring carbon dioxide[227]. Particle diameter distributions of the synthetic wastewater solutions are measured. According to the

measurements, particle sizes vary below 40 µm. After synthetic wastewater is prepared, 2 hours is given to the yeast to grow.

Table 6.1 Composition of the synthetic wastewater

Composition	Concentration (mg/L)
Alginate	75.7
Yeast	145
Microcrystalline Cellulose	95
Bovine serum albumin (BSA)	91.3
$CaCl_2$ (Calcium chloride)	190.2
$C_{18}H_{36}O_2$ (Stearic acid)	462.5
KCl (Potassium chloride)	425.7
$CaCO_3$ (Calcium carbonate)	118.5

6.1.3 Operating Conditions

All 5 membranes have been used as separation media to examine the effects of pore size on MBR performance. The synthetic wastewater given in Table 6.1 was used as influent. The initial effluent flow rate was 0.36 m^3/d. Backwash was applied two times per hour, and the backwash duration was 2 minutes. Backwash intensity was 0.72 m^3/d, and the aeration intensity was 0.85 m^3/d. A minute-long relaxation was applied after 5 minutes of operation throughout the filtration process. The treatments were operated continuously for 8 hours for all membranes.

6.1.4 Analytical Methods

6.1.4.1 Clean Water Permeability (CWP)

The water flux meter located at the College of Textiles, NCSU measures how much water passes in a unit time through the medium at a predetermined pressure (Figure 5.6). The area

of the circular specimen is 45 cm^2. Clean water was poured into the vessel, and pressured gas was added. Subsequently, the quantity of water passing through the nonwoven was measured on a weighing scale. Three specimens of each medium were tested and results are obtained in the unit of g/sec per 45.5 cm^2 at 0.2 Bar. Additionally, intrinsic resistances were calculated according to the following equation:

$$R_t = \frac{\Delta p}{\vartheta . \mathrm{J}} \tag{6.1}$$

Where J is permeation flux (m^3/m^2s); Δp is the transnonwoven pressure (Pa); ϑ is the viscosity of the permeate (Pa.s); R_m is the resistance (m^{-1})

6.1.4.2 Water Quality Analysis

Chemical oxygen demand (COD) is a measure of the oxygen equivalent amount of organic materials which are subject to oxidation by potassium dichromate in a 50% sulfuric acid solution. This test is conducted by Hatch Method #8000 based on the Reactor Digestion Method[228], which is USEPA approved for reporting wastewater analysis (Federal Register, April 21,1980, 45(78)26811-26812). The measurement range is from 20 to 1500 mg/L. Once the oxidation step is completed, the amount of dichromate which is consumed is measured calorimetrically. Colorimetric measurement is quicker and easier to run compared to titration method, and does not require additional reagents. It can be operated in 3 hours while the biochemical oxygen demand (BOD) test takes 5days. This test is carried out at NCSU Environmental Engineering Lab.

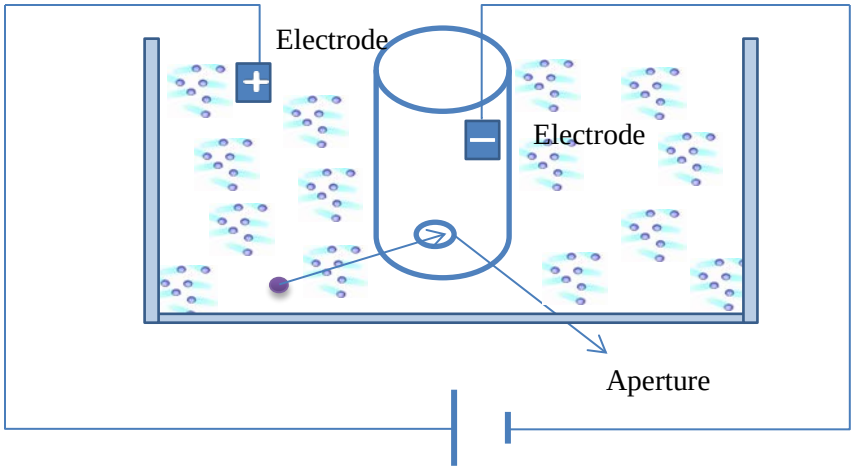

Figure 6.3 Schematic view of the Coulter principle

Turbidity, which is affected by suspended and colloidal materials, is the indication of water clarity. Even though turbidity is not a direct indication of health risk, it is performed frequently in wastewater treatment plants[229,230]. This test is conducted through a Hach® 2100N Laboratory turbidimeter by the Nephleometric method according to ASTM D7315, which also meets the requirements of EPA Method 180.1.

Table 6.2 The summary of the characteristics of the membranes

Sample ID	Membrane Material	Mean Flow Pore Size (µm)	Largest Pore Size (µm)	Thickness (µm)	Solid Volume Fraction	Basis Weight (g/m^2)
M	PVDF	0.82	1.5	125	0.34	75
NW0	PBT	3.02	5.5	211	0.47	130
NW1	PBT	9.05	18.5	255	0.33	110
NW2	PBT	18.12	32.8	343	0.27	120
NW3	PBT	29.79	65.9	571	0.17	130

Particle Counting and Size Analyzer

The electrical sensing zone (ESZ), aka the Coulter principle (Figure 6.3), provides size distribution in number, volume and surface area in a single measurement. Particles which are present in a diluted solution are pulled through a small aperture separating electrodes which

an electric current passes through. While a particle passes through that aperture, a difference in impedance occurs. The Coulter principle indicates that the change in this pulse is proportional to the volume of the particles that passed through the aperture[231]. The particle size is then calculated accordingly. The Coulter principle is not affected by optical properties, density, color or shape of the particle where measurements are reported in terms of spherical diameter in light blockage and scattering methods[230,232,233]. Furthermore, particle size analysis can show the nominal pore size of dynamic membrane layer. A Multisizer™ 4 Coulter counter from Beckman Coulter®, Inc (FL, US) is used for particle counting and size analyses. A volume of 1 ml was taken from each sample. It was then diluted 1:20 with BCI ISOTON 2 (electrolyte) in order not to block the aperture. Counting was conducted in volumetric mode (1000 µl) with a 70 µm aperture tube.

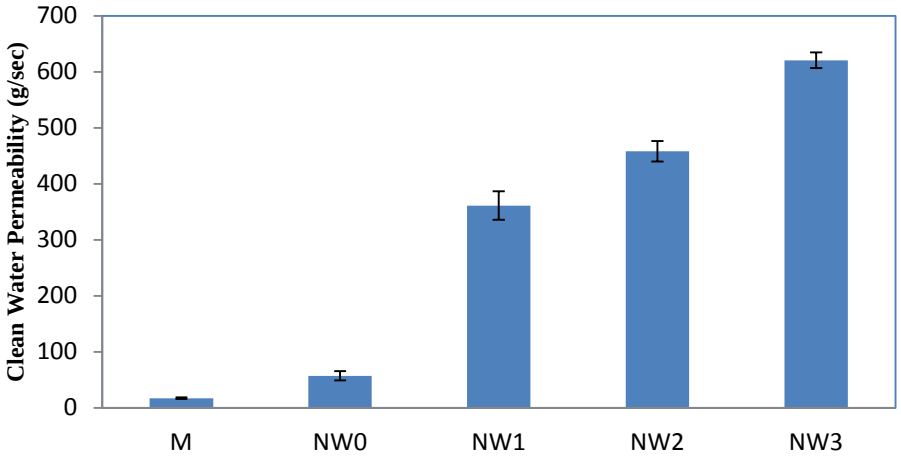

Figure 6.4 Clean water permeabilities of the membranes

6.1.4.3 Filtration Resistance Analyses

Total filtration resistance (R_t) is the summation of nonwoven intrinsic resistance (R_m), cake resistance (R_c), pore narrowing resistance (R_n) and pore blocking resistance (R_b). R_c and R_n

are considered to be reversible fouling where R_b is considered to be irreversible fouling[234]. After the experiment is completed, R_t is measured with clean water according to Eq. 6.1.

6.2 Results and Discussion

6.2.1 Membrane Characterization

Table 6.2 shows the characteristics of the membranes used in this study. Pore sizes range from 0.82 to 29.79 µm. Nonwoven membranes have much bigger pore size than the commercial PVDF membrane. The largest detected pores are critical in nonwoven membranes, because particles can pass through these bigger pores and affect the filtration efficiency significantly. The largest pore diameter of the NW3 was 65.9 µm, while largest pore of the NW0 was 5.5 µm. Largest detected pore size increased as mean flow pore size increased.

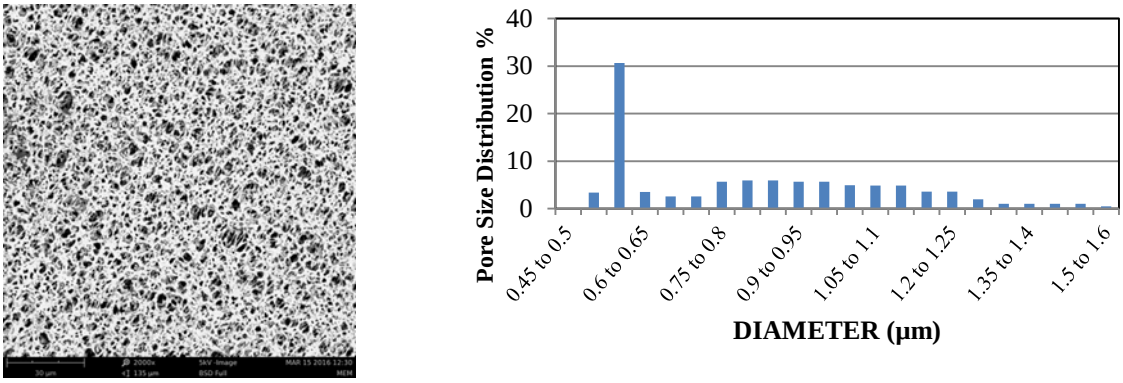

Figure 6.5 SEM image and the pore size distribution of the PVDF membrane

Manufacturer provided the pore size of the PVDF membrane as 0.65 µm. However, mean flow pore size of the membrane measured as 0.82 µm. It is thought that the pore size difference may have occurred due to wettability of the PVDF. The solid volume fraction

(SVF) of NW0, NW1, and NW2 are quite larger than typical nonwovens due to the calendering effect. Sample NW0 has the highest SVF while NW3 has the lowest SVF. Basis weights of the nonwoven membranes were kept high compared to the PVDF membrane in order to achieve sufficient tensile properties.

Figure 6.4 shows that the clean water permeabilities (CWPs) of the membranes range from 17 to 621 g/sec per 45.5 cm^2 at 0.2 Bar. The CWPs obtained for all nonwovens are much higher than the commercial PVDF membrane. Nonwovens are very permeable because of their larger mean flow pore size, lower SVF and interconnected pore structures. Clean water permeability increases as the mean flow pore size increases and SVF decreases. Standard errors of nonwoven membranes were found larger compared to the PVDF membrane. Non-uniformity of basis weight and/or non-homogeneity of SVF may have led to the variation in CWPs.

Figure 6.5 shows SEM images of the PVDF membrane. The membrane has a narrower pore size distribution compared to the nonwovens. Also, the structure of the membrane is compeletely different compared to the nonwovens. In nonwoven structure there are gaps between the fibers. Interconnected pores are formed by randomly overlapping fibers (Figure 6.6). This complex fiber and pore network result in different pore structure compared to the commercial membrane.

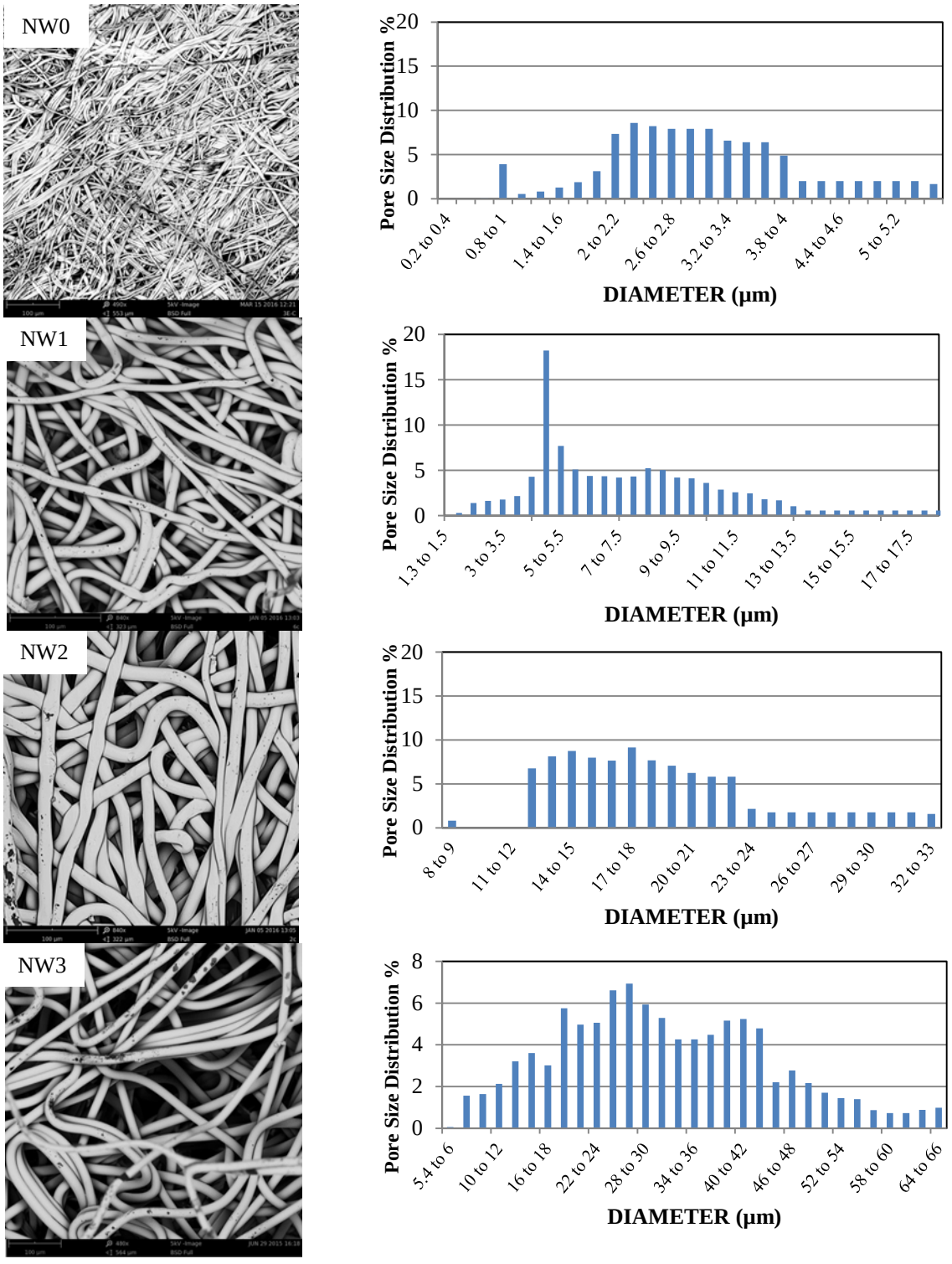

Figure 6.6 SEM images and the pore size distributions of the nonwoven membranes

Figure 6.6 shows the SEM images and pore size distributions of the nonwoven membranes. As seen from the SEM images, NW0 has tightly packed structure with a smooth surface. Pore size ranged from 0.8 to 5.5 µm, where the fiber size was 3.1 µm. It has the narrowest pore size distribution among the nonwoven membranes. Pore size distribution of NW1 ranged from 1.5 to 18 µm. Average fiber diameter of the NW1 was 10.04 µm while the average fiber diameter of the NW2 was 13.27 µm. Pore size distributions of NW2 and NW3 were broad compared to the other nonwoven membranes.

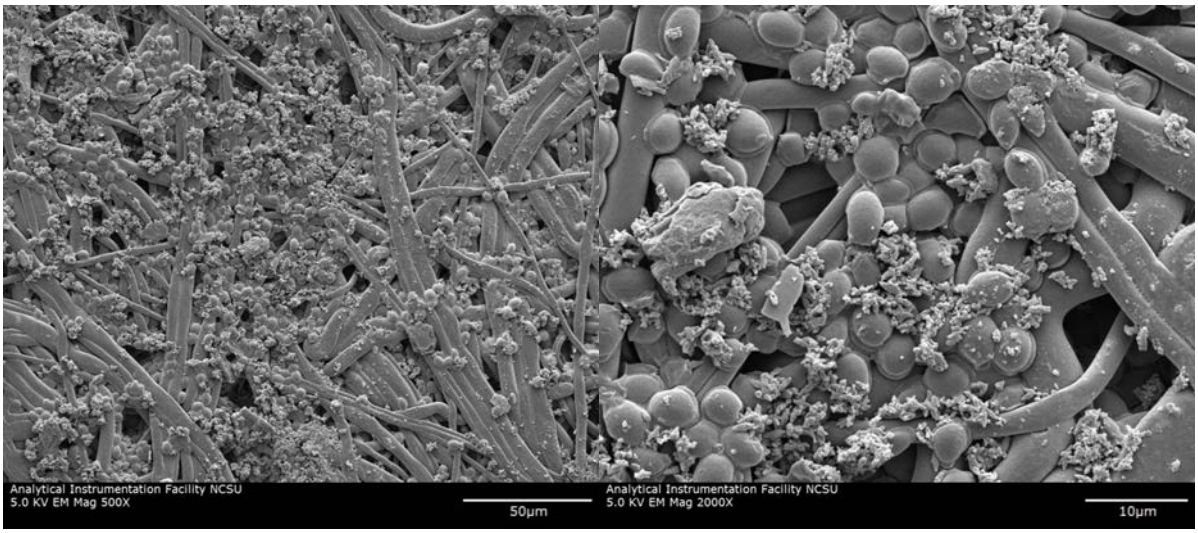

Figure 6.7 SEM images of the surface of the NW0 after filtration

6.2.2 Treatment Performance

The virgin structure of NW0 consisting of random overlapped fibers is shown in Figure 6.6, while the fouled structure of the same media can be seen in Figure 6.7. The yeast cells, which have a diameter of about 3 to 7 µm, commonly appear as ellipsoid-shaped[235,236]. Therefore, it is thought that the spherical shaped particles correspond to the yeast cells.

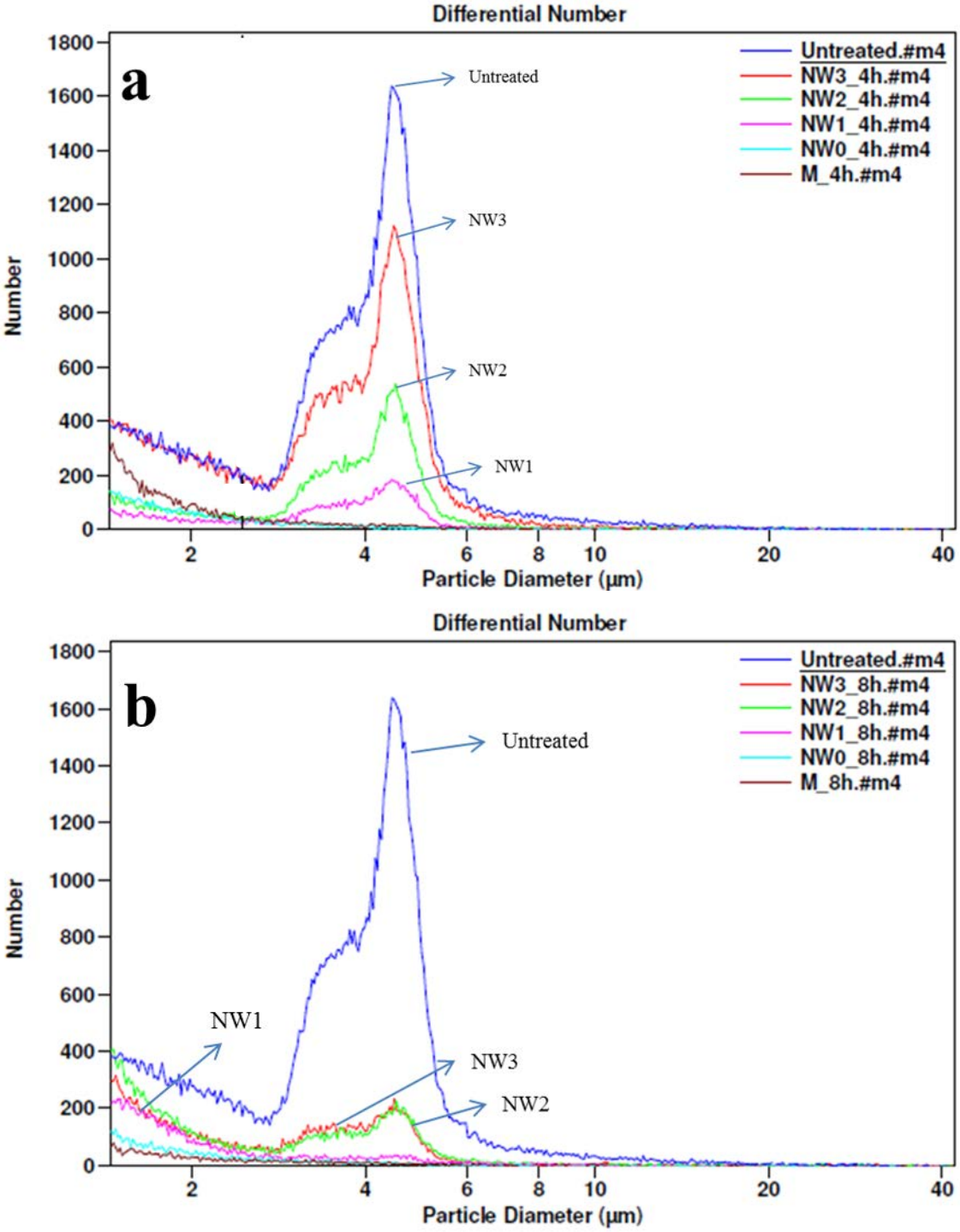

Figure 6.8 Particle size distributions a) after 4 hours, b) after 8 hours filtration

Other particles could be cellulose and calcium carbonate. The size of the microcrystalline cellulose is provided as 20 µm by the manufacturer (Sigma-Aldrich), while 80 % of the calcium carbonate particles are smaller than 2 µm[237].

Membrane	R_m (10^{10} m^{-1})	R_t (10^{10} m^{-1})	R_m/R_t
M	5.97	15.23	0.392
NW0	1.78	25.09	0.071
NW1	0.28	28.67	0.010
NW2	0.22	26.88	0.008
NW3	0.16	11.65	0.014

Table 6.3 Resistances of the membranes after the batch filtration tests

According to the particle counting calculations, 90% of the particles in the raw wastewater were smaller than 27.86 µm, and 75% were smaller than 16.75 µm. The total counted number of particles was 90,449 for the raw wastewater. After 4 h treatment, the total counted number of particles was 67,751 for sample NW3, 25,489 for sample NW2, 10,683 for sample NW1 and 6,232 for sample NW0. The total counted number of particles was 9,768 for the membrane. The number of counted particles decreased with decreasing mean flow pore size after 4 h treatment. After 8 h treatment, similar behavior was observed for the number of counted particles. Figure 6.8 shows the particle size distributions of the influent and the effluents. A peak was observed around 5 µm for the influent (indication of yeast cells). This peak has been identified for NW3, NW2, and NW1 after 4 h treatment. However, the number of counted particles around 5 µm decreased significantly after 8 h treatment for NW3, NW2, and NW1. No peaks were observed for NW0 or for the PVDF membrane. There is no significant change in the particle size distributions of NW0 and the PVDF membrane with time. Generally, the total counted number of particles decreases with decreasing mean flow

pore size for each treatment. The number of counted particles for NW3 and NW2 are close to each other after 8 h. The difference between the numbers of counted particles decreased as the filtration time increased.

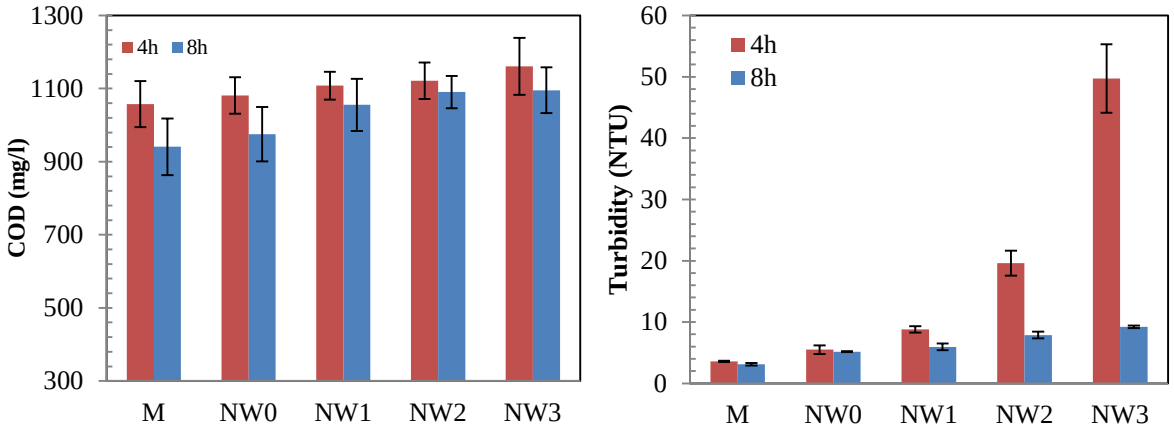

Figure 6.9 Water quality parameters of the effluents

Table 6.3 shows the intrinsic resistances (R_m) and total filtration resistances (R_t) of the membranes after the batch filtration tests. NW3, with the largest mean flow pore size, had the lowest total filtration resistance. Since 90% of the particles in the raw wastewater were smaller than 27.86 µm (the mean flow pore size of the NW3 was 29.79 µm), most of particles passed through NW3. The second-lowest total filtration resistance after NW3 was exhibited by the commercial membrane. Since the membrane acted as a surface filter, a small amount of particles blocked the pores. This is why the membrane had a low filtration resistance. R_m/R_t ratio demonstrates that PVDF membrane has a lower initial fouling ratio compared to the nonwoven membranes. The wide pore size distributions and high surface area of the nonwovens may have triggered the fast fouling. Surface filters lead to less internal fouling resistance in water filtration applications because most of the particles are blocked

before entering into the structure. R_m/R_t ratio indicates that NW0 behaved like a surface filter compared to the other nonwoven membranes, because the initial fouling ratio was lower compared to the other nonwoven membranes.

Figure 6.9 shows the water quality parameters of the effluents. COD value of the influent was 1327 g/ml with a standard error of 52.5. COD removal efficiency was from 5 to 30 % for all membranes. COD values increases slightly with increasing mean flow pore size, and decreases slightly with filtration time. The COD values indicate that filtration duration was not sufficient for higher COD removal efficiencies, since COD is the indirect concentration indication of all contaminants such as suspended and dissolved particles. Figure 6.9 also shows the turbidi-meter results of the effluents. The average turbidity value of the influent was 213 NTU. Turbidity removal efficiencies were between 65 and 97%. The membrane removed most of the suspended particle at the early stage of the filtration. This is why the effluent from the membrane had the lowest turbidity value. However, as mean flow pore size increases, turbidity removal decreased at the early stage of the filtration. NW2 and NW3 have higher turbidity values after 4 h treatment compared to other membranes.

6.3 Conclusions

The effects of nonwoven pore size on traditional submerged bioreactor performance have been investigated in terms of fouling and effluent quality. A comparison of the nonwoven media with the typical membrane was also undertaken. Effluent quality and filtration resistance results revealed that separation performance of nonwovens is governed by the pore size and its distribution with regard to influent particle size distribution. R_m/R_t ratios in the

Table 6.3 proved that the filtration resistances of nonwovens increased faster compared to the membrane, indicating pore blocking by particles in the nonwoven media. Therefore, optimization of pore characteristics is required in order to achieve low-fouling nonwovens.

7. Conclusions and Recommendations

7.1 Overall Conclusions

The current research focused on the formation of nonwoven membranes and their liquid filtration performances in a typical membrane bioreactor. Nonwovens have many potential applications in particle separation applications. A review of the literature exposed that pore size and its distribution are the critical parameters in microfiltration. Therefore, there has been extensive interest in producing nonwoven media at given pore size. For this reason, a basis for designing and producing nonwovens at given pore size have been developed. Validations of the existing mean pore size models and the model that we developed in this study have been carried out for three series of nonwoven fabrics. These models verified that there are two structure properties that are directly related to mean pore size of nonwovens: fiber diameter and solid volume fraction. The validation results revealed that Wrotnowski's model has the best agreement with the data in the range studied here. However, our model is better predictor than Wrotnowski's model only for highly porous (uncalendered) webs having small fibers (<4μm).

Three different setups have been investigated for the formation of nonwoven membranes: post-processing through heat press, laminator, and heated calender rollers. An ideal nonwoven separation media should have narrow pore size distribution, and smooth surface. Although the calendering narrowed the pore size distribution, we were not able to achieve this structure and there were still large pores. The heated steel-steel roller configuration, where the gap between the rollers was predetermined, gave the most promising results

according to the SEM images and basic web characteristics. The results revealed that smooth, membrane-like, and yet permeable structures have been formed after the calendering through this setup. Moreover, controlled compaction (compared to other setups) was achieved.

We tried to reach to the target mean flow pore size after web formation through calendering. If the thickness, fiber diameter, and basis weight of the fabric are measured after the web formation, pore size requirements can be achieved by determining the solid volume fraction with the help of the right model. However, the anticipated mean pore sizes were lower than the measured mean flow pore size.

After all nonwoven membranes were fabricated, performances of the selected membranes with different pore size were tested in the bioreactor to determine their fouling behavior and effluent quality. Nonwovens were very permeable because of their larger mean flow pore size and lower solidity. Standard errors of nonwovens' CWPs were found larger compared to the commercial membrane. This might be due to the differences in basis weight and solid volume fraction in the webs. SEM images of nonwoven membranes showed the unique structure of the webs. Pore structure of the nonwovens is completely different from the PVDF membrane. According to water quality tests and particle counting analyses, effluent quality is mainly driven by the mean flow pore size. According to the filtration resistance results, nonwovens showed faster initial fouling compared to the PVDF membrane, indicating pore blocking. The wide pore size distributions of the nonwovens may have triggered the fast fouling. It was also found that NW0 can be regarded as surface filter while

other nonwoven membranes can be regarded as depth filter, because the initial fouling ratio of the NW0 was lower compared to the other nonwoven membranes.

Nonwovens cannot be a straight replacement in bioreactors as separation media yet. Operation conditions should be adapted. Additionaly, calendering reduced the pore size to a useful level however pore size distribution is still wide.

7.2 Recommendations for Future Work

Existing mean pore size models underestimate the fiber orientation distribution which affects the pore characteristics. A novel model that utilizes the fiber orientation distribution in addition to fiber size and solid volume fraction is required to precisely predict the mean pore diameter in nonwovens.

Fouling still seems to be the main drawback of nonwoven in particle separation applications. The nonwoven membrane reactor system with low fouling could be achieved through selecting the appropriate nonwoven characteristics. Optimization of pore characteristics such as pore structure, pore size, and pore size distribution is required. In particular, further study is required to obtain narrower pore size distributions of melt-processed nonwovens.

Similar effluent qualities could be achieved in nonwovens and membranes when their pore sizes were close. However, greater fouling is expected from nonwovens due to the high surface area. During long-term operation, high fouling increases the operation cost and the bioreactor may require earlier membrane replacement. In the literature it has been shown that hydrophilic membranes have better antifouling property compared to hydrophobic

membranes. Making the filter more hydrophilic through surface treatment techniques can reduce the fouling of the nonwovens.

Long term (more than one month) MBR fouling of nonwoven membranes (with comparing a typical membrane) must be put in perspective for the cost of filter replacement. During long-term operation, a dynamic layer (cake layer or secondary membrane) is formed. This layer acts as another membrane on top of the original membrane. Function of dynamic membrane formation on nonwovens could be investigated during long term operation, as well.

Since the structure of the pores in nonwovens is different from typical membranes, hydrodynamic properties such as hydraulic retention time of bioreactor may affect the nonwoven fouling behavior in a different way. Therefore, the influence of hydrodynamic parameters on the fouling behavior of nonwovens can also be studied.

References

1. Angelakis, A. N. & Spyridakis, D. S. A brief history of water supply and wastewater management in ancient Greece. *Water Sci. Technol. Water Supply* **10,** 618 (2010).

2. Wachinski, A. *Membrane Processes for Water Reuse*. (McGraw-Hill Professional, 2012).

3. Lofrano, G. & Brown, J. Wastewater management through the ages: a history of mankind. *Sci. Total Environ.* **408,** 5254–5264 (2010).

4. Simonovic, S. P. *Managing Water Resources: Methods and Tools for a Systems Approach*. (Routledge, 2012).

5. Mohanty, K. & Purkait, M. K. *Membrane Technologies and Applications*. (CRC Press, 2011).

6. Judd, S. *The MBR Book: Principles and Applications of Membrane Bioreactors for Water and Wastewater Treatment*. (Elsevier, 2011).

7. Wang, L. K., Hung, Y.-T., Lo, H. H. & Yapijakis, C. *Handbook of Industrial and Hazardous Wastes Treatment*. (CRC Press, 2004).

8. Meng, F. *et al.* Recent advances in membrane bioreactors (MBRs): Membrane fouling and membrane material. *Water Res.* **43,** 1489–1512 (2009).

9. Park, H.-D., Chang, I.-S. & Lee, K.-J. *Principles of Membrane Bioreactors for Wastewater Treatment*. (CRC Press, 2015).

10. Rushton, A., Holdich, R. G. & Ward, A. S. *Solid-liquid filtration and separation technology*. (Wiley-VCH, 2000).

11. Mukhopadhyay, A. in *Composite Non-Woven Materials* (eds. Das, D. & Pourdeyhimi, B.) 164–210 (Woodhead Publishing, 2014).

12. Chapman, R. *Applications of Nonwovens in Technical Textiles*. (Elsevier, 2010).

13. Kumar, R. S. *Textiles for industrial applications*. (Taylor & Francis, 2013).

14. Cheremisinoff, N. P. *Liquid filtration*. (Butterworth-Heinemann, c1998.).

15. *e-CFR: TITLE 40—Protection of Environment*. *Electronic Code of Federal Regulations* **TITLE 40—Protection of Environment,**

16. Côté, P., Buisson, H., Pound, C. & Arakaki, G. Immersed membrane activated sludge for the reuse of municipal wastewater. *Desalination* **113,** 189–196 (1997).

17. Scott, S. Application of Membrane Bioreactor Technology to Wastewater Treatment and Reuse.

18. Stephenson, R. L. & Jr, J. B. B. *The Industrial Wastewater Systems Handbook*. (CRC Press, 1997).

19. Sanin, F. D., Clarkson, W. W. & Vesilind, P. A. *Sludge Engineering: The Treatment and Disposal of Wastewater Sludges*. (DEStech Publications, Inc, 2011).

20. Fields, K. A., Chen, A. H., Division, N. R. M. R. L. (U S.) W. S. and W. R. & Wang, L. *Arsenic removal from drinking water by coagulation/filtration and lime softening plants*. (National Risk Management Research Laboratory, Office of Research and Development, U.S. Environmental Protection Agency, 2000).

21. Halling-Sørensen, B. & Jorgensen, S. E. *The Removal of Nitrogen Compounds from Wastewater*. (Elsevier, 1993).

22. Sedlak, R. I. *Phosphorus and Nitrogen Removal from Municipal Wastewater: Principles and Practice, Second Edition*. (CRC Press, 1991).

23. *Physical and chemical Characteristics- Fact sheets*.

24. Engineering, H. D. R. *Handbook of public water systems*. (John Wiley & Sons, 2001).

25. Lingireddy, S. *Control of Microorganisms in Drinking Water*. (ASCE Publications, 2002).

26. Kirmeyer, G. J. *Guidance Manual for Maintaining Distribution System Water Quality*. (American Water Works Association, 2000).

27. Marsh, H. & Reinoso, F. R. *Activated Carbon*. (Elsevier, 2006).

28. Calabrò, V. in *Handbook of Membrane Reactors* 3–53 (Elsevier, 2013).

29. Yang, S.-T. *Bioprocessing for Value-Added Products from Renewable Resources: New Technologies and Applications*. (Elsevier, 2011).

30. *Membrane BioReactors WEF Manual of Practice No. 36*. (McGraw-Hill Professional, 2011).

31. Gao, D. *et al.* Current research and development of controlling membrane fouling of MBR. *Afr. J. Biotechnol.* **8,** (2009).

32. Le-Clech, P., Chen, V. & Fane, T. A. G. Fouling in membrane bioreactors used in wastewater treatment. *J. Membr. Sci.* **284,** 17–53 (2006).

33. Chang, I.-S., Le Clech, P., Jefferson, B. & Judd, S. Membrane Fouling in Membrane Bioreactors for Wastewater Treatment. *J. Environ. Eng.* **128,** 1018–1029 (2002).

34. Weiner, R. F. *Environmental Engineering*. (Butterworth-Heinemann, 2003).

35. Cleary, J. & Eckenfelder, W. W. *Activated Sludge Technologies for Treating Industrial Wastewaters: Design and Troubleshooting*. (DEStech Publications, Inc, 2013).

36. Larsen, B. *Math Handbook for Wastewater Treatment Plant Operators: Math Fundamentals and Problem Solving*. (Bob Larsen, 2010).

37. Carstensen, F., Apel, A. & Wessling, M. In situ product recovery: Submerged membranes vs. external loop membranes. *J. Membr. Sci.* **394–395,** 1–36 (2012).

38. Tien, C. *Principles of Filtration*. (An Elsevier Title, 2012).

39. Ramakrishna, S., Ma, Z. & Matsuura, T. *Polymer Membranes in Biotechnology: Preparation, Functionalization and Application*. (Imperial College Press, 2011).

40. Sun, F. Y. *et al.* Hybrid biofilm-membrane bioreactor (Bf-MBR) for minimization of bulk liquid-phase organic substances and its positive effect on membrane permeability. *Bioresour. Technol.* **198,** 772–780 (2015).

41. Chae, S. R., Kang, S. T., Watanabe, Y. & Shin, H. S. Development of an innovative vertical submerged membrane bioreactor (VSMBR) for simultaneous removal of organic matter and nutrients. *Water Res.* **40,** 2161–2167 (2006).

42. Zuo, D. & Li, H. Study on Processing Condition of Submerged Rotating MBR for Wastewater Treatment. in *International Conference on Energy and Environment Technology, 2009. ICEET '09* **2,** 775–778 (2009).

43. Chen, T. K. & Chen, J. N. Combined membrane bioreactor (MBR) and reverse osmosis (RO) system for thin-film transistor-liquid crystal display TFT-LCD, industrial wastewater recycling. *Water Sci. Technol. J. Int. Assoc. Water Pollut. Res.* **50,** 99–106 (2004).

44. Psoch, C. & Schiewer, S. Critical flux aspect of air sparging and backflushing on membrane bioreactors. *Desalination* **175,** 61–71 (2005).

45. Phattaranawik, J., Fane, A. G., Pasquier, A. C. S. & Bing, W. A novel membrane bioreactor based on membrane distillation. *Desalination* **223,** 386–395 (2008).

46. Kouakou, E., Salmon, T., Toye, D., Marchot, P. & Crine, M. Gas–liquid mass transfer in a circulating jet-loop nitrifying MBR. *Chem. Eng. Sci.* **60,** 6346–6353 (2005).

47. Oshiki, M., Awata, T., Kindaichi, T., Satoh, H. & Okabe, S. Cultivation of Planktonic Anaerobic Ammonium Oxidation (Anammox) Bacteria Using Membrane Bioreactor. *Microbes Environ.* **28,** 436–443 (2013).

48. Tian, J., Chen, Z., Nan, J., Liang, H. & Li, G. Integrative membrane coagulation adsorption bioreactor (MCABR) for enhanced organic matter removal in drinking water treatment. *J. Membr. Sci.* **352,** 205–212 (2010).

49. Meng, F., Chae, S.-R., Shin, H.-S., Yang, F. & Zhou, Z. Recent Advances in Membrane Bioreactors: Configuration Development, Pollutant Elimination, and Sludge Reduction. *Environ. Eng. Sci.* **29,** 139–160 (2011).

50. Peinemann, K.-V. & Nunes, S. P. *Membrane Technology: Volume 4: Membranes for Water Treatment*. (John Wiley & Sons, 2010).

51. Zhang, J., Chua, H. C., Zhou, J. & Fane, A. G. Factors affecting the membrane performance in submerged membrane bioreactors. *J. Membr. Sci.* **284,** 54–66 (2006).

52. Strathmann, H. *Introduction to Membrane Science and Technology*. (Wiley, 2011).

53. Zhu, J., Zhao, X. & He, C. Zwitterionic SiO2 nanoparticles as novel additives to improve the antifouling properties of PVDF membranes. *RSC Adv.* **5,** 53653–53659 (2015).

54. Jing-Feng, W. *et al.* Comparison and Analysis of Membrane Fouling between Flocculent Sludge Membrane Bioreactor and Granular Sludge Membrane Bioreactor. *PLoS ONE* **7,** (2012).

55. Hilal, N., Kochkodan, V., Al-Khatib, L. & Levadna, T. Surface modified polymeric membranes to reduce (bio)fouling: a microbiological study using E. coli. *Desalination* **167,** 293–300 (2004).

56. Drews, A. Membrane fouling in membrane bioreactors—Characterisation, contradictions, cause and cures. *J. Membr. Sci.* **363,** 1–28 (2010).

57. Takht Ravanchi, M., Kaghazchi, T. & Kargari, A. Application of membrane separation processes in petrochemical industry: a review. *Desalination* **235,** 199–244 (2009).

58. Sagle, A. & Freeman, B. Fundamentals of membranes for water treatment. *Future Desalination Tex.* **2,** 137–154 (2004).

59. Allgeier, S., Alspach, B. & Vickers, J. Membrane filtration guidance manual. *U. S. Environ. Prot. Agency US* (2005).

60. NATH, K. *MEMBRANE SEPARATION PROCESSES*. (PHI Learning Pvt. Ltd., 2008).

61. Ho, W. S. W. & Sirkar, K. K. *Membrane Handbook*. (Springer Science & Business Media, 1992).

62. Zeman. *Microfiltration and Ultrafiltration: Principles and Applications*. (CRC Press, 1996).

63. Ang, W. L., Mohammad, A. W., Hilal, N. & Leo, C. P. A review on the applicability of integrated/hybrid membrane processes in water treatment and desalination plants. *Desalination* doi:10.1016/j.desal.2014.03.008

64. Zhang, C. H., Dong, Y. Y. & Zhang, F. J. Modeling of PVA Modified Non-Woven for Submerged Membrane Bioreactor Treating Synthetic Wastewater. *Adv. Mater. Res.* **356,** 1109–1117 (2012).

65. Basile, A. & Nunes, S. *Advanced Membrane Science and Technology for Sustainable Energy and Environmental Applications*. (Elsevier, 2011).

66. Spellman, F. R. *Handbook of Water and Wastewater Treatment Plant Operations, Third Edition*. (CRC Press, 2013).

67. Lazarova, V., Choo, K.-H. & Cornel, P. *Water-energy Interactions in Water Reuse*. (IWA Publishing, 2012).

68. Basile, A. *Handbook of Membrane Reactors: Reactor Types and Industrial Applications*. (Elsevier, 2013).

69. Evaluating filtration media: A comparison of polymeric membranes and nonwovens. *Filtr. Sep.* **35,** 912–914 (1998).

70. Federation, W. E. *Membrane BioReactors WEF Manual of Practice*. (McGraw Hill Professional, 2011).

71. Kiso, Y. *et al.* Wastewater treatment performance of a filtration bio-reactor equipped with a mesh as a filter material. *Water Res.* **34,** 4143–4150 (2000).

72. Satyawali, Y. & Balakrishnan, M. Treatment of distillery effluent in a membrane bioreactor (MBR) equipped with mesh filter. *Sep. Purif. Technol.* **63,** 278–286 (2008).

73. Walker, M., Banks, C. J. & Heaven, S. Development of a coarse membrane bioreactor for two-stage anaerobic digestion of biodegradable municipal solid waste. *Water Sci. Technol. J. Int. Assoc. Water Pollut. Res.* **59,** 729–735 (2009).

74. Wang, W., Jung, Y.-J., Kiso, Y., Yamada, T. & Min, K.-S. Excess sludge reduction performance of an aerobic SBR process equipped with a submerged mesh filter unit. *Process Biochem.* **41,** 745–751 (2006).

75. Li, W.-W. *et al.* Integration of aerobic granular sludge and mesh filter membrane bioreactor for cost-effective wastewater treatment. *Bioresour. Technol.* **122,** 22–26 (2012).

76. Jung, Y.-J., Koh, H.-W., Shin, W.-T. & Sung, N.-C. Wastewater Treatment Using Combination Of MBR Equipped With Non-Woven Fabric Filter And Oyster-Zeolite Column. *Environ. Eng. Res.* **10,** 247–256 (2005).

77. Moghaddam, M., Satoh, H. & Mino, T. Effect of important operational parameters on performance of coarse pore filtration activated sludge process. *Water Sci. Technol.* **46,** 229–236 (2002).

78. Alavi Moghaddam, M. R., Guan, Y., Satoh, H. & Mino, T. Filter clogging in coarse pore filtration activated sludge process under high MLSS concentration. *Water Sci. Technol.* **54,** 55 (2006).

79. Guo, W. *et al.* Roles of sponge sizes and membrane types in a single stage sponge-submerged membrane bioreactor for improving nutrient removal from wastewater for reuse. *Desalination* **249,** 672–676 (2009).

80. Zhang, X. *et al.* Formation of dynamic membrane in an anaerobic membrane bioreactor for municipal wastewater treatment. *Chem. Eng. J.* **165,** 175–183 (2010).

81. Chu, L. & Li, S. Filtration capability and operational characteristics of dynamic membrane bioreactor for municipal wastewater treatment. *Sep. Purif. Technol.* **51,** 173–179 (2006).

82. Fan, B. & Huang, X. Characteristics of a Self-Forming Dynamic Membrane Coupled with a Bioreactor for Municipal Wastewater Treatment. *Environ. Sci. Technol.* **36,** 5245–5251 (2002).

83. Jeison, D., Días, I. & van Lier, J. B. Anaerobic membrane bioreactors: Are membranes really necessary? *Electron. J. Biotechnol.* **11,** 0–0 (2008).

84. Ersahin, M. E. *et al.* A review on dynamic membrane filtration: materials, applications and future perspectives. *Bioresour. Technol.* **122,** 196–206 (2012).

85. Kiso, Y. *et al.* Coupling of sequencing batch reactor and mesh filtration: operational parameters and wastewater treatment performance. *Water Res.* **39,** 4887–4898 (2005).

86. Li, W.-W. *et al.* Filtration behaviors and biocake formation mechanism of mesh filters used in membrane bioreactors. *Sep. Purif. Technol.* **81,** 472–479 (2011).

87. Fuchs, W. *et al.* Influence of operational conditions on the performance of a mesh filter activated sludge process. *Water Res.* **39,** 803–810 (2005).

88. Hutten, I. M. *Handbook of Nonwoven Filter Media*. (Elsevier, 2007).

89. Tiraferri, A., Yip, N. Y., Phillip, W. A., Schiffman, J. D. & Elimelech, M. Relating performance of thin-film composite forward osmosis membranes to support layer formation and structure. *J. Membr. Sci.* **367,** 340–352 (2011).

90. Hilal, N., Kochkodan, V., Nigmatullin, R., Goncharuk, V. & Al-Khatib, L. Lipase-immobilized biocatalytic membranes for enzymatic esterification: Comparison of various approaches to membrane preparation. *J. Membr. Sci.* **268,** 198–207 (2006).

91. Zhang, S. *et al.* Well-constructed cellulose acetate membranes for forward osmosis: Minimized internal concentration polarization with an ultra-thin selective layer. *J. Membr. Sci.* **360,** 522–535 (2010).

92. Zanetti, F., De Luca, G. & Sacchetti, R. Performance of a full-scale membrane bioreactor system in treating municipal wastewater for reuse purposes. *Bioresour. Technol.* **101,** 3768–3771 (2010).

93. McCutcheon, J. R. & Elimelech, M. Influence of membrane support layer hydrophobicity on water flux in osmotically driven membrane processes. *J. Membr. Sci.* **318,** 458–466 (2008).

94. Oh, S. J., Kim, N. & Lee, Y. T. Preparation and characterization of PVDF/TiO2 organic–inorganic composite membranes for fouling resistance improvement. *J. Membr. Sci.* **345,** 13–20 (2009).

95. Lohokare, H. R., Bhole, Y. S. & Kharul, U. K. Effect of support material on ultrafiltration membrane performance. *J. Appl. Polym. Sci.* **99,** 3389–3395 (2006).

96. Gander, M., Jefferson, B. & Judd, S. Membrane bioreactors for use in small wastewater treatment plants: membrane materials and effluent quality. *Water Sci. Technol.* **41,** 205–211 (2000).

97. Chang, I.-S., Gander, M., Jefferson, B. & Judd, S. J. Low-Cost Membranes for Use in a Submerged MBR. *Process Saf. Environ. Prot.* **79,** 183–188 (2001).

98. Alavi Moghaddam, M. R., Satoh, H. & Mino, T. Performance of coarse pore filtration activated sludge system. *Water Sci. Technol. J. Int. Assoc. Water Pollut. Res.* **46,** 71–76 (2002).

99. Chang, M.-C., Tzou, W.-Y., Chuang, S.-H. & Chang, W.-K. Application of non-woven fabric material in membrane bioreactor processes for industrial wastewater treatment. in *5th international membrane science and technology conference, Sydney* 10–14 (2003).

100. Zhi-Guo, M., Feng-lin, Y. & Xing-wen, Z. MBR focus: do nonwovens offer a cheaper option? *Filtr. Sep.* **42,** 28–30 (2005).

101. Chang, M.-C., Horng, R.-Y., Shao, H. & Hu, Y.-J. Performance and filtration characteristics of non-woven membranes used in a submerged membrane bioreactor for synthetic wastewater treatment. *Desalination* **191,** 8–15 (2006).

102. Horng, R. Y., Shao, H., Chang, W. K. & Chang, M. C. The feasibility study of using non-woven MBR for reduction of hydrolysed biosolids. *Water Sci. Technol. J. Int. Assoc. Water Pollut. Res.* **54,** 85–90 (2006).

103. Chang, W.-K., Hu, A. Y.-J., Horng, R.-Y. & Tzou, W.-Y. Membrane bioreactor with nonwoven fabrics as solid–liquid separation media for wastewater treatment. *Desalination* **202,** 122–128 (2007).

104. Ho, J. H., Khanal, S. K. & Sung, S. Anaerobic membrane bioreactor for treatment of synthetic municipal wastewater at ambient temperature. *Water Sci. Technol. J. Int. Assoc. Water Pollut. Res.* **55,** 79–86 (2007).

105. An, Y., Wang, Z., Wu, Z., Yang, D. & Zhou, Q. Characterization of membrane foulants in an anaerobic non-woven fabric membrane bioreactor for municipal wastewater treatment. *Chem. Eng. J.* **155,** 709–715 (2009).

106. Horng, R.-Y. *et al.* Application of TiO2 photocatalytic oxidation and non-woven membrane filtration hybrid system for degradation of 4-chlorophenol. *Desalination* **245,** 169–182 (2009).

107. Ren, X. *et al.* Novel membrane bioreactor (MBR) coupled with a nonwoven fabric filter for household wastewater treatment. *Water Res.* **44,** 751–760 (2010).

108. Bjorge, D. *et al.* Initial testing of electrospun nanofibre filters in water filtration applications. *WATER SA* **36,** 151–155 (2010).

109. Chuang, S.-H., Lin, P.-K. & Chang, W.-C. Dynamic fouling behaviors of submerged nonwoven bioreactor for filtration of activated sludge with different SRT. *Bioresour. Technol.* **102,** 7768–7776 (2011).

110. Bilad, M. R., Westbroek, P. & Vankelecom, I. F. J. Assessment and optimization of electrospun nanofiber-membranes in a membrane bioreactor (MBR). *J. Membr. Sci.* **380,** 181–191 (2011).

111. Chuang, S.-H., Chang, W.-C., Chang, M.-C. & Hu, K.-L. Filtration performances of a novel submerged nonwoven filter for particle separation. *Desalination* **279,** 163–169 (2011).

112. Lee, J.-Y., Choi, B.-K., Ahn, K.-H., Maeng, S. K. & Song, K.-G. Characteristics of flux and gel layer on microfilter and non-woven fabric filter surface based on anoxic–aerobic MBRs. *Bioprocess Biosyst. Eng.* **35,** 1389–1398 (2012).

113. Meng, F. *et al.* A novel nonwoven hybrid bioreactor (NWHBR) for enhancing simultaneous nitrification and denitrification. *Biotechnol. Bioeng.* **110,** 1903–1912 (2013).

114. He, Y., Zhang, W., Rao, P. & Jin, P. Diatomite- and polyvinyl alcohol-modified nonwoven fabric in membrane bioreactor for wastewater reclamation. *Desalination Water Treat.* **0,** 1–7 (2014).

115. He, Y., Zhang, W., Rao, P. & Jin, P. Performance of diatomite/iron oxide modified nonwoven membrane used in membrane bioreactor process for wastewater reclamation. *Water Sci. Technol. J. Int. Assoc. Water Pollut. Res.* **70,** 533–539 (2014).

116. Wang, C., Chen, W.-N., Hu, Q.-Y., Ji, M. & Gao, X. Dynamic fouling behavior and cake layer structure changes in nonwoven membrane bioreactor for bath wastewater treatment. *Chem. Eng. J.* **264,** 462–469 (2015).

117. A wastewater game-changer. Available at: http://www.wme.com.au/categories/water/April2_2014.php. (Accessed: 12th November 2015)

118. Fujii, T., Sugino, H., Rouse, J. D. & Furukawa, K. Characterization of the microbial community in an anaerobic ammonium-oxidizing biofilm cultured on a nonwoven biomass carrier. *J. Biosci. Bioeng.* **94,** 412–418 (2002).

119. Tsushima, I., Ogasawara, Y., Kindaichi, T., Satoh, H. & Okabe, S. Development of high-rate anaerobic ammonium-oxidizing (anammox) biofilm reactors. *Water Res.* **41,** 1623–1634 (2007).

120. Liu, C., Yamamoto, T., Nishiyama, T., Fujii, T. & Furukawa, K. Effect of salt concentration in anammox treatment using non woven biomass carrier. *J. Biosci. Bioeng.* **107,** 519–523 (2009).

121. Bhatti, Z. I., Toda, H. & Furukawa, K. p-Nitrophenol degradation by activated sludge attached on nonwovens. *Water Res.* **36,** 1135–1142 (2002).

122. Wang, T., Zhang, H., Yang, F., Li, Y. & Zhang, G. Start-up and long-term operation of the Anammox process in a fixed bed reactor (FBR) filled with novel non-woven ring carriers. *Chemosphere* **91,** 669–675 (2013).

123. Ni, S.-Q., Lee, P.-H., Fessehaie, A., Gao, B.-Y. & Sung, S. Enrichment and biofilm formation of Anammox bacteria in a non-woven membrane reactor. *Bioresour. Technol.* **101,** 1792–1799 (2010).

124. Chang, W.-K., Chang, M.-C., Horng, R.-Y. & Shao, H. Membrane bioreactor using non-woven fabric filtration. (2004).

125. Kloos, S. D. & Wang, S. Non-woven membrane bioreactor and its fouling control method. (2012).

126. 张王冠, 张敏超, 洪仁阳 & 邵信. Membrane bioreactor using non fabric filtration. (2003).

127. 张文启 & 沈勇. Non-woven fabric floc dynamic membrane bioreactor for sewage treatment. (2012).

128. 孟志国, 杨凤林 & 张兴文. Integrated non-woven cloth bioreactor. (2005).

129. 张敏超, 洪仁阳, 萧碧莲 & 邵信. Anaerobic non-woven thin-film bioreactor and waste water treatment method. (2010).

130. 张兴文, 杨凤林 & 孟志国. Integral non-woven fabric biological reactor. (2006).

131. Wu, Y., Huang, X., Wen, X. & Chen, F. Function of dynamic membrane in self-forming dynamic membrane coupled bioreactor. *Water Sci. Technol. J. Int. Assoc. Water Pollut. Res.* **51,** 107–114 (2005).

132. Loderer, C., Gahleitner, B., Steinbacher, K., Stelzer, C. & Fuchs, W. Dynamic filtration – A novel approach for critical flux determination using different textiles. *Sep. Purif. Technol.* **120,** 410–414 (2013).

133. Bjorge, D. *et al.* Performance assessment of electrospun nanofibers for filter applications. *Desalination* **249,** 942–948 (2009).

134. Kim, H.-C. *et al.* Electrospun nanofibrous PVDF–PMMA MF membrane in laboratory and pilot-scale study treating wastewater from Seoul Zoo. *Desalination* **346,** 107–114 (2014).

135. Lesjean, B., Tazi-Pain, A., Thaure, D., Moeslang, H. & Buisson, H. Ten persistent myths and the realities of membrane bioreactor technology for municipal applications. *Water Sci. Technol.* **63,** 32–39 (2011).

136. Mafirad, S., Mehrnia, M. R. & Sarrafzadeh, M. H. Effect of membrane characteristics on the performance of membrane bioreactors for oily wastewater treatment. *Water Sci. Technol.* **64,** 1154 (2011).

137. Marle, C. *Multiphase flow in porous media*. (Editions Technip, 1981).

138. Al-hadidi, A. M. M. Limitations, improvements, alternatives for the silt density index. (University of Twente, 2011).

139. van der Marel, P. *et al.* Influence of membrane properties on fouling in submerged membrane bioreactors. *J. Membr. Sci.* **348,** 66–74 (2010).

140. Seo, G. T., Moon, B. H., Lee, T. S., Lim, T. J. & Kim, I. S. Non-woven fabric filter separation activated sludge reactor for domestic wastewater reclamation. *Water Sci. Technol. J. Int. Assoc. Water Pollut. Res.* **47,** 133–138 (2003).

141. Li, T. Dependence of filtration properties on stainless steel medium structure. *Filtr. Sep.* **34,** 265–273 (1997).

142. Wang, X. Y. & Gong, R. H. Thermally bonded nonwoven filters composed of bi-component polypropylene/polyester fiber. II. Relationships between fabric area density, air permeability, and pore size distribution. *J. Appl. Polym. Sci.* **102,** 2264–2275 (2006).

143. Ho, C. & Zydney, A. L. Overview of Fouling Phenomena and Modeling Approaches for Membrane Bioreactors. *Sep. Sci. Technol.* **41,** 1231–1251 (2006).

144. Bacchin, P., Derekx, Q., Veyret, D., Glucina, K. & Moulin, P. Clogging of microporous channels networks: role of connectivity and tortuosity. *Microfluid. Nanofluidics* **17,** 85–96 (2013).

145. Chandler, M. & Zydney, A. Effects of membrane pore geometry on fouling behavior during yeast cell microfiltration. *J. Membr. Sci.* **285,** 334–342 (2006).

146. *Advanced Membrane Technology and Applications*. (John Wiley & Sons, Inc., 2008).

147. Lalia, B. S., Kochkodan, V., Hashaikeh, R. & Hilal, N. A review on membrane fabrication: Structure, properties and performance relationship. *Desalination* **326,** 77–95 (2013).

148. Yoon, S.-H. *Membrane Bioreactor Processes: Principles and Applications*. (CRC Press, 2015).

149. Vrijenhoek, E. M., Hong, S. & Elimelech, M. Influence of membrane surface properties on initial rate of colloidal fouling of reverse osmosis and nanofiltration membranes. *J. Membr. Sci.* **188,** 115–128 (2001).

150. Yu, L.-Y., Xu, Z.-L., Shen, H.-M. & Yang, H. Preparation and characterization of PVDF–SiO2 composite hollow fiber UF membrane by sol–gel method. *J. Membr. Sci.* **337,** 257–265 (2009).

151. Yan, L., Li, Y. S., Xiang, C. B. & Xianda, S. Effect of nano-sized Al2O3-particle addition on PVDF ultrafiltration membrane performance. *J. Membr. Sci.* **276,** 162–167 (2006).

152. Dereli, R. K. *et al.* Potentials of anaerobic membrane bioreactors to overcome treatment limitations induced by industrial wastewaters. *Bioresour. Technol.* **122,** 160–170 (2012).

153. Carroll, T., Booker, N. A. & Meier-Haack, J. Polyelectrolyte-grafted microfiltration membranes to control fouling by natural organic matter in drinking water. *J. Membr. Sci.* **203,** 3–13 (2002).

154. Jung, C.-W., Son, H.-J. & Kang, L.-S. Effects of membrane material and pretreatment coagulation on membrane fouling: fouling mechanism and NOM removal. *Desalination* **197,** 154–164 (2006).

155. Korikov, A. P., Kosaraju, P. B. & Sirkar, K. K. Interfacially polymerized hydrophilic microporous thin film composite membranes on porous polypropylene hollow fibers and flat films. *J. Membr. Sci.* **279,** 588–600 (2006).

156. Gholap, S. G., Badiger, M. V. & Gopinath, C. S. Molecular origins of wettability of hydrophobic poly(vinylidene fluoride) microporous membranes on poly(vinyl alcohol) adsorption: Surface and interface analysis by XPS. *J. Phys. Chem. B* **109,** 13941–13947 (2005).

157. Yoon, K. *et al.* High flux ultrafiltration membranes based on electrospun nanofibrous PAN scaffolds and chitosan coating. *Polymer* **47,** 2434–2441 (2006).

158. Zhang, C.-H., Yang, F., Wang, W.-J. & Chen, B. Preparation and characterization of hydrophilic modification of polypropylene non-woven fabric by dip-coating PVA (polyvinyl alcohol). *Sep. Purif. Technol.* **61,** 276–286 (2008).

159. Wang, C., Yang, F., Liu, L.-F., Fu, Z. & Xue, Y. Hydrophilic and antibacterial properties of polyvinyl alcohol/4-vinylpyridine graft polymer modified polypropylene non-woven fabric membranes. *J. Membr. Sci.* **345,** 223–232 (2009).

160. Wang, C. *et al.* High flux and antifouling filtration membrane based on non-woven fabric with chitosan coating for membrane bioreactors. *Bioresour. Technol.* **101,** 5469–5474 (2010).

161. Iqbal, Y. M. & & Iqbal, S. &. *Colloidal & Surface Chemistry*. (Discovery Publishing House, 1996).

162. Seo, G. T., Moon, B. H., Park, Y. M. & Kim, S. H. Filtration characteristics of immersed coarse pore filters in an activated sludge system for domestic wastewater reclamation. *Water Sci. Technol.* **55,** 51 (2007).

163. Daels, N. *et al.* The use of electrospun flat sheet nanofibre membranes in MBR applications. *Desalination* **257,** 170–176 (2010).

164. Trussell, R. S., Merlo, R. P., Hermanowicz, S. W. & Jenkins, D. Influence of mixed liquor properties and aeration intensity on membrane fouling in a submerged membrane bioreactor at high mixed liquor suspended solids concentrations. *Water Res.* **41,** 947–958 (2007).

165. Fan, F. & Zhou, H. Interrelated effects of aeration and mixed liquor fractions on membrane fouling for submerged membrane bioreactor processes in wastewater treatment. *Environ. Sci. Technol.* **41,** 2523–2528 (2007).

166. Meng, F., Yang, F., Shi, B. & Zhang, H. A comprehensive study on membrane fouling in submerged membrane bioreactors operated under different aeration intensities. *Sep. Purif. Technol.* **59,** 91–100 (2008).

167. Bae, T.-H. & Tak, T.-M. Interpretation of fouling characteristics of ultrafiltration membranes during the filtration of membrane bioreactor mixed liquor. *J. Membr. Sci.* **264,** 151–160 (2005).

168. Hilal, N., Ogunbiyi, O. O., Miles, N. J. & Nigmatullin, R. Methods Employed for Control of Fouling in MF and UF Membranes: A Comprehensive Review. *Sep. Sci. Technol.* **40,** 1957–2005 (2005).

169. Fane, A., Beatson, P. & Li, H. Membrane fouling and its control in environmental applications. *Water Sci. Technol.* **41,** 303–308 (2000).

170. Ndinisa, N. V., Fane, A. G. & Wiley, D. E. Fouling Control in a Submerged Flat Sheet Membrane System: Part I – Bubbling and Hydrodynamic Effects. *Sep. Sci. Technol.* **41,** 1383–1409 (2006).

171. Pradhan, M., Vigneswaran, S., Kandasamy, J. & Aim, R. B. Combined effect of air and mechanical scouring of membranes for fouling reduction in submerged membrane reactor. *Desalination* **288,** 58–65 (2012).

172. Wu, J., Le-Clech, P., Stuetz, R. M., Fane, A. G. & Chen, V. Effects of relaxation and backwashing conditions on fouling in membrane bioreactor. *J. Membr. Sci.* **324,** 26–32 (2008).

173. Zsirai, T., Buzatu, P., Aerts, P. & Judd, S. Efficacy of relaxation, backflushing, chemical cleaning and clogging removal for an immersed hollow fibre membrane bioreactor. *Water Res.* **46,** 4499–4507 (2012).

174. Kim, J., Cai, Z. & Benjamin, M. M. Effects of adsorbents on membrane fouling by natural organic matter. *J. Membr. Sci.* **310,** 356–364 (2008).

175. Wu, B., An, Y., Li, Y. & Wong, F. S. Effect of adsorption/coagulation on membrane fouling in microfiltration process post-treating anaerobic digestion effluent. *Desalination* **242,** 183–192 (2009).

176. Wu, J., Chen, F., Huang, X., Geng, W. & Wen, X. Using inorganic coagulants to control membrane fouling in a submerged membrane bioreactor. *Desalination* **197,** 124–136 (2006).

177. Mishima, I. & Nakajima, J. Control of membrane fouling in membrane bioreactor process by coagulant addition. *Water Sci. Technol.* **59,** 1255 (2009).

178. Pearce, G. Introduction to membranes: Fouling control. *Filtr. Sep.* **44,** 30–32 (2007).

179. Liu, C. *et al.* Membrane chemical cleaning: from art to science. *Pall Corp. Port Wash. NY* **11050,** (2001).

180. Liao, B. Q., Bagley, D. M., Kraemer, H. E., Leppard, G. G. & Liss, S. N. A Review of Biofouling and Its Control in Membrane Separation Bioreactors. *Water Environ. Res.* **76,** 425–436 (2004).

181. Kopitar, D., Skenderi, Z. & Mijovic, B. Study on the Influence of Calendaring Process on Thermal Resistance of Polypropylene Nonwoven Fabric Structure. *J. Fiber Bioeng. Inform.* **7,** 1–11 (2014).

182. Kopitar, D., Skenderi, Z. & Rukavina, T. Impact of calendering process on nonwoven geotextiles hydraulic properties. *Text. Res. J.* **84,** 66–77 (2014).

183. Bhat, G. S. Development of structure and properties during thermal calendering of polylactic acid (PLA) fiber webs. *EXPRESS Polym. Lett.* **2,** 49–56 (2008).

184. Sakthivel, S., JJ, E. A. & Ramachandran, T. Development of Needle-Punched Nonwoven Fabrics from Reclaimed Fibers for Air Filtration Applications. *J. Eng. Fabr. Fibers JEFF* **9,** (2014).

185. Zhang, C. H., Dong, Y. Y. & Zhang, F. J. Modeling of PVA Modified Non-Woven for Submerged Membrane Bioreactor Treating Synthetic Wastewater. *Adv. Mater. Res.* **356–360,** 1109–1117 (2011).

186. Agarwal, S., Greiner, A. & Wendorff, J. H. Functional materials by electrospinning of polymers. *Prog. Polym. Sci.* **38,** 963–991 (2013).

187. Albrecht, W., Fuchs, H. & Kittelmann, W. *Nonwoven Fabrics: Raw Materials, Manufacture, Applications, Characteristics, Testing Processes*. (John Wiley & Sons, 2006).

188. *Handbook of nonwovens*. (CRC Press [u.a.], 2007).

189. Cheryan, M. *Ultrafiltration and Microfiltration Handbook*. (CRC Press, 1998).

190. Ciocoiu, M., Haghi, A. K. & Zaikov, G. E. (Gennadiĭ E. *Materials behavior : research methodology and mathematical models*. (Apple Academic Press, 2015).

191. Das, D. & Neckář, B. in *Composite Non-Woven Materials* 30–57 (Elsevier, 2014).

192. Bhatia, S. K. & Suits, L. D. *Recent Developments in Geotextile Filters and Prefabricated Drainage Geocomposites*. (ASTM International, 1996).

193. Abdel-Ghani, M. S. & Davies, G. A. Simulation of non-woven fibre mats and the application to coalescers. *Chem. Eng. Sci.* **40,** 117–129 (1985).

194. Kopitar, D., Skenderi, Z. & Rukavina, T. Infuence of Pressure on Water Permeability and Characteristic Opening Size of Nonwoven Geotextiles. *J. Fiber Bioeng. Inform.* **6,** 103–115 (2013).

195. Berlin, A. A., Joswik, R. & Vatin, N. I. (Nikolai I. *Engineering textiles : research methodologies, concepts, and modern applications*. (Apple Academic Press, 2016).

196. Rawal, A., Kameswara Rao, P. V., Russell, S. & Jeganathan, A. Effect of fiber orientation on pore size characteristics of nonwoven structures. *J. Appl. Polym. Sci.* **118,** 2668–2673 (2010).

197. Dai, X.-Q. (Xiaoqun), Li, Y. (Yi) & Textile Institute (Manchester, E. *Biomechanical engineering of textiles and clothing*. (CRC Press ; Woodhead Publishing, c2006.).

198. Chawla, K. K. *Fibrous materials*. (Cambridge University Press, 1998).

199. Kim, H. S. & Pourdeyhimi, B. A note on the effect of fiber diameter, fiber crimp and fiber orientation on pore size in thin webs. *Int. Nonwovens J.* **9,** 15–19 (2000).

200. Lombard, G., Rollin, A. & Wolff, C. Theoretical and Experimental Opening Sizes of Heat-Bonded Geotextiles. *Text. Res. J.* **59,** 208–217 (1989).

201. Faure, Y. H., Gourc, J. P. & Gendrin, P. Structural study of porometry and filtration opening size of geotextiles. *Geosynth. Microstruct. Perform.* **1076,** 102–119 (1990).

202. Rawal, A. Structural analysis of pore size distribution of nonwovens. *J. Text. Inst.* **101,** 350–359 (2010).

203. Wrotnowski, A. Felt Filter Media. *Filtr. Sep.* 426–431 (1968).

204. Wrotnowski, A. C. Nonwoven Filter Media. *Chern Eng Prog* **58,** 61–67 (1962).

205. Giroud, J. P. Granular filters and geotextile filters. in *Proceedings of Geofilters* **96,** 565–680 (1996).

206. Tsai, P. Characterization of melt blown web properties using air flow technique. *Int. Nonwovens J.* **8,** 36–40 (1999).

207. Neckář, B. & Ibrahim, S. Theoretical Approach for Determining Pore Characteristics Between Fibers. *Text. Res. J.* **73,** 611–619 (2003).

208. Lifshutz, N. On the ‘mean flow’pore size distribution of microfiber and nanofiber webs. *INJ Spring* 18–23 (2005).

209. Simmonds, G. E., Bomberger, J. D. & Bryner, M. A. Designing Nonwovens to Meet Pore Size Specifications. *J. Eng. Fabr. Fibers JEFF* **2,** 1–15 (2007).

210. Davies, C. . Air Filtration. *Acad. Press* (1976).

211. Neckář, B. & Das, D. *Theory of structure and mechanics of fibrous assemblies and yarns*. (Woodhead Pub. India, 2012).

212. Jena, A. & Gupta, K. Liquid extrusion techniques for pore structure evaluation of nonwovens. *Int. Nonwovens J.* **12,** 45–53 (2003).

213. Jena, A. & Gupta, K. Characterization of pore structure of filtration media. *FluidParticle Sep. J.* **14,** 227–241 (2002).

214. Jena, A. & Gupta, K. Pore volume of nanofiber nonwovens. *Int Nonwovens J* **14,** 25–30 (2005).

215. Kallmes, O. & Corte, H. The structure of paper, I. The statistical geometry of an ideal two dimensional fiber network. *Tappi J* **43,** 737–752 (1960).

216. *Mathematical Modeling for Flow and Transport Through Porous Media*. (Springer Science & Business Media, 2013).

217. Vallabh, R., Banks-Lee, P. & Seyam, A.-F. New Approach for Determining Tortuosity in Fibrous Porous Media. *J. Eng. Fabr. Fibers JEFF* **5,** 7–15 (2010).

218. Koponen, A., Kataja, M., Timonen, J. & Kandhai, D. Simulations of Single-Fluid Flow in Porous Media. *Int. J. Mod. Phys. C* **9,** 1505–1521 (1998).

219. Katsoufidou, K., Yiantsios, S. G. & Karabelas, A. J. Experimental study of ultrafiltration membrane fouling by sodium alginate and flux recovery by backwashing. *J. Membr. Sci.* **300,** 137–146 (2007).

220. Bergman, L. W. Growth and maintenance of yeast. *Two-Hybrid Syst. Methods Protoc.* 9–14 (2001).

221. Wiley, Lastwiley & Clavier. *Kirk-Othmer Food and Feed Technology, 2 Volume Set*. (John Wiley & Sons, 2007).

222. Harris, P. *Food Gels*. (Springer Science & Business Media, 2012).

223. Ferguson, L. & Grafton-Cardwell, E. E. *Citrus Production Manual*. (UCANR Publications, 2014).

224. Wink, D. J., Fetzer-Gislason, S. & McNicholas, S. *The Practice of Chemistry*. (Macmillan, 2003).

225. *Industrial Chemistry*. (Krishna Prakashan Media, 1991).

226. Hauser, B. *Drinking Water Chemistry: A Laboratory Manual*. (CRC Press, 2001).

227. Feilden, B. *Conservation of Historic Buildings*. (Routledge, 2007).

228. Jirka, A. M. & Carter, M. J. Micro semiautomated analysis of surface and waste waters for chemical oxygen demand. *Anal. Chem.* **47,** 1397–1402 (1975).

229. Environment, W. F. *Basic Laboratory Procedures for Wastewater Examination*. (Water Environment Federation, 2002).

230. Association, A. P. H., Association, A. W. W., Bridgewater, L., Rice, E. W. & Federation, W. E. *Standard methods for the examination of water and wastewater.* (American Public Health Association, c2012.).

231. bibliography.pdf. Available at: https://www.beckmancoulter.com/wsrportal/bibliography?docname=BR-10052C_Multisizer_4.pdf. (Accessed: 3rd February 2016)

232. Graham, M. D. The Coulter Principle: Foundation of an Industry. *J. Assoc. Lab. Autom.* **8,** 72–81 (2003).

233. Zhang, H., Chon, C. H., Pan, X. & Li, D. Methods for counting particles in microfluidic applications. *Microfluid. Nanofluidics* **7,** 739–749 (2009).

234. Choo, K.-H. & Lee, C.-H. Membrane fouling mechanisms in the membrane-coupled anaerobic bioreactor. *Water Res.* **30,** 1771–1780 (1996).

235. Giaever, G. *et al.* Functional profiling of the Saccharomyces cerevisiae genome. *Nature* **418,** 387–391 (2002).

236. Satyanarayana, T. & Kunze, G. *Yeast Biotechnology: Diversity and Applications*. (Springer Science & Business Media, 2009).

237. Tegethoff, F. W. *Calcium Carbonate: From the Cretaceous Period into the 21st Century*. (Birkhäuser, 2012).

Appendices

Appendix A - TGA Curves of the PBT Resins

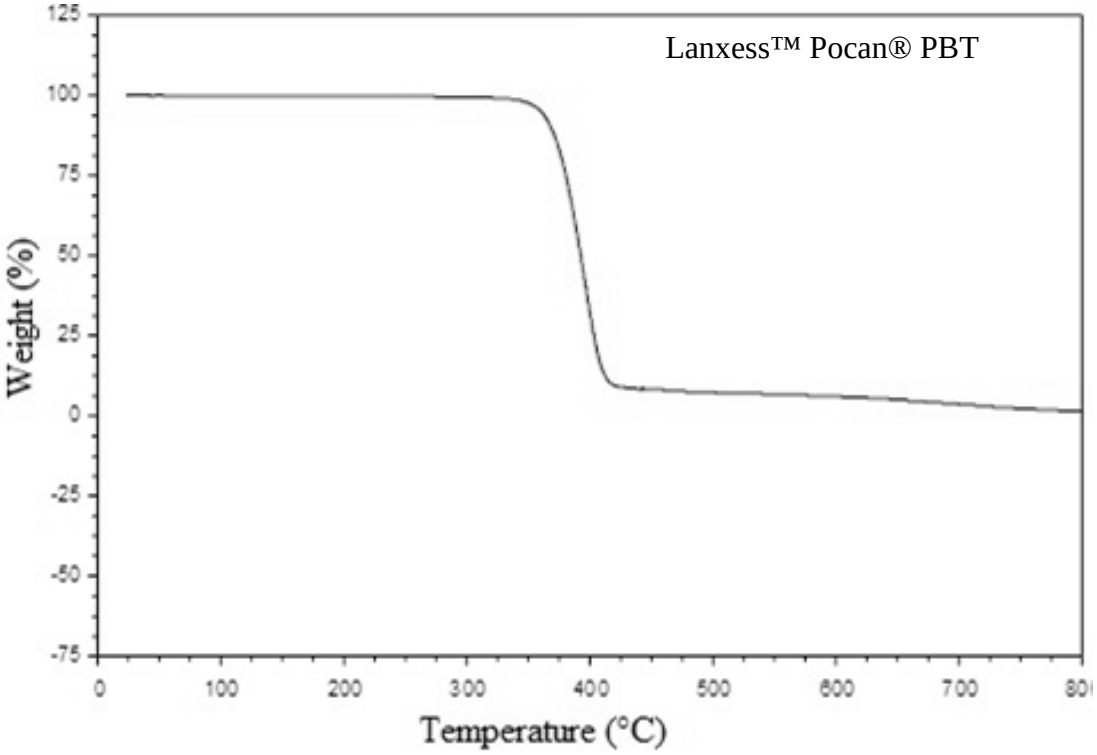

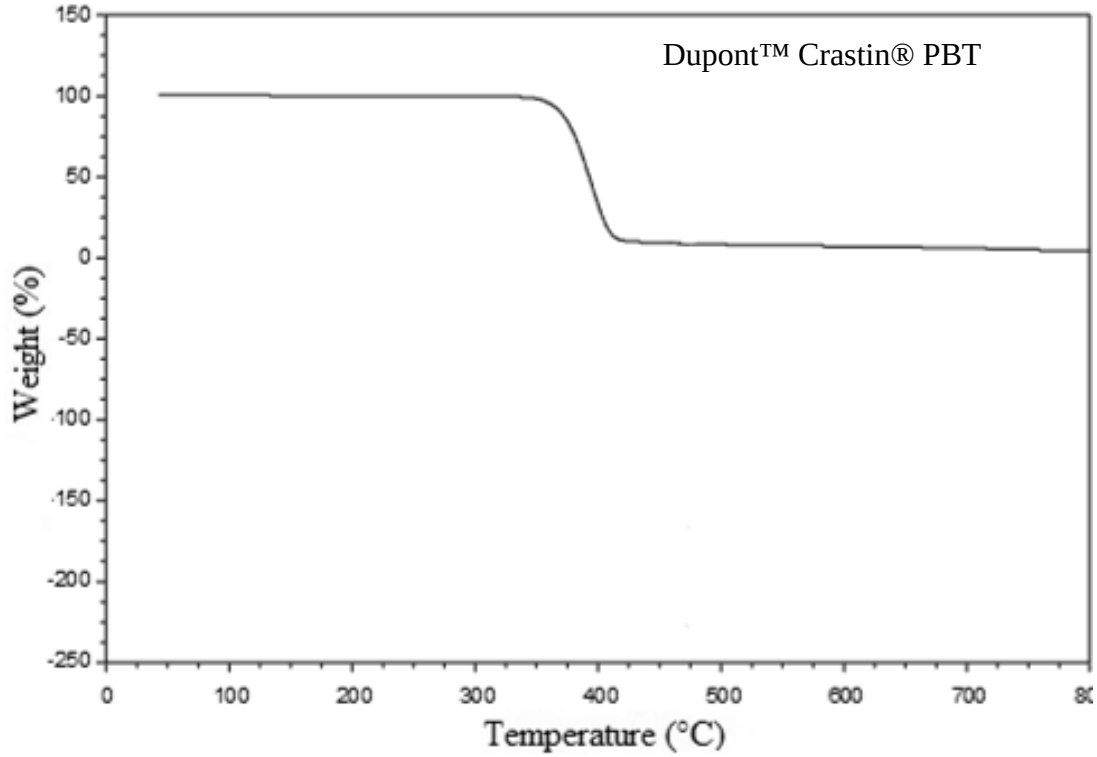

Appendix B - DSC Curves of the PBT Resins